FABRICATION OF LOW TEMPERATURE CO-FIRED CERAMIC (LTCC)-BASED SENSOR AND MICRO-FLUIDIC STRUCTURES

THÈSE N^{O} 3696 (2007)

PRÉSENTÉE LE 2 MARS 2007

À LA FACULTÉ DES SCIENCES ET TECHNIQUES DE L'INGÉNIEUR

Laboratoire de production microtechnique 2

SECTION DE MICROTECHNIQUE

ÉCOLE POLYTECHNIQUE FÉDÉRALE DE LAUSANNE

POUR L'OBTENTION DU GRADE DE DOCTEUR ÈS SCIENCES

PAR

Hansu BIROL

M. Sc. in sensor systems technology, Hochschule für Technik, Karlsruhe, Allemagne
de nationalité turque

acceptée sur proposition du jury:

Prof. Y. Perriard, président du jury
Prof. P. Ryser, directeur de thèse
Dr A. Dziedzic, rapporteur
Prof. G. L. Messing, rapporteur
Prof. P. Muralt, rapporteur

ÉCOLE POLYTECHNIQUE
FÉDÉRALE DE LAUSANNE

Lausanne, EPFL
2007

Ancüm, Bupum, biricik Alline'm ve
eşsiz Antonio Carlos Jobim'e

Summary

Low temperature co-fired ceramic (LTCC) technology has attracted remarkable attention in fabrication of sensors and micro-fluidic devices in the last decade. Although structuring planar LTCC foils, which are processed and screen-printed with thick-films, seems straight forward, major problems are encountered once basic sensor features such as cavities and micro-channels are desired within the sensor module. Therefore, this study aims to accomplish two major tasks: development of an advanced technique for fabrication of well-defined and integrated cavities in LTCC and production of novel sensors by using new design parameters and compatible materials systems.

Concerning the former objective, we developed graphite-based sacrificial (GB) pastes, which was screen-printed on LTCC, stacked with additional layers and fired. Cavities were formed by removal of sacrificial pastes during different stages of firing: GB was oxidized during sintering of the LTCC module.

We selected membrane with inlet and outlet channels as our model device to study the oxidation kinetics of the GB paste as a function of graphite particle size, paste formulation, heating rate, channel dimensions and LTCC open-pore closure behavior and its effects on the membrane features. We found that higher heating rates (> 2.5 °C/min) shifted the oxidation of the paste to higher temperature as expected, whereas lower rates resulted in burnout and LTCC densification at lower temperatures, changing the cavity from a swollen to sagged structure, respectively. Channel dimensions were also found to have a direct influence on membrane swelling such that wider (400 μm) and thicker (> 70 μm of printed paste) channels permitted increased oxygen intake and played the major role in oxidation of the paste, after the closure of LTCC open porosity. We produced membranes within a diameter range of 7-18 mm and well-defined spacing of 13 to 100 μm. Displacement of largest membranes, which can be used as sensitive pressure sensors at sub-20 mbar range, were characterized in terms of applied pressure and membrane swelling. A hysteretic behavior of membrane displacement was observed as a function of swelling, which was absent in case of relatively flat membranes.

In the second part of the thesis, fabrication of novel, LTCC-based sensors as an alternative to alumina-based ones was covered. Promising device applications were realized using distinctive properties of LTCC such as low thermal conductivity (an order of magnitude lower than alumina), design flexibility, fine substrate thicknesses (40 μm), lower elastic modulus, etc. Thus, we demonstrated three LTCC-based sensors detecting gas viscosity, force

and inclination. Physical principle, materials selection, fabrication procedure and performance of these sensors were explained in detail.

The materials compatibility, which is one of the utmost important parameters to assure the quality and the performance of the sensors, was discussed by using various materials characterization techniques and instruments. Differential shrinkage between LTCC tape and thick-film components and the process-dependent-tape shrinkage were found to be the major challenges, which also present the main boundaries of this technology today. In order to avoid the former problem, we modified thick-film terminations by mixing with network-forming additives such as quartz so that its shrinkage behavior was matched to LTCC. This facilitated utilization of thinner LTCC substrates, which is one of the figure of merits, for improved force sensing. The shrinkage of the sensor module, on the other hand, was compensated by manipulating design parameters in light of observed dimensional changes.

Finally, future perspectives for structuring LTCC are presented, where an alternative technique to GB pastes is presented: mineral-based sacrificial pastes. In spite of similarity to GB pastes in processing conditions and parameters, these new pastes are formulated by a mixture of high and low melting temperature mineral (CaO) and glass (B_2O_3), respectively, where a consolidated state is formed that is etched by acid after firing. It was observed that the technique results in well-defined spacing and efficient removal characteristics. On the other hand, shrinkage mismatch to that of LTCC remains a problem.

Keywords: LTCC, sensors, micro-fluidic, sacrificial layers

Version Abrégée

La technologie en céramique co-cuite à basse température (LTCC) a attiré une forte attention dans la fabrication de capteurs et de dispositifs micro fluidiques dans la dernière décennie. Bien que la structuration de feuilles de LTCC, qui sont traitées et sérigraphiées avec des couches épaisses, ne semble pas problématique, des problèmes important apparaissent si des éléments de structure tels que des cavités et des micro-canaux sont désirés dans le module de capteur. Par conséquent, cette étude vise à accomplir deux objectifs principaux : développement d'une technique avancée pour la fabrication de cavités bien définies et intégrées dans le LTCC et la production de types de capteurs novateurs en employant de nouveaux paramètres de conception et systèmes compatibles de matériaux.

Pour le premier objectif, nous avons développé les pâtes (GB) sacrificielles à base de graphite, qui ont été sérigraphiées sur le LTCC, recouvertes avec des couches additionnelles de LTCC et cuites. Des cavités ont été crées par la disparition des pâtes sacrificielles pendant différentes étapes de la cuisson: le GB a été oxydé pendant le frittage du module de LTCC.

Nous avons choisi la membrane avec des canaux d'admission et de sortie comme notre dispositif modèle pour étudier la cinétique d'oxydation du GB en fonction de la granulométrie du graphite, de la formulation de la pâte, du taux de chauffage, des dimensions des canaux et du processus de fermeture de la porosité ouverte du LTCC et ses effets sur les dispositifs de membrane. Nous avons constaté que des taux de chauffage plus élevées décalent l'oxydation de la pâte vers des températures plus élevés, comme prévu, tandis que des taux inférieurs ont pour conséquence une oxydation et une densification de LTCC à plus basse température, donnant respectivement des cavités gonflées ou affaissées. Les dimensions des canaux se sont également avérées avoir une influence directe sur le gonflement de la membrane : des canaux plus larges et plus épais facilitent l'oxydation et jouent le rôle principal dans l'oxydation de la pâte après disparition de la porosité ouverte du LTCC. Nous avons produit des membranes dans une gamme de diamètre de 7-18 millimètres et d'espacement bien défini du 13 à 100 μm. Le déflexion des plus grandes membranes, qui peuvent être utilisées en tant que capteurs de pression sensibles à moins de 20 mbar, a été caractérisée en fonction de la pression pour des membranes présentant différents degrés de gonflement initial. Nous avons observé un comportement d'hystérésis du déplacement de la membrane en fonction du gonflement, qui disparaît pour des membranes relativement plates.

Dans la deuxième partie de la thèse, la fabrication de capteurs novateurs à base de LTCC comme alternative à l'alumine a été étudiée. Des examples prometteurs de dispositifs ont été réalisées en utilisant les propriétés du LTCC telles que la faible conductivité thermique (un ordre de grandeur plus basse que l'alumine), la souplesse de conception, les épaisseurs fines de substrat (40µm), le module élastique inférieur, etc. Ainsi, nous avons présenté trois capteurs basés sur le LTCC, mesurant la viscosité de gaz, la force et l'inclinaison. Le principe, le choix de matériaux, le procédé de fabrication et la réalisation de ces capteurs ont été expliqués en détail.

La compatibilité de matériaux, qui est l'un des aspects déterminants, a été étudiée en utilisant diverses techniques de caractérisation des matériaux. Le retrait différentiel au frittage entre la bande de LTCC et les compositions de couches épaisses se sont avérés être les défis principaux, qui présentent également les limites principales de cette technologie aujourd'hui. Afin de contrôler le retrait, nous avons modifié des compositions couches épaisses en incorporant des additifs tels que le quartz, de sorte que son comportement au retrait soit ajusté à celui du LTCC. Ceci a permis l'utilisation de substrats plus minces de LTCC, rendant possible la fabrication de capteurs plus sensibles. Le retrait du module du capteur, d'autre part, a été compensé en changeant les dimensions initiales en fonction des premiers essais.

Finalement, de futures perspectives de structurer le LTCC ont été examinées et une technique alternative aux pâtes de GB est présentée: des pâtes sacrificielles minérales. Malgré la similitude aux pâtes graphite du point de vue de la fabrication, ces nouvelles pâtes sont basées sur un mélange d'une poudre minérale réfractaire (CaO) et d'un fondant (B_2O_3), où on forme un matériau soluble dans l'acide après cuisson à l'acide. Des caractéristiques prometteuses, telles qu'une dissolution facile après cuisson et une structuration bien définie du LTCC, ont été observées. Cependant, le choix des matériaux doit encore être amélioré pour obtenir un retrait plus compatible à celui du LTCC.

Mots-clés: LTCC, capteurs, microfluidique, couches sacrificielles

Table of Contents

1 INTODUCTION

1.1 LTCC technology: history and development

Microelectronics is a multi-billion dollar industry today, offering consumers a wide range of products such as mobile phones, wireless communication systems, portable computers, DVD players, flat panel displays, storage medias, etc. (figure 1.1.). This is an outcome of the successful combination of a broad spectrum of technologies with the remarkable advancements in materials science [1]. However the key technology, which completes the two and determines the performance, reliability and cost of the final product, is microelectronics packaging [1-3]. Whether it is an integrated circuit (IC) on a silicon chip (e.g. solid state devices, logic and memory components of computers, etc.) or a microsystem on a multi-chip module (MCM), which are the basic functional segments of such devices, packaging plays an important role by providing mechanical support, robustness, hermeticity, power and signal transmission to/from ICs, in addition to many other functions [3].

Apparatus	iPod nano	Nokia E61 mobile phone	Sony DSC T5 digital camera	Sony Vaio VGNTX 751 PB laptop
$d_{longest}$ (cm)	8.7	11.7	9.4	27.2
d_{medium} (cm)	4	7	6	19.6
$d_{shortest}$ (cm)	0.7	1.4	2	2.8
weight (g)	43	144	113	1200

Figure 1.1. Indispensable features of new electronics: smaller, lighter and more functional.

A simple microelectronic package can be visualized as a planar interconnect board (= substrate) providing housing for discrete ICs. The circuits are flip-chipped or bonded on this layer, which is previously printed with electronic components for circuit wiring. This type of packaging medium, in which the multiple ICs and components are confined into one single layer, is called MCM (Figure 1.2.) [4] and it is further classified in terms of the substrate used: MCM-L, MCM-C and MCM-D, where L, C and D represent laminate or printed circuit board

(PCB), ceramic and organics/inorganics deposited on a carrier, respectively [5, 6]. Among these substrates, the ceramics exhibit desired thermal and electrical characteristics compared to polymers [7, 8]. Although this hybrid system seems a straightforward solution, it is insufficient to respond to the demands of new packages seeking high functional density and wiring, smaller sizes, robustness etc. [4].

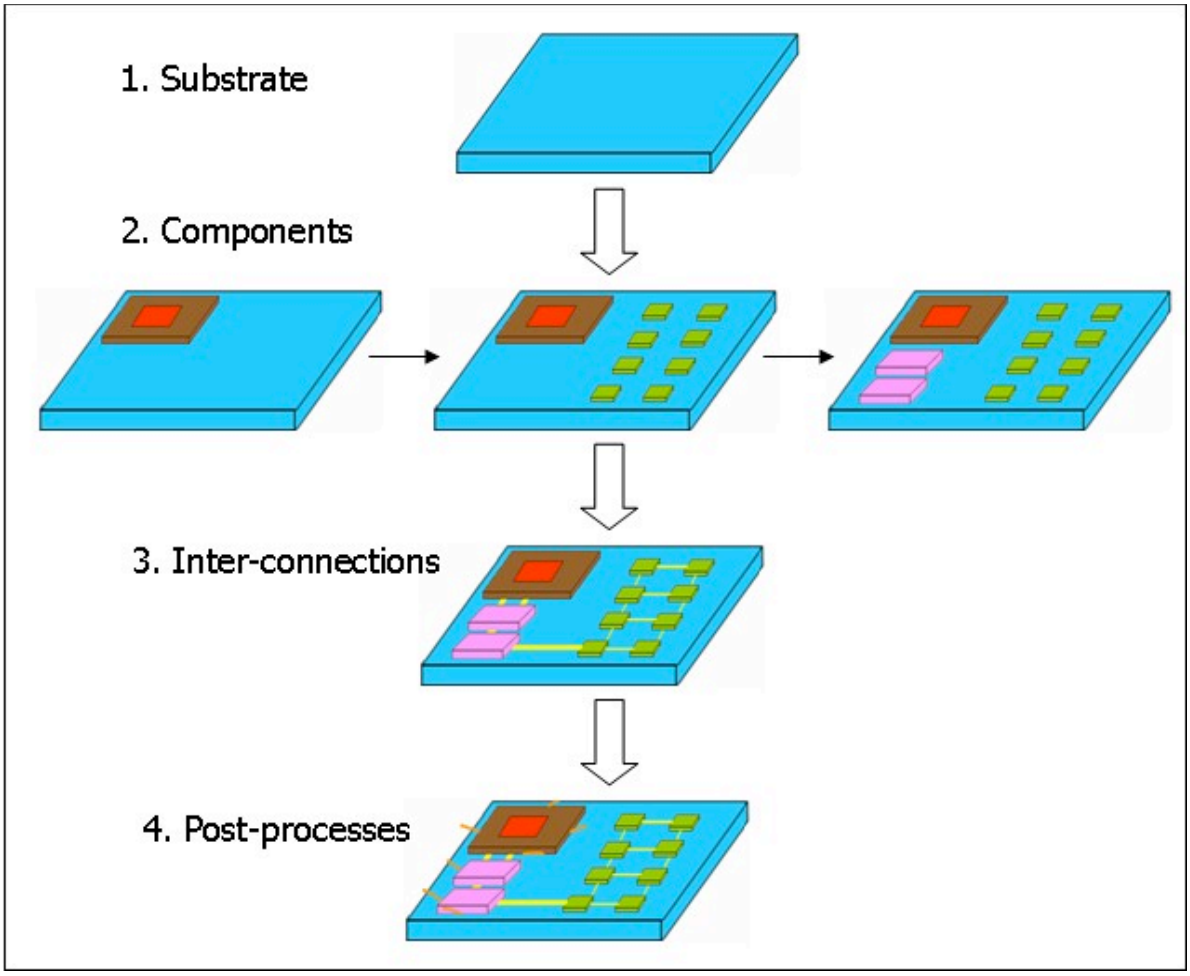

Figure 1.2. A simple microelectronic package: components confined into one single layer.

An advanced microelectronic package, on the other hand, is based on the integration of active and passive electronic components such as filters, digital and controlled impedance RF interconnects, RLC elements (R = resistor, L = inductor, and C = capacitor), etc… into a multilayer ceramic (MLC) module (figure 1.3.) [4, 5, 9]. These components are integrated within (= embedded, buried) and/or onto the surface layers, facilitating the fabrication of a monolithic structure with increased functionality/size ratio, performance and reliability. The communication between the components is enhanced by the electrical vias, which increase the

wiring density and decrease signal path by intelligent design concepts. The packaging method based on this technique is called multi-chip integrated circuit (MCIC) and it is divided into three sub-groups [4]: thick-film [10], low temperature co-fired ceramic (LTCC) and high-temperature co-fired ceramic (HTCC) [4].

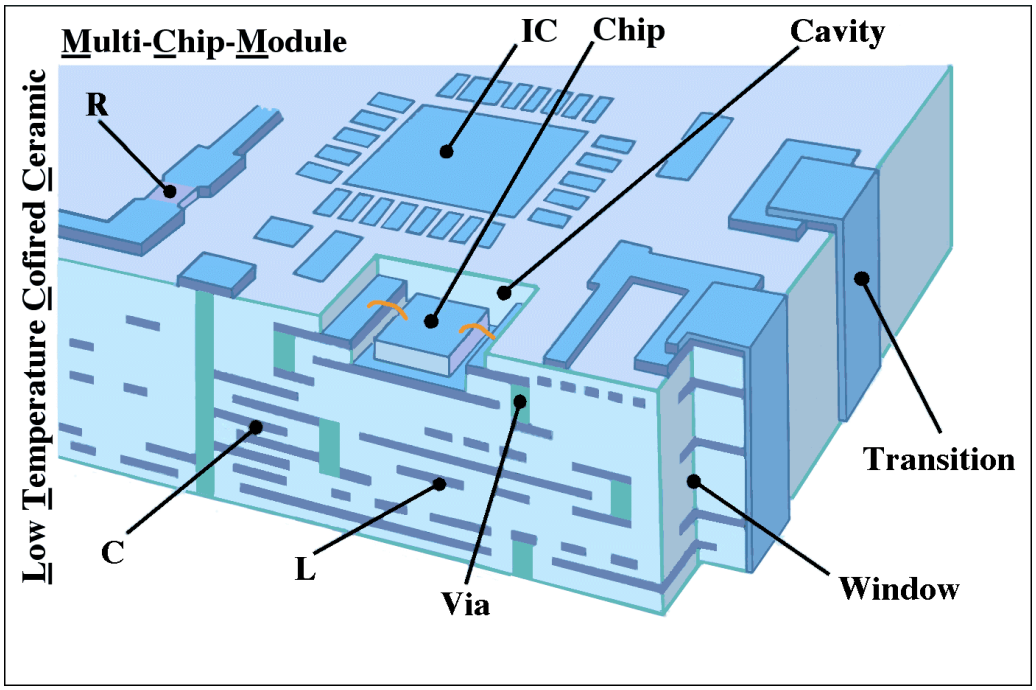

Figure 1.3. An advanced microelectronic package: components are integrated onto/into the entire module (image from "Microwave Engineering Europe", Aug/Sep 97: A 3D representation of Murata's hybrid module in LTCC).

The development of MCIC technology was driven by the need for increased interconnect density, higher signal transmission and clock rates for digital and microwave electronics in the early 1990s [7, 9]. Although MCIC, in general, was used in military, space applications, etc. [4], LTCC-based MCIC technology made its own breakthrough in the telecommunication field, which is one of the fastest growing segments in the consumer electronics industry [11, 12]. Mobile phones (0.9-2 GHz), wireless local networks - Bluetooth (2.4 GHz), global positioning systems (GPS, 1.6 GHz), broadband access connection systems (5.8-40 GHz), etc. are some of the examples to LTCC applications in the RF field [11-15].

The history of LTCC technology actually dates back to early 80s, when it was first developed by Hughes and DuPont for military systems [16, 17]. Commercialization of the technology, which was accelerated after the co-operation of LTCC tape producers such as DuPont, Heraeus and Ferro with packaging companies in the late 80s, broadened the

application areas to avionics and automotive industries [17, 18]. We have been witnessing versatile applications in sensors, micro-fluidics, etc. in the last decade, which have become increasingly popular [19-34]. These relatively recent LTCC applications will be the main interest area of this thesis, with a focus on their fabrication technique using a special method. Although LTCC technology is cited as the most intelligent packaging concept for realization of highly functional, reliable and low-cost electronic devices [36], it is evident that such a progress can be achieved by using advanced materials systems, which play the major role in the functionality and reliability of packages manufactured.

1.2 LTCC materials system

1.2.1 Definition of key terms: low temperature and cofiring

As discussed in the previous section, the substrate is the fundamental component of any microelectronic package [36]. The circuits are soldered on it, thus, forming the surface mount(able) device (SMD), and the connection between these devices are facilitated by the electrodes. In a typical LTCC materials system, the substrate is the fired LTCC sheet, whereas all other active and/or passive electronic components listed previously are the functional elements of the system integrated/screen-printed in the overall multilayer structure.

Instead of explaining these components directly, it would be more appropriate to emphasize the two key features of the technology primarily, which are actually explicitly-defined in the name itself: low temperature and cofired ceramic.

The former term refers to LTCC sintering temperature below 950 °C (usually the 850-900 °C range), which is relatively low compared to that of classical ceramic substrates such as α-Al_2O_3, around 1650 °C [37]. Before elucidating further, the right question here should be “why low temperature?” to make the link to the second term and to better understand the technology as a whole.

Selection of internal electrodes in MLCs has always been a challenge since it has impacts on reliability and cost of the overall system. The conductors employed, particularly in the case of reliable and high performance devices, are expected to exhibit various properties: high electrical conductivity and migration resistance, compatibility with other materials in the system, ease of producing solder/wire interconnection bonds with good electrical and mechanical integrity, good adhesion to substrate, good definition and fireability in air, etc.

[38]. In spite of a wide range of alternatives, previous studies on the thermodynamic behavior of electrodes have shown that only noble metals are stable in air over a temperature range commonly used (800-1100 °C) during the sintering of substrates [38-40]. Thus, Ag, Au, Cu have been extensively used in the fabrication of MLC devices requiring high speed and undisturbed signal transmission, fast switch times (GHz range), high performance, etc. for a long time. Ag/Pd is also a conductor of high interest, as it possesses complete miscibility and thus, a wide range of melting temperatures that can be manipulated by changing the Ag/Pd ratio; however, it exhibits a unique problem: oxidation of Pd. This leads to expansion of the electrode and a tendency to interact with the surrounding dielectric substrate as a result of the resulting oxide phases [38, 40-44].

There is one significant feature common to these electrodes, which is their low melting temperature (T_m): Ag, Au and Cu at 961, 1063 and 1083 °C, respectively [38]. Therefore the application of these electrodes, which is a fundamental requirement for fabrication of reliable and high performance devices, imposes strict condition on the substrates to be used: *low temperature* sintering [37, 45]. Obviously, the term "low" refers to a temperature value that is lower than the melting temperature of the electrodes listed above: below 1000 °C. This condition has been the driving force for developing novel substrates for fabricating the hybrid microelectronic systems of the future.

The birth of LTCC technology occurred as a result of these requirements and efforts in the early 80s based on the idea of firing the low temperature sintered multilayer ceramic with the high conductivity thick-film electrodes simultaneously, hence the term *cofiring* is introduced [46-48].

1.2.2 Description of the components

The push towards low temperature sintering substrates lead to the introduction of a new type of material in multilayer ceramic technologies: glass-ceramics. These are polycrystalline solids containing residual glass phase, which are derived from the controlled crystallization of glasses [49, 50]. Successful preparation of the glass-ceramics depends on the homogeneous distribution of the crystallization sites (crystal nuclei) throughout the glass and the appropriate heat treatment, which yields 50 to 100% of crystalline at the end of the process [50]. Besides traditional glass-forming techniques like forming, shaping and heating, glass-ceramics can be processed via powder route by slip casting, tape casting (LTCC), etc. [49].

The glass, in addition to its presence in the composition of the substrates, is also used in other components of the package: passive electronic components such as thick-film conductors and resistors, in which it has functions other than promoting densification. Therefore, from here on, we will be explaining the two main components of a typical LTCC materials system - LTCC sheets and integrated passives - individually, for a better understanding.

The substrates employed in microelectronic packages must fulfill various requirements: ideally low dielectric constant for successful signal transmission, high dielectric strength, low dissipation factors particularly at high frequencies, well-matched thermal coefficient of expansion (TCE) to that of printed components, ability to withstand the 500-1000 °C temperature range, high mechanical strength, smooth surfaces, free of surface distortion, visual defects, physical and chemical compatibility, low cost in high volume production [51]. Most of the substrates used in microelectronics are ceramic or ceramic-based materials such as alumina, beryllia, magnesia, zirconia and glass-ceramics [48, 51]. It is evident that the selection of the substrate is related to the application of interest, which requires a careful evaluation of these candidates considering their electrical, thermal, mechanical and chemical properties. LTCC substrates, which are glass-ceramics in their nature, fulfill most of these prerequisites, in addition to other benefits such as flexibility in design and fabrication, low firing temperatures, etc. Their production, on the other hand, combines some of the very fundamental and sophisticated techniques of the ceramics processing science such as ceramic powder preparation [52, 53], colloidal processing [54, 55] and tape-casting [56, 57].

From a general perspective, LTCC tapes are thick layers prepared by tape-casting a glass-ceramic slurry on polymeric carriers at varying thicknesses (30-350 μm) [6]. Glass, which is the key material of this mixture to lower sintering temperature [1, 58, 59], is prepared by melting the raw materials mixed at desired composition, quenching the molten liquid and grinding the solidified structure for powdering. It is introduced into the ceramic either as a low softening point glass or as a fully devitrifying (crystallizing) glass during firing [60, 61].

In the former case, the glass frit facilitates low temperature sintering by liquid phase sintering (LPS), which facilitates increased diffusivity and mass transport compared to solid state sintering. It softens at a relatively low glass transition temperature forming the liquid, which leads to neck-formation by viscous flow. This is followed by liquid spread over ceramic

particles (fillers), the stage during which small particles dissolve and precipitate on larger ones, in addition to wetting and rearrangement [62-65]. The LPS of insoluble systems is referred to as non-reactive liquid phase sintering (NLPS), which requires a sufficient amount of glass for full density [65]. The final density is a strong function of the filler size and volume, heating rate, temperature, etc [62]. On the other hand, the LPS of systems containing low viscosity and high reactivity glass against crystalline phase constitutes the reactive sintering [66].

The other approach, which suggests the utilization of fully-devitrifying glass as the starting material, has also been employed in LTCC tapes and is considered more advantageous compared to the low softening point glass, from thermomechanical and dielectric merits [60, 61]. A clear and well-organized description of glass compositions that are used in commercial LTCC tape systems and the corresponding sintering mechanisms are explained in [66, 67].

The filler is the other inorganic constituent of the tape, which either reacts with the glass and forms a new phase (not a full reaction necessarily) or remains as is [14, 37]. Depending on the type of the filler and the phases forming upon firing, physical, thermal and electrical properties are determined. Therefore the glass, which is used to reduce the sintering temperature, should have the minimum effect on such properties of the base ceramic [68] (particularly in cases where the “as is” filler properties such as PZT, thick-films, etc. are sought. In other cases, such as anorthite, on the other hand, the glass-filler reaction is an expected one). Al_2O_3, $BaTiO_3$, $CaTiO_3$, $SrTiO_3$, $MgCaTiO_3$, $CaZrO_3$ are examples to the dielectric ceramic materials [69]. Among many others, the reaction of Al_2O_3 with CaO-Al_2O_3-SiO_2-B_2O_3 glass, which leads to formation of anorthite phase [70, 71], has various advantages other than promotion of low temperature densification: lower thermal expansion coefficient, high-heat deformation resistance, high compatibility with conductors [72].

There are also alkali and alkaline earth modifiers in the LTCC tapes, which provide required flow and densification characteristics to the tape at desired firing temperature [73]. Li_2O, Na_2O, K_2O, CaO, MgO, SrO are some of these elements, which play a critical role in reducing the viscosity of glass. However, excess flow upon firing is avoided by partial crystallization of the glass, which is initiated by the reaction with the ceramic filler in the glass matrix [73].

The final constituent of an LTCC tape is the organic vehicle, which facilitates casting of the composition that is composed of glass, ceramic fillers and alkaline/earth alkaline

modifiers. This organic medium, in which the crystalline and amorphous materials are dispersed, is comprised of a polymeric binder that is dissolved in a volatile organic/aqueous solvent and other optional constituents such as plasticizers, release agents, stabilizing agents, dispersing agents, etc [73]. The binder provides certain amount of strength and toughness to the thin sheets and surrounds powder particles by anchoring itself to their surface. It creates a 3-D-interconnected skeleton of the resin [74]. The optimum binder is the one that can be used at smallest amounts with the maximum quantity of functional solids [73]. This is an important term as it is related to the shrinkage of the tape upon firing: closer packing (less binder amount) leads to reduced shrinkage (dimensional change) [75]. The solvent, which is to dissolve the binder completely, on the other hand, is expected to evaporate from the rest ideally at low temperatures (< 120 °C) of drying process [73]. The main criteria for a liquid to be a solvent in the dispersion are similar chemical structure (functional groups) to that of the binder and providing a medium, in which the constituents are well-dispersed [74]. Dispersion is also and mainly facilitated by the dispersant, which is used to avoid agglomeration of small particles. The last major constituent of the organic vehicle, plasticizer, is the key material determining the plasticity, workability of LTCC tape during cutting, punching, lamination, etc. and thus, it must prevent cracking of tape [73]. Further information for the major components of organic vehicle, other than those discussed in tape casting literature in general, can alternatively be found in [76-80].

Therefore, the properties of an ideal organic vehicle in light of these discussions are: good application of composition, appropriate viscosity and rheological behavior, appropriate wettability of the substrate and solids, good drying rate, good firing properties and good dried film strength to withstand rough handling, no chemical reactivity with the inorganics [73, 81, 82].

The last step prior to casting of LTCC sheets is the slurry processing, which consists of milling, deairing and filtering processes. Milling is conducted in order to disperse the slurry and it is performed in a preferred sequence: initially the powder, solvent and the dispersant is milled, which is followed by addition of binder and plasticizer and re-milling. This sequence of components introduction into the process avoids the competition for adsorption on the particles between the dispersant and binder/plasticizer and reduces the mechanical damage of the binder molecules by shorter milling periods [82]. Deairing, on the other hand, is applied to

prevent formation of bubbles in the cast tape, which is followed by filtering the slurry through a sieve to filter dirt, undissolved organics, milling debris, etc. [82].

The last step in LTCC tape manufacturing is tape casting. This is performed by transferring the prepared slurry from a reservoir onto a moving tape carrier by a doctor blade (figure 1.4.) [56, 57, 82, 83], which actually determines the thickness of the cast slurry with constant rheological behavior [84]. The carrier is usually an organic film and it is expected to have a smooth surface, which is coated with additional elements to avoid excessive adhesion of the slurry. Tape casting is completed by the drying process [83], during which the solvent is evaporated, thus allowing the particles and binder to form a flexible sheet with sufficient strength to be stripped from the carrier [82]. Drying occurs on the surface of the cast slurry, which hosts the solvents transported to the surface by capillary forces introduced by air flow. Further drying is controlled by solvent diffusion into the channels and surface [82].

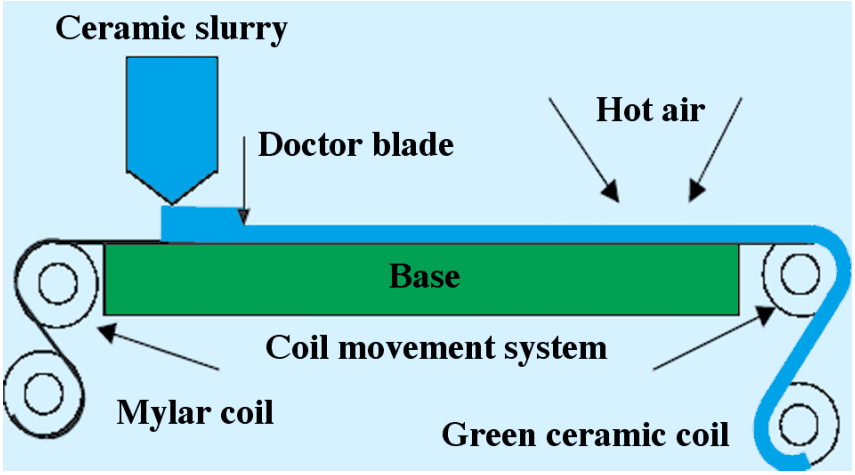

Figure 1.4. Principle of tape casting: slurry is poured on the carrier sheet and dried (image from [16]).

Today, there are a number LTCC tape manufacturers and their products, depending on the application, vary as a function of the chemical, physical and electrical properties of the ceramic filler and glass used, constituents of the organic vehicle, processing, etc. [8, 85-88].

The passives, on the other hand, are integrated between the layers, providing significant advantages over discretely-deposited components: active/passive trimming, reduced area and weight, increased packaging efficiency and interconnect density, increased reliability as a result of solderless-connections and most important of all reduced cost (figure 1.5.) [5, 10, 89]. Thus, the cost can be effectively reduced in the design phase of devices, once the appropriate substrate and the interconnection technology are identified [89].

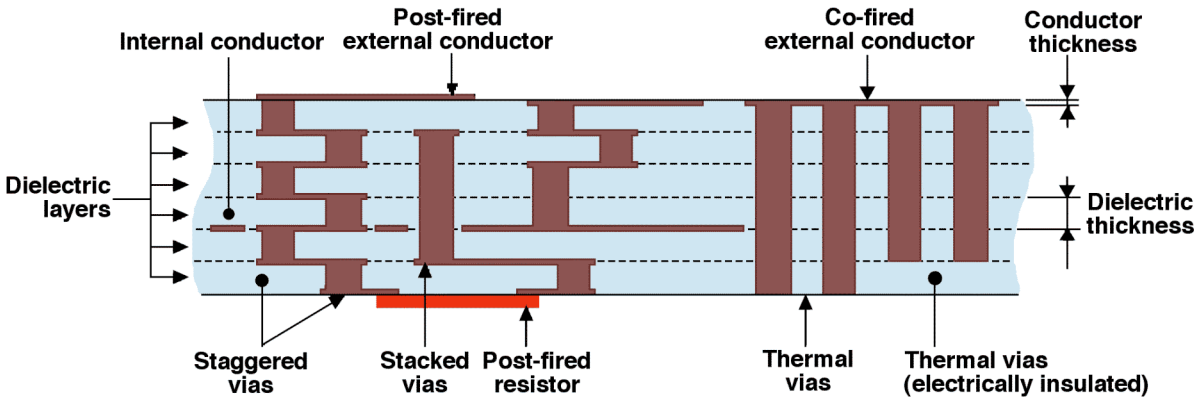

Figure 1.5. Saving volume, robustness, increased functional density by integrated passive components and vias (image from Defence R&D Canada).

Integrated passives are the electronic components of the (LTCC) multilayer circuits such as conductors, resistors, capacitors and inductors, which are screen-printed on LTCC layers (figure 1.5.). For the sake of clarity, we will focus on thick-film conductors since they constitute the largest quantity of the printed material used in a hybrid microcircuit [90]. We will also briefly discuss the fundamentals of thick-film resistors, which are the essential elements of the sensors and devices that will be introduced in the proceeding sections.

Thick-film conductor pastes are composed of three main ingredients: the functional phase, which consists of finely-divided particles of metals such as Ag, Au, Pd, Pt, Al, Cu, Ni, etc., glass frit/oxide and organic vehicle facilitating dispersion of particles and screen-printing [90-94]. Glass, apart from enhancing low temperature densification, determines the resistivity and binds the metal particles together and to the substrate [90-92]. The chemistry of the glass has an important role in determining the adhesion strength of the fired film on the substrate [90]. Thus, the conductors, according to this glass characteristic, are classified as fritted (containing a low-melting glass such as $Pb/B_2O_3/SiO_2$), fritless/oxide bonded (only a small amount of active oxides such as CuO, CdO, NiO, etc.) and glass + oxide [90]. However, glass must also exhibit physical and chemical compatibility with LTCC tapes during firing, in addition to other features at post-processing such as solder-wetting, leach resistance, which is the chemical inertness of conductor to dissolution in the solder, migration resistance [90, 95 and 96].

Thick-film resistors (TFRs), on the other hand, are the most interesting class of thick-films, which can be used either as a passive circuit element or as a sensing element such as thermistors (positive/negative temperature coefficient, PTC/NTC respectively), piezoresistors,

etc. [97-104]. They are composite materials, in which a submicron crystalline conductive phase, usually ruthenium dioxide (RuO_2) or ruthenate ($Bi_2Ru_2O_7$ or $Pb_2Ru_2O_{6.5}$) is mixed with much larger glass particles of high-lead silicate glass in an organic vehicle [97, 98]. The glass phase plays the major role in determining the final microstructure by penetrating into the conductor clusters and dispersing them randomly in the glass matrix upon softening above the glass transition temperature [97-99]. Previous studies have demonstrated that conduction, in such a media, is facilitated by the electrons tunneling through very thin glass layers between fine conductor particles [105-113]. Therefore, the resistivity is a strong function of the conductor fraction and particle size, the glass composition and the microstructure and it can vary over 10 orders of magnitude (~ 10^{-4} to 10^5 Ω.cm) as a function of these values [110]. Thick-film resistors, which are buried in LTCC multilayers, are further expected to exhibit physical and chemical compatibility for increased reliability [113].

1.2.3 Cofiring and technological challenges

Manufacturing LTCC multilayer systems is a multi-step process [6, 114], which can be summarized in the following order:

1.2.3.1 Slitting and blanking

The desired amount of tape is cut from the "ready to use" tape roll (cast and dried) and the working tape(s) for a pre-determined design is brought down to ideal size (figure 6).

1.2.3.2 Pre-conditioning

The tapes are stabilized at elevated temperatures (e.g. 120 °C) for a short time, which is followed by overnight stabilization at ambient temperature (figure 1.6.).

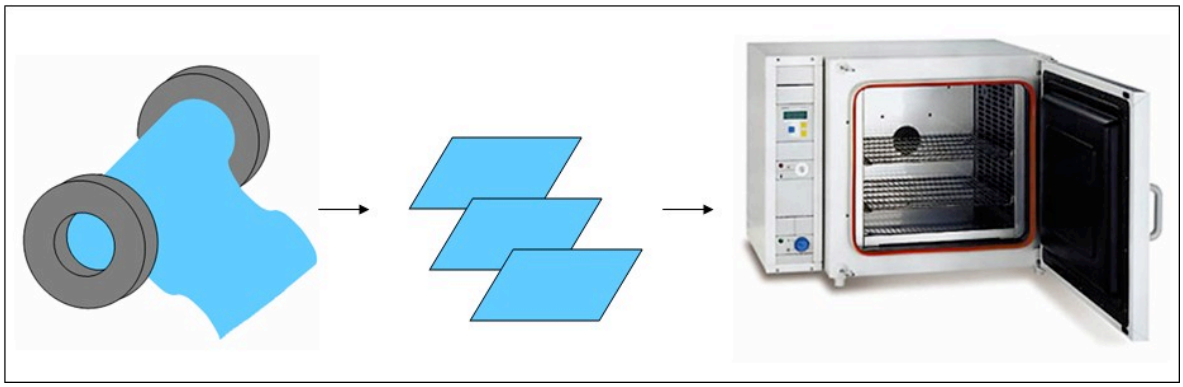

Figure 1.6. Slitting from the roll and preconditioning at a certain temperature and time interval.

1.2.3.3 Forming vias, planar geometrical structures

Vias and/or 2-D geometries such as rectangles are punched, machine or laser cut. The selection of machining parameters such as punch pressure, laser power, etc. has to be optimized to avoid tape deterioration [116]. Moreover, the structural and functional layers of the desired final device must be well planned at this stage: architectural features, layouts for thick-film deposition, etc.

1.2.3.4 Via filling

The vias are filled on each layer using the recommended materials and processes, which can be found on the product list of tape manufacturers (figure 1.7., list of tape manufacturers in [88]).

1.2.3.5 Screen-printing

Thick-film components, which are developed to exhibit physical and chemical compatibility with the LTCC tape of choice, are usually provided by the tape manufacturer and this set of components is referred to as the LTCC materials system.

The screens, which define the pattern and the amount of the deposited film, are fabricated by stretching a finely woven mesh over a frame (e.g. cast aluminium) [117]. The mesh, through which the paste is forced, is characterized by its size and density (lines/inch), tension, orientation and material (figure 1.7.) [117-118]. Therefore, the mesh selection is a critical step and it is influenced by the required line definition of the pattern and the paste being used. Mesh count (strands/inch) and filament (forms the mesh) diameter determine the mesh opening and the relation between the filament diameter and the mesh opening is inverse for a given mesh count: the smaller the filament diameter, the larger the mesh opening, which allows greater volume of ink deposition (figure 1.8.) [117].

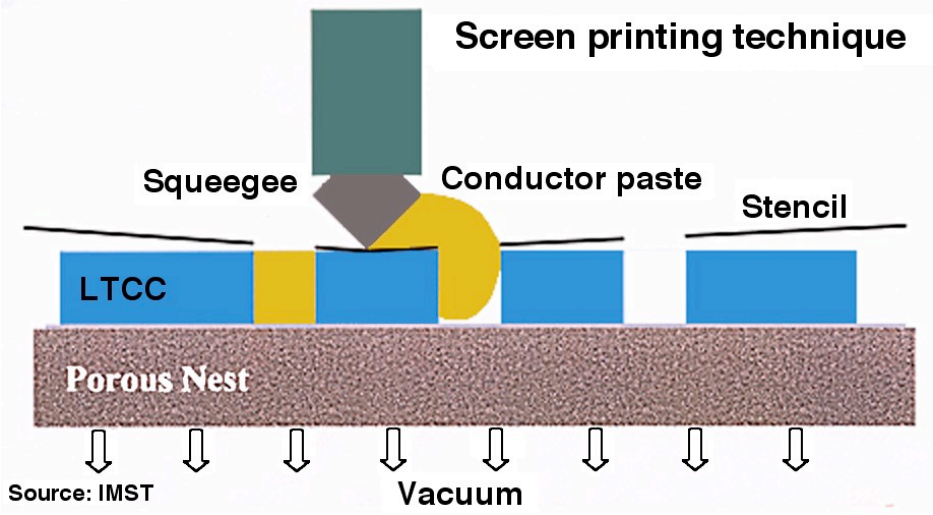

Figure 1.7. Screen-printing process: via filling (image from IMST).

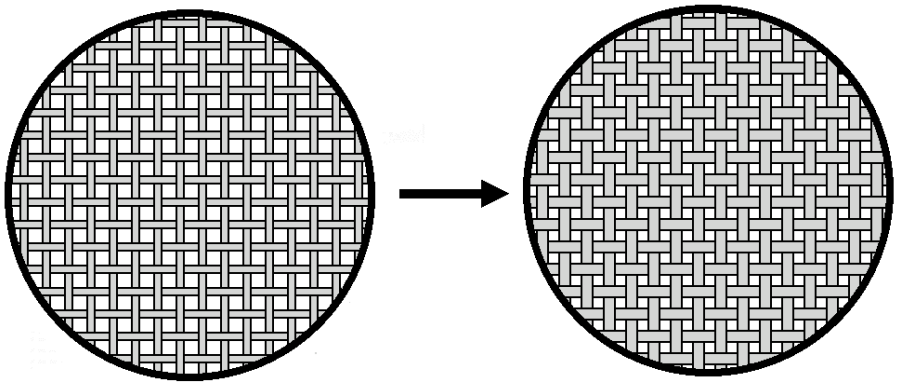

Figure 1.8. Reduced mesh opening (on the right) as a result of increased filament diameter (image from Coates Circuit Products).

The screen manufacture, on the other hand, is a step-wise procedure: frame and screen fabric selection, fabric attachment to the frame, deposition of the image of the layout to be printed over the screen, etc. [117]. Once these steps are defined and the screen is manufactured, the LTCC tape to be printed is carefully placed at a small distance to the screen and on porous alumina, which is connected to a pump that applies negative pressure to the tape. This is an obligatory step to avoid the LTCC tape remaining stuck to the screen after printing.

The screen-printed layers are first leveled at the ambient temperature and then in the oven at temperatures indicated by the manufacturers (ca. 100-150 °C). This is followed by inspecting the quality of the printed layers: line width, profile, thickness, etc.

1.2.3.6 Stacking and lamination

Registered LTCC sheets are stacked by a pin system [116] to form multilayers (figure 1.9.).

The stacked LTCC sheets are then laminated (figure 1.10.). Lamination is ideally performed under a uniaxial press and on a heating plate, which is heated to an elevated temperature (~ 100 °C) to enhance interpenetration of the particles via evaporated organics path (figure 1.11.). The quality of lamination is very important for the integrity of the system after firing; interfaces free of traces and defects, which are initiated by organics burnout, in addition to a homogenous microstructure are the main quality parameters. Certain techniques are reported to improve this step such as the introduction of a double sided adhesive tape into the LTCC layers [119-123]. According to this approach, the adhesive tape melts and exerts a capillary force on the tapes, making them closer to each other, which results in a rearrangement of the particles in the interface. Therefore the lamination is facilitated at low temperatures and pressures, avoiding the deformations observed in the other case.

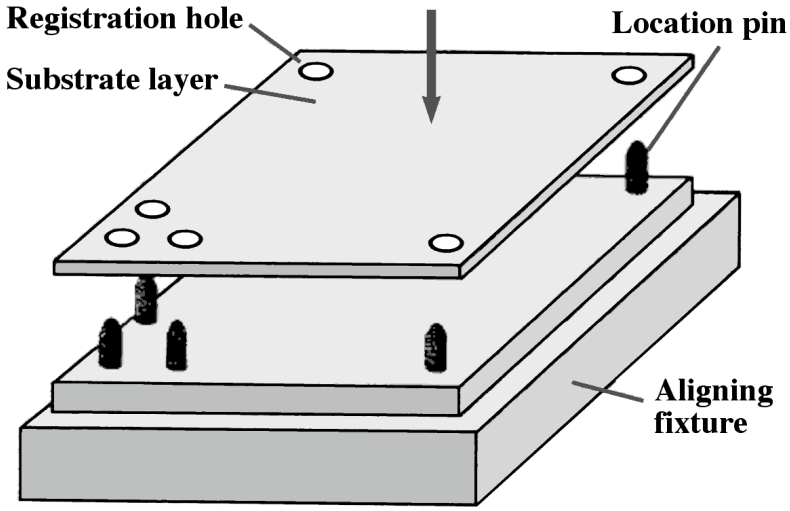

Figure 1.9. Stacking the registered layers using pin-alignment (image from [16]).

Figure 1.10. Lamination using uni-axial press.

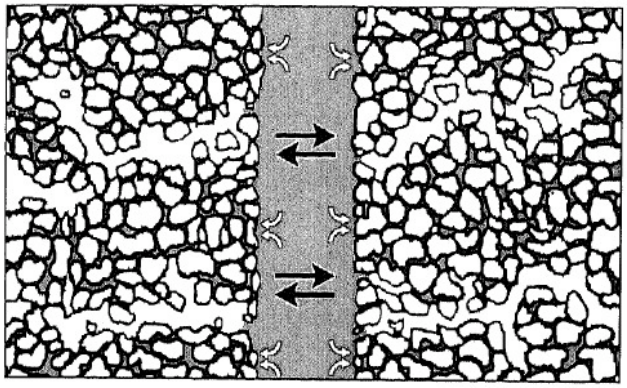

Figure 1.11. Inter-penetration of layers by organics diffusion at elevated temperatures (image from [119]).

1.2.3.7 Cofiring

Laminated LTCC layers with integrated thick-film components are cofired in homogenously-circulating air. This process is based on simultaneous firing of the materials in their green state (unfired state) and it differs from post-firing, in which the thick-films are fired on sintered LTCC substrates. Firing is usually performed according to a two-step-profile that is defined by the tape manufacturer at two dwell temperatures: organics burnout and peak firing (sintering) temperature (figure 1.12.) [46, 47].

Organics burnout is facilitated by oxidation of the organic vehicle in the tape and in the pastes, at a temperature above the boiling temperature of the binder, which is usually around 450-500 °C (certain binder types can decompose as well instead of boil). Unless careful processing parameters are selected (slow heating rates, etc.), this can be an aggressive process, which can result in delamination, bubble formation at the integrated passives, increased porosity, etc. Moreover sufficient time should be given for complete binder removal at the selected dwell temperature. The details of the binder burnout process have been given elsewhere [124-127].

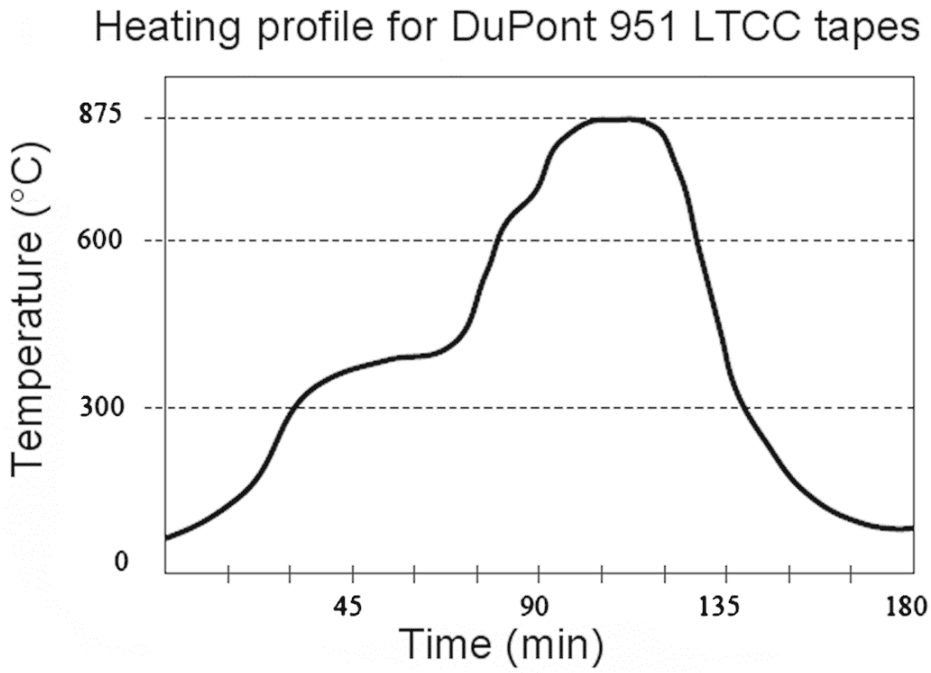

Figure 1.12. Heating profile for DuPont 951 tapes (image from DuPont).

Cofiring materials in their green state leads to increased materials interactions compared to post-firing. Therefore materials compatibility becomes a major concern as it determines the properties and the performance of the cofired electronic components. It has long been known that materials compatibility in an LTCC system is mainly determined by the physical and chemical properties of the glass in the components and the processing conditions [128-146]. Glass softens and liquefies over the glass transition temperature and thus, facilitates the material transport between the LTCC components (figure 1.13.). The driving force for this transport is thermodynamics: excess ion in a component flows to the component with deficient concentration to annul the gradient [128]. The important parameter, at this point, is the glass

viscosity (and softening point), which is a strong function of the composition: ions promoting network formation such as SiO_2 and Al_2O_3 increase viscosity, thus avoiding excessive interaction and resulting in a narrow interaction zone [128].

Peak firing temperature and time, as in other steps, are given by the LTCC manufacturer, with typical conditions being around 875 °C and 20 min. Both of these parameters should be selected carefully, as they determine the phases formed. The essence of cofiring can be summarized as the densification step that is completed until the onset of crystallization, which continues until the end of peak firing.

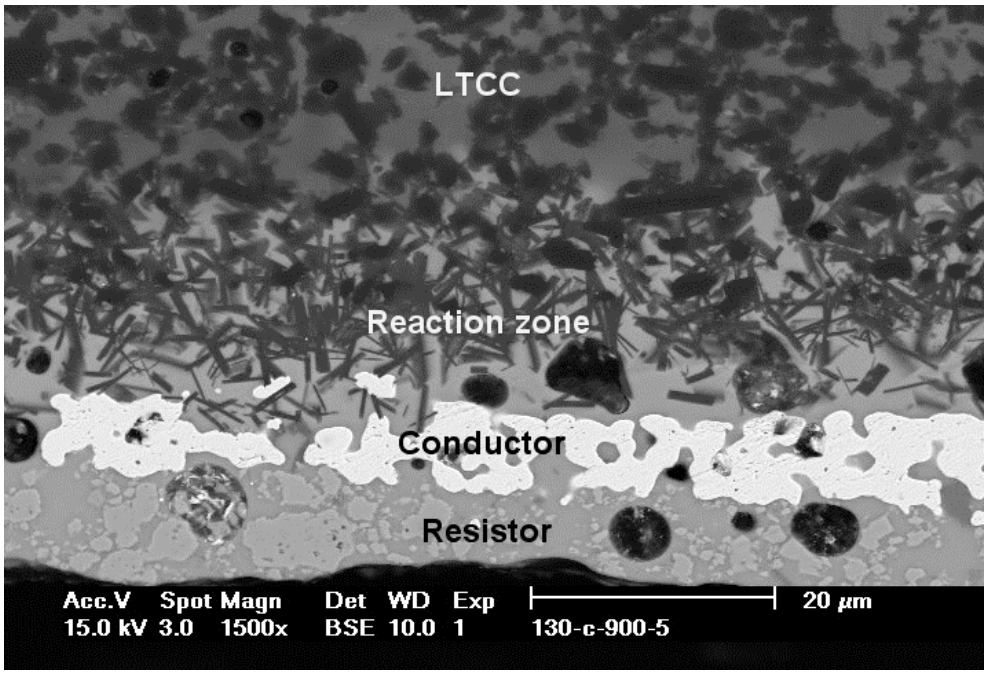

Figure 1.13. Excessive reaction an the LTCC-conductor-resistor boundary: reaction zone formed.

1.2.3.8 Surface layer printing

The surface of the cofired LTCC structure is printed with passive components such as resistors, etc. and/or with other pastes to attach devices (packaging), using recommended materials and processes.

1.2.3.9 Final inspection and singulation

Finally, the complete structure is inspected and cut to final size.

The overall procedure, which is well-established and straight-forward, is summarized in figure 1.14. However, the technology still faces major challenges such as the shrinkage of LTCC tapes and/or compatibility issues of the components.

Shrinkage of tapes (~ 14±1 % in x, y and z dimensions for a DuPont 951 LTCC tape [114]), which occurs as a result of the organics burnout and densification, has to be considered carefully at the early stages of device production, as it introduces uncertainty in the dimensional accuracy of the cofired structures. Although the shrinkage values and the tolerances get smaller as the technology continuously adapts to high-yield packaging efficiency, difficulties in dimensional control pose problems for reliable manufacturing.

A second problem related to shrinkage occurs between neighboring components such as LTCC-resistor, LTCC-electrode: differential shrinkage mismatch, due to the thick-film components, having an earlier onset of densification temperatures than LTCC. As a result, they sinter prior to LTCC tapes and deform the tapes, leading to warpage, camber, etc. [39, 142-144, 147-151].

As a major challenge, chemical compatibility on the other hand, is ascribed to the glass, which facilitates (increased) material transport between components during LPS. The extent of the resulting interaction between the components is set by the principles of thermodynamics and it can lead to variation of the resistance of the buried resistors or the destruction of the fine conductor lines, for instance [142-144].

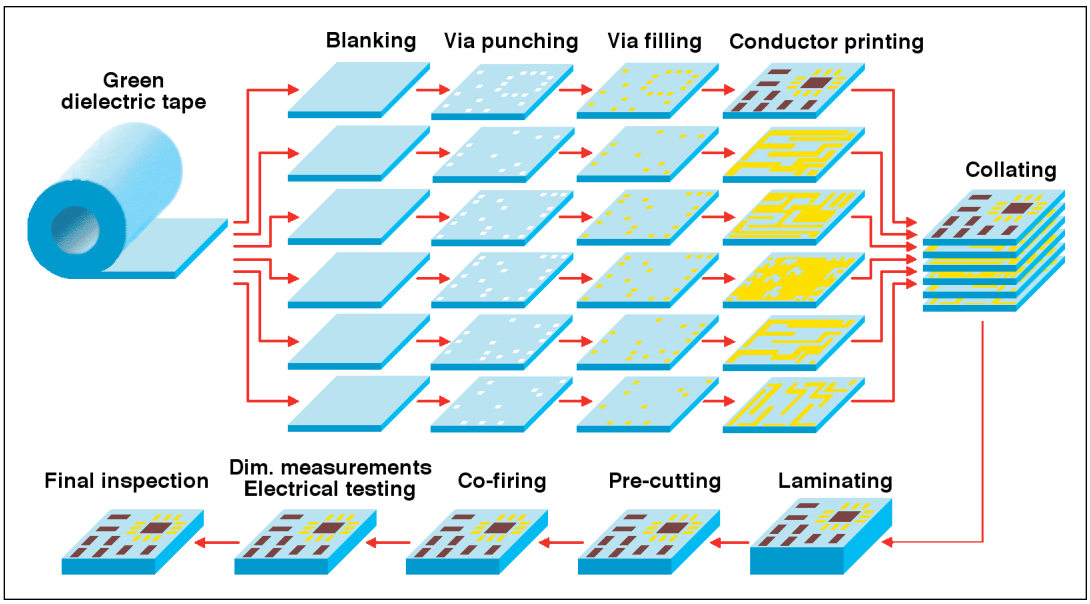

Figure 1.14. LTCC processing: from slurry to multilayer package (image from DT Microcircuits).

1.2.4 Present and future trends

Recent developments and future perspectives in LTCC materials development are driven by two major factors: materials compatibility issues and new application areas, imposing additional restrictions on the chemistry of the tapes. Glass-free, lead-free, zero-shrinkage LTCC tapes systems and pressure-assisted sintering, at this point, are some of the popular research interests.

As discussed previously, glass is the major constituent in the LTCC tape, which leads to chemical incompatibility, unless its composition is optimized with glass in other components. Moreover, its existence in a number of phases increases the possibility of reactions with the metal electrode and imposes complexity for LTCC processing [151]. Therefore, a glass-free system is always preferable as long as low sintering substrates with desired dielectric properties are produced [151, 152]. Selection of such system imposes restrictions primarily on melting point, compatibility with Ag conductors, etc. Recent studies address $CaGeO_3$ and $CaGe_2O_5$ as potential candidates for low temperature sintering, glass-free substrates [151].

Lead-free LTCC tapes are another popular area that is growing rapidly for packaging of multi-systems such as “lab on chip” and bio-applications [152, 153]. The principle restriction on the tapes to be used for these applications is the exclusion of toxic materials such as lead, cadmium, etc., which are sometimes included in the glass formulation. In spite of the narrower materials selection window, new lead-free LTCC tapes (systems) are shown to demonstrate densification and electrical performance that is well-comparable to that of lead-bearing compositions [154-157].

Another very interesting development is in the area of non-shrinking tapes, which receives a growing attention for circuit designers and high-scale circuit manufacturers. Introduced into the market, first by Heraeus [158], these tapes are reported to shrink in (x, y) and z directions by ca. 0.2 % and 32 %, respectively and thus, maintain very tight tolerances [159]. Extremely low shrinkage on x, y dimensions of the tape is a remarkable improvement for production, eliminating the need for insertion of sacrificial layers, etc. to reduce shrinkage tolerances [160]. Since the screen-printed layout remains almost the same on the non-shrinking tape after firing, it is also extremely practical, precise and cost-saving (figure 1.15.).

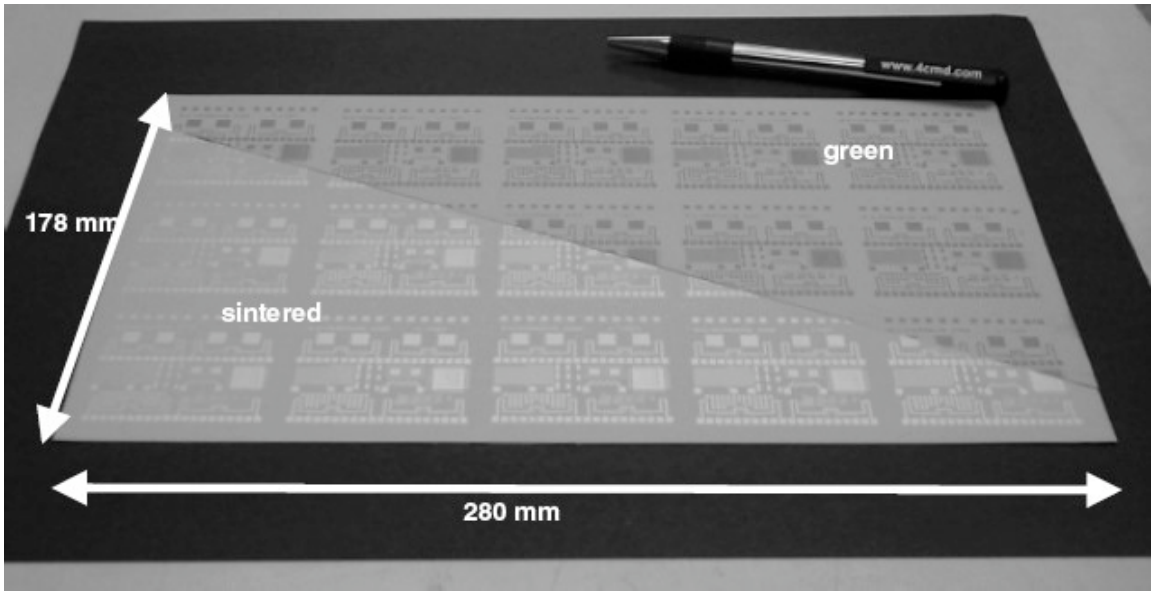

Figure 1.15. Heralock, Zero-shrink tape: laminate before (on the right hand side) and after sintering. Shrinkage in x, y dimensions of the sintered body is almost negligible (image from [161]).

The sintering mechanism by which these tapes remain shrink-free is referred to as self-constrained sintering [67, 161]. In this approach (Heralock tapes from Heraeus), a three-layer-tape is formed by wet on wet ceramic slurry deposition, where the top and bottom layers contain low temperature softening glass and ceramic particles and the mid-layer is a refractory with wetting agent. Wetting agent promotes glass flow from the outer layers into the porous layer during firing. More work on the fundamentals of self-constrained sintering can be found in references [162-163].

From a general point, the techniques for zero-shrinkage LTCC sintering are developed to suppress the in-plane shrinkage in LTCC [164]. A big portion of these techniques are based on constraining the tape by using additional sacrificial layers (pressureless assisted sintering, PLAS) or by fixing the tape on a previously-sintered substrate (tape on substrate, TOS or LTCC on metal, LTCC-M) [165, 166]. Another approach is based on the application of pressure during firing and it is called pressure-assisted sintering (PAS) [164].

1.3 LTCC technology as an alternative solution for device packaging

The characteristic properties of the LTCC materials systems have been discussed so far and in this section, the advantages these properties provide for device applications will be overviewed.

1.3.1 Traditional application areas

LTCC technology was originally confined in the early 80s to the telecommunication and avionics sector, until the LTCC tapes were fully commercialized upon increasing customer demands and application areas [16-18]. Today, LTCC is the major materials system for production of advanced high-frequency components such as filters, antennas, integrated RF modules, etc., which are used in portables, cars, etc. (figure 1.16.) [11, 14, 167, 168].

Figure 1.16. A broad range of LTCC applications: from telecommunication to automotives (images from Ericson, Darfon, Epcos, DT Microcircuits Corporation).

The common requirements of such devices are high and undisturbed signal propagation speeds especially at high frequencies, faster switching, high reliability against mechanical, thermal and environmental perturbations and surely low costs [11, 14, 169-171]. These demands as a function of materials properties are briefly discussed in the following:

1.3.1.1 Dielectric constant, ε

Enhancing the speed (reducing the propagation delay time) is closely related to the improvement of the media speed and reduction of the wiring length. The material property, which controls the media speed (υ) is the dielectric constant (ε) and their relation is given by:

$$\upsilon = c / \varepsilon^{0.5}$$

Therefore, reducing the dielectric constant has a direct effect in increasing the propagation speed and thus, reducing the delay time [2, 171]. Moreover, a smart design can further reduce the wiring length by using vias effectively.

1.3.1.2 Quality factor, Q

The quality factor, Q of the dielectric media is inversely related to the transmission power loss of a wave signal ($Q = f_o / \Delta f$). The signal loss is mainly due to the conduction loss of the conductor at high frequencies, whereas it is due to the dielectric loss of the substrate at low frequencies [129]. Therefore, low loss conductors such as Ag, Au, etc. are the only choices in applications requiring low loss and high frequency.

1.3.1.3 Temperature coefficient of resonant frequency, T_f

T_f measures the shift of resonant frequency of a dielectric resonating circuit over a temperature change. The dielectric is expected to have a T_f value close to zero, so that the components in the package demonstrate stable dielectric properties under temperature fluctuations and provide high quality filtering [14].

1.3.1.4 Coefficient of thermal expansion, CTE

CTE is an important parameter as it affects the Si-based ICs attached. Therefore, the substrate is expected to exhibit CTE values close to that of Si [7, 170] in order to avoid deformations such as cracks, delaminations etc. between the substrate and the attached components due to shrinkage mismatch.

LTCC technology, which unites substrate-thick-film-co-firing and device integration processes optimally, covers most of these requirements and it is, thus, still one of the few materials system employed for fabrication of telecommunication devices.

1.3.2 Recent applications

Beside its ideal dielectric properties for devices operating at high-frequencies, LTCC offers numerous advantages for other packaging applications such as optics [172], automotives [173-175], avionics [175], MEMS (micro electro-mechanical systems) [176], microsystems [177], sensors [28, 33, 178-184], micro-fluidics [185-187], biotechnology [153, 189] etc. The versatility of applications is a consequence of the attractive features of the LTCC materials system such as ease of tape handling and structuring, high-density packaging, chemical and

thermal stability, possibility to unite electro-mechanical functions in one system, reduced cost by high-yield and low turn-around times, etc.

1.4 Structuring LTCC

Multilayer LTCC structures are usually fabricated following a well-established and straight forward procedure, as discussed previously. However, most of the devices such as MEMS, sensors, micro-fluidics, etc. possess additional features such as cavities, channels, membranes, which require utilization of more sophisticated techniques for fabrication. At this point, structuring LTCC becomes a critical issue and this plays a major role in determining the quality of fabricated structures. From a general point of view, methods to fabricate such LTCC structures depend on the final dimensions in addition to the desired device specifications [17], which can be classified as passive and active techniques.

In the former approach, LTCC sheets are machined and cavities are fabricated by stacking and laminating these layers in addition to non-machined, complete layers at the top and bottom (figure 1.17.). Therefore, structuring is facilitated by the machined tape itself, whilst lamination is the crucial step that has to be optimized to bond the LTCC layers efficiently [190-192]. However, the major problem concerning this technique is the poor lamination due to insufficiently-transmitted lamination pressure through the layers and delamination following firing (figure 1.18.). Moreover sagging is widely observed in such structures: unsupported layers sag upon lamination and glass softening over glass transition temperature [17, 195], thus, the cavity is destroyed. Although new methods to improve lamination are reported such as utilization of molds [193, 194], this approach has yet drawbacks for fabrication of a wide-range of reliable micro-fluidic devices.

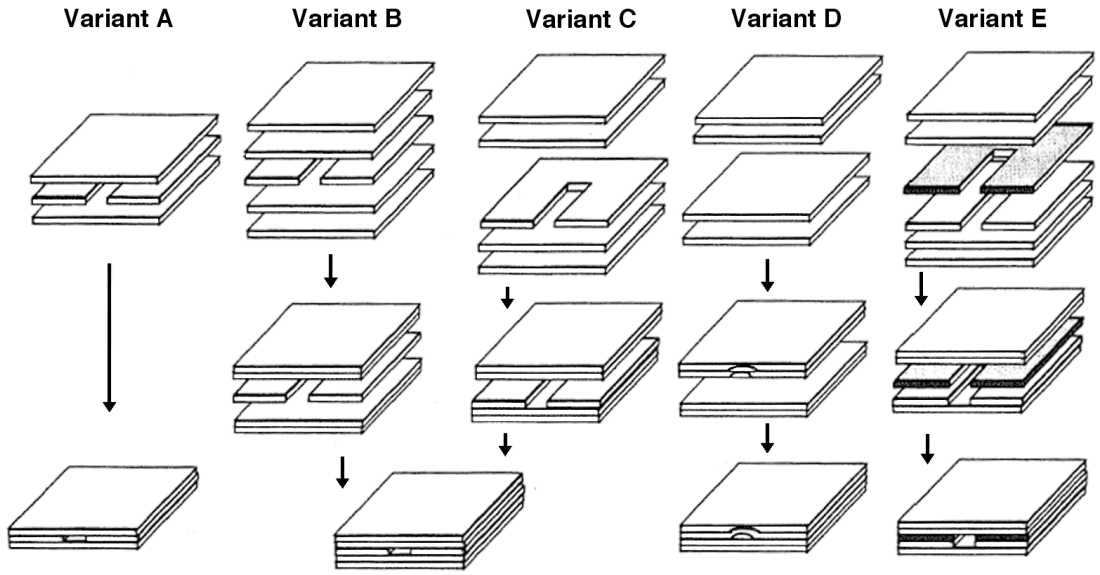

Figure 1.17. Realization of cavities in LTCC without using sacrificial material (image from [190]).

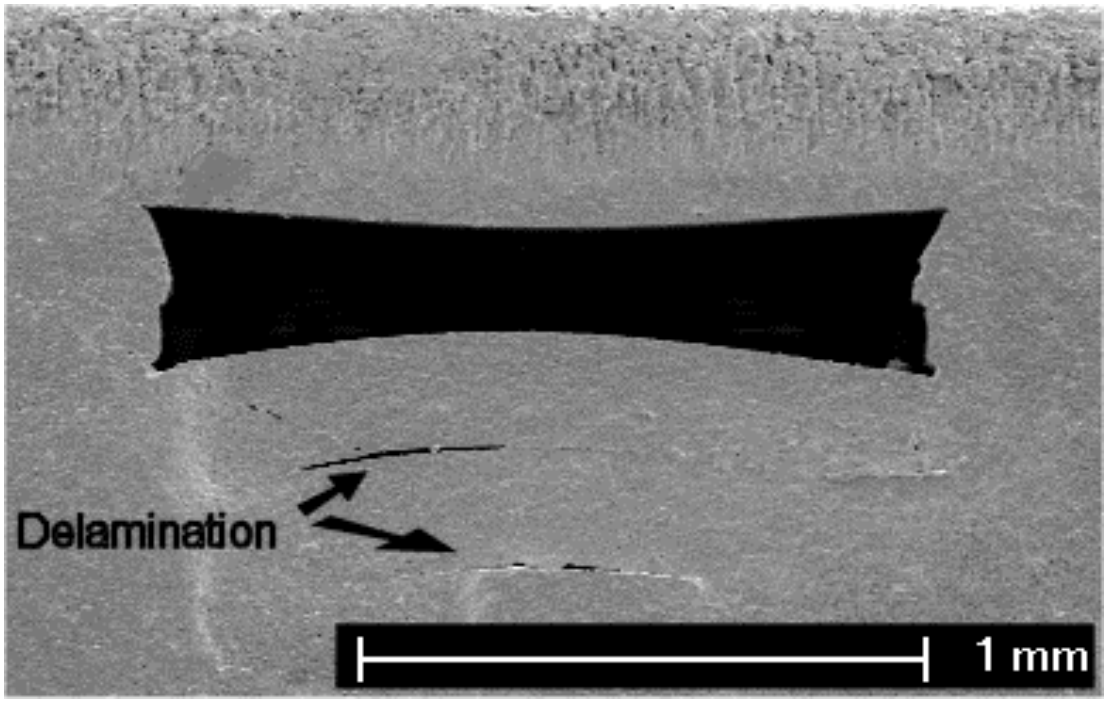

Figure 1.18. Delamination due to lack of a supporting layer = sacrificial material (image from [200]).

Active methods, on the other hand, are based on utilization of a fugitive phase that can be removed following/during firing [195-201], in addition to rarely-cited chemical processes [202]. The general requirements of a fugitive phase (sacrificial layer) are various: easy

deposition into cavities or on tapes, shrinkage-match to LTCC, chemical inertness to avoid interaction with tapes, sufficient flow ability to withstand lamination pressure, etc. [195].

The fugitive materials, independent of the functional phase, are prepared by a similar route: the functional material (the fugitive phase) is mixed with an organic vehicle to facilitate deposition on tapes, which is followed by lamination and firing. Depending on its nature, the fugitive phase is removed either following firing by etching in case of glass frit or mineral-based sacrificial pastes [195, 197] or during firing by oxidation in case of graphite-based fugitive paste, carbon tape [198-201].

1.5 Objective and construction of thesis

The starting point of thesis is based on the idea of fabricating novel, LTCC-based sensors with micro-fluidic structures, which are smartly-packaged, reliable, cost-efficient and yet with superior performance to its existing alternatives in the market. The objectives of thesis, within this perspective, can be summarized as follows:

- development of a technique based on graphite sacrificial paste, which can be screen-printed, laminated and fully-removed during firing, to support LTCC layers against sagging and delamination during processing,
- preparing and selecting the ideal paste, which should exhibit fundamental characteristics such as ideal rheology for printing, stability, etc., in a systematic way, using design of experiments,
- determining main processing parameters and understanding their nature and interrelations,
- analyzing the effects of processing parameters on selected device, which is membrane,
- evaluating the efficiency of the developed technique: device characterization

According to this outline, thesis is constructed in the following order:

Chapter 2. Background of graphite sacrificial paste

Processing and characterization of pastes

Chapter 3. Fabrication of micro-fluidic structures

Effect of processing conditions on membranes

Chapter 4. Evaluation of membranes

Structural properties, membrane displacement versus pressure

Chapter 5. Sensors based on LTCC technology

Viscosity, force, inclination sensors

Chapter 6. Summary and conclusions

Chapter 7. Future perspectives

Minerals based sacrificial pastes

References

1. R.R. Tummala, “Ceramic and glass-ceramic packaging in the 1990s”, J. Am. Ceram. Soc., 1991, 74 [5], 895-908.

2. U. Chowdhry and A.W. Sleight, “Ceramics substrates for microelectronic packaging”, Ann. Rev. Mater. Sci., 1987, 17, 323-340.

3. G. Kelly, J. Alderman, C. Lyden and J. Barrett, “Microsystem packaging: lessons from conventional low cost IC packaging”, J. Micromech. Microeng., 1997, 7, 99-103.

4. S. Al-Taei, D. Haigh and G. Passiopoulos, “Multilayer ceramic integrated circuits (MCICs) technology and passive circuit design”, Proceedings of the London Communication Symposium 2001, 10-11 September 2001, 6th Annual London Conference on Communications, 139-142.

5. “Handbook of Thick-film Technology”, Edited by K.E.G. Pitt, Electrochemical Publications Ltd., 2nd Edition, 2005, 479-480.

6. M. Jackson, M. Pecht, S.B. Lee and P. Sandborn, “Integral, embedded and buried passive technologies”, from the archive of the Calce Electronics and Products Center, 2003.

7. V.A. Chiriac and T.-Y. Tom Lee, “Thermal assessment of RF integrated LTCC front end module (FEM)”, IEEE Trans. Adv. Pack., 2004, 27 (3), 545-557.

8. R. Kulke, M. Rittweger, PO. Uhlig, C. Günner, “LTCC-multilayer ceramic for wireless and sensor applications”, 2001, IMST GmbH, paper available on: http://www.taconic-add.com/pdf/technicalarticles--ltccmultilayer.pdf.

9. R.L. Brown, A.A. Shapiro and P.W. Polinski, “The integration of passive components into MCMs using advanced low-temperature cofired ceramics”, The International Journal of Microcircuits and Electronic Packaging, 1993, 16 (4), 328-338.

10. “Thick-film Sensors”, Edited by M. Prudenziati, Elsevier, 1994, 3-32, 59-111.

11. S.X. Dai, R.-F. Huang, D.L. Wilcox, Sr., “Temperature stable, low loss and low fire dielectric for consumer wireless applications”, Proceedings of the First Chine International Conference on High-Performance Ceramics, October 1998, Beijing, 338-341.

12. P. Barnwell, W. Zhang, J. Lebowitz, K. Jones, N. MacDonald, C. Free and Z. Tian, “An investigation of the properties of LTCC materials and compatible conductors for their use in wireless applications”, Proceedings of the IMAPS International Symposium on Microelectronics, 2000, Boston, 659–664.

13. H. Jantunen, “Low temperature co-fired ceramic (LTCC) materials for telecommunication devices”, PhD thesis, Department of Electrical Engineering, University of Oulu, Finland, 2001, 15.

14. S.X. Dai, R.-F. Huang, D.L. Wilcox, Sr., “Use of titanates to achieve a temperature-stable low temperature cofired ceramic dielectric for wireless applications”, J. Amer. Ceram. Soc., 2002, 85 [4], 828-832.

15. R.L. Brown and W.R. Smith, “Embedded passive functions for RF and mixed-signal circuits”, 1997, Proceedings of the 1997 IEEE International Conference on Multichip Modules, 351-356.

16. M.R. Gongora-Rubio, “Non-packaging applications of LTCC technology”, Presentation, Conference of Pan-American Advanced Studies Institute, Micro-electro mechanical Systems, June 2004.

17. M.R. Gongora-Rubio, P. Espinoza-Vallejos, L. Sola-Laguna, J.J. Santiago-Avilés, “Overview of low temperature co-fired ceramics tape technology for meso-system technology (MsST)”, Sensor. Actuat. A-Phys., 2001, 89, 222-241.

18. S. Annas, “Advances in low temperature co-fired ceramic (LTCC) for ever increasing microelectronic applications", IEEE Elect. Comp. Tech. Conf., 2003, 1691-1693.

19. R. Bauer, K.-J. Wolter and W. Sauer, “Three dimensionally-formed thick-film devices with low temperature co-fired ceramic multilayer technology”, ISHM Proceedings, 1995, 481-486.

20. H.Teterycz, L.J.Golonka, J.Kita, R.Bauer, B.W. Licznerski, K. Nitsch and K. Wisniewski, “New design of an SnO_2 gas sensor on LTCC”, Sensor. Actuat. B-Chem., 1998, 47, 100-103.

21. L.J.Golonka, B.W. Licznerski, K. Nitsch, H. Teterycz, R. Bauer and K.J. Wolter, “Examples of gas sensors by application of thick-film technology”, Proceedings of the 43rd International Scientific Colloquium, TU Ilmenau, 1998, 465-470.

22. M.G-Rubio, L.S.-Laguna, M. Smith and J.J.S.-Aviles, “LTCC technology multilayer eddy-current proximity sensor for harsh environments”, Proceedings of the International Symposium on Microelectronics, 1999, 676-681.

23. M.G-Rubio, L.M.S-Laguna, P.J. Moffett and J.J.S-Aviles, “The utilization of LTCC-ML technology for meso-scale EMS, a simple thermistor based flow sensor”, Sensor. Actuat. A-Phys., 1999, 73, 215-221.

24. H. Lynch, J.Park, P.A.E-Valejos, J.J. S-Aviles and L.S-Laguna, “Meso-scale pressure transducers utilizing LTCC tapes”, Proceedings of the Materials Research Society Symposium, 1999, 546, 177-182.

25. M.A. Fonseca, J.M. English, M. von Arx and M.G.Allen “High-temperature characterization of ceramic pressure sensors”, Proceedings of the 11th International Conference on Solid-State Sensors and Actuators, Eurosensors XV, Digest of Technical Papers, 2001, 1, 486-489.

26. T. Thelemann, H. Thust and M. Hintz, “Using LTCC for microsystems”, Microelectrocnics International, 2002, 19, 19-23.

27. R.A. Blechschmidt-Trapp, O. Hohlfeld, R. Muller and R. Werthschutzky, “Piezoresistive sensors for medical applications exemplified by a probe for measure pressure in the rectum”, Biomed. Tech. (Berl)., 2002, 47 (3), 43-47.

28. T. Pisarkiewicz, A. Sutor, P. Potempa, W. Maziarz, H. Thust and T. Thelemann, “Microsensor based on low temperature cofired ceramics and gas sensitive thin-film”, Thin Solid Films, 2003, 436, 84-89.

29. W.K. Jones, Y. Liu and M. Gao, “Micro heat pipes in low temperature cofire ceramic (LTCC) substrates”, IEEE T. Compon. Pack. Manuf. Technol., 2003, 26 (3), 110-115.

30. K.A. Peterson, S.B. Rohde, T.S. Turner, R. Stokes and A. Casias, “Novel structures in ceramic interconnect technology”, Proceedings of the Ceramic Interconnect Technology Conference, 2003, 223-228.

31. T.Y. Tsai, N.H. Tai and I.N. Lin, “Characteristics of nanotube electron field emission devices prepared by LTCC process”, Diam. Relat. Mater., 2004, 13, 982-986.

32. K.A. Peterson, K.D. Patel, C.K. Ho, S.B. Rohde, C.D. Nordquist, C.A. Walker, B.D. Wroblewski and M. Okandan, “Novel microsystem applications with new techniques in low temperature co-fired ceramics”, Int. J. Appl. Ceram. Technol., 2005, 2 (5), 345-363.

33. K.L. Zhang, S.K. Chou and S.S. Ang, “Development of a low-temperature co-fired ceramic solid propellant microthruster”, J. Micromech. Microeng., 2005, 15, 944-952.

34. L.J. Golonka, H. Roguszczak, T. Zawada, J. Radojewski, I. Grabowskab, M. Chudy, A. Dybko, Z. Brzozka and D. Stadnik, “LTCC based microfluidic system with optical detection”, Sensor. Actuat. B-Chem., 2005, 111-112, 396-402.

35. Report from: http://www.imaps.org/cii/cii_roadmap_2002.pdf.

36. “Ceramic Materials for Eelectronics”, Edited by R.C. Buchanan, 2nd edition, Marcel Dekker, 1991, Chapter 9: Multilayer Ceramic Technology, 488-526.

37. M. Eberstein and W.A. Schiller, “Development of high-permittivity glasses for microwave LTCC tapes”, Glass Sci. Technol., 2003, 76 (1), 8-16.

38. S.F. Wang, J.P. Dougherty, W. Huebner and J.G. Peppin, “Silver-palladium thick-film conductors”, J. Am. Ceram. Soc., 1994, 77 (12), 3051-3072.

39. J.H. Jean and C.R. Chang, “Camber development during cofiring Ag-based low-dielectric constant ceramic package”, J. Mater. Res., 1997, 12 (10), 2743-2750.

40. J.G. Peppin, “Subsolidus phase relations in the system Pd-Ag-O and application to multilayer ceramic capacitor electrodes”, Adv. Ceram. Mater., 1988, 3 (5), 517-319.

41. S.F. Wang and W. Huebner, “Thermodynamic modeling of equilibrium subsolidus phase relations in the Ag-Pd-O_2 system”, J. Am. Ceram. Soc., 1991, 74 (6), 1349-1353.

42. S.F. Wang, W. Huebner and C.Y. Huang, “Correlation of subsolidus phase relations in the Ag-Pd-O system to oxidation reduction kinetics and dilatometric behavior”, J. Am. Ceram. Soc., 1992, 75 (8), 2232-2239.

43. S.F. Wang and W. Huebner, “Interaction of Ag/Pd metallization with lead and bismuth oxide-based fluxes in multilayer ceramic capacitors”, J. Am. Ceram. Soc., 1992, 75 (9), 2339-2352.

44. T. Garino and M. Rodriguez, “Behavior of silver and palladium mixtures during heating”, J. Am. Ceram. Soc., 2000, 83 (11), 2709-2714.

45. M. Valant and D. Suvorov, “Chemical compatibility between silver electrodes and low-firing binary-oxide compounds: conceptual study”, J. Am. Ceram. Soc., 2000, 83 (11), 2721-2729.

46. W.A. Vitriol and J.I. Steinberg, “Development of a low temperature cofired multilayer ceramic technology”, Proceedings of the International Symposium on Microelectronics, ISHM 1983, 593-598.

47. R.G. Pond and W.A. Vitriol, “Custom packaging in a thick-film house using low temperature cofired multilayer ceramic technology”, Proceedings of the International Symposium on Microelectronics, ISHM 1984, 268-271.

48. Y. Shimada, K. Utsumi, M. Suzuki, H. Takamiza, M. Nitta and T. Watari, “Low firing temperature multilayer glass-ceramic substrate”, IEEE T. Compon. Hybr., 1983, CHMT-6 (4), 382-388.

49. “Glasses and Glass-Ceramics”, Edited by M.H. Lewis, Chapman and Hall, 1989, 226-271.

50. “Glass-Ceramic Materials”, Z. Strnad, Elsevier, 1986, 9-10, 114-127.

51. “Thick-film Sensors”, Edited by M. Prudenziati, Elsevier, 1994, 59-71.

52. “Introduction to the Principles of Ceramic Processing”, J.S. Reed, John Wiley and Sons, 1995, 255-276.

53. F.F. Lange, “Powder processing science and technology for increased reliability”, J. Am. Ceram. Soc., 1989, 72 (1), 3-15.

54. J. A. Lewis, “Colloidal processing of ceramics”, J.A. Lewis, J. Am. Ceram. Soc., 2000, 83 (10), 2341-2359.

55. R.G. Horn, “Surface forces and their action in ceramic materials”, J. Am. Ceram. Soc., 1990, 73 (5), 1117-1135.

56. R.E. Mistler, “Tape casting: past, present, potential”, Am. Ceram. Soc. Bull., October 1998, 82-265.

57. “Materials Science and Technology, A Comprehensive Treatment, 17A, Processing of Ceramics”, Edited by R.J. Brook, John Wiley and Sons, 1996, “Tape casting”, by H. Hellebrand, 190-260.

58. S.F. Wang, W. Huebner and J.P. Dougherty JP, “Correlation of wettability and interfacial reaction to the densification and dielectric properties of fluxed- BaTiO3”, Proceedings of the Ninth IEEE International Symposium on Applications of Ferroelectrics, August 1994, University Park, PA, USA, 581-584.

59. X. Kuang, G. Carotenuto and L. Nicolais, “A review of ceramic sintering and suggestions on reducing sintering temperatures”, Adv. Perform. Mater., 1997, 4, 257-274.

60. H. Jantunen, R. Rautioaho, A. Uusimäki and S. Leppävuori, „Compositions of $MgTiO_3$-$CaTiO_3$ ceramic with two borosilicate glasses for LTCC technology”, J. Eur. Ceram. Soc., 2000, 20, 2331-2336.

61. H. Jantunen, R. Rautioaho, A. Uusimäki and S. Leppävuori, „Compositions of $MgTiO_3$-$CaTiO_3$ ceramic with two borosilicate glasses for LTCC technology”, J. Am. Ceram. Soc., 2000, 83 (11), 2855-2857.

62. A. Mohanram, “Co-sintering of integrated ceramics: fundamentals, observations and design guidelines” PhD thesis, Department of Materials Science and Engineering, The Pennsylvania University, Pennsylvania, 2005, 8-12.

63. W.S. Hackenberger, T.R. Shrout, J.P. Dougherty and R.F. Speyer, “Real time observations of LTCC substrate and conductor materials”, ISHM’92 Proceedings, 1992, 82-87.

64. W.S. Hackenberger, T.R. Shrout, J.P. Dougherty and R.F. Speyer, “Sintering phenomena and microstructural development in LTCC multilayer substrates”, ISHM’93 Proceedings, 1993, 215-220.

65. J.H. Jean and T.K. Gupta, “Liquid-phase sintering in the glass-cordierite system”, J. Mater. Sci., 1992, 27 (6), 1575-1584.

66. T. Rabe, M. Gemeinert and W.A. Schiller, “Development of advanced low temperature co-fired ceramics (LTCC) ”, Key Eng. Mat., 2004, 264-268, 1181-1184.

67. T. Rabe and W.A. Schiller, “Zero shrinkage of LTCC by self-constrained sintering”, Proceedings of the Ceramic Interconnect and Ceramic Microsystems Technologies (CICMT), 2005.

68. H. Jantunen, A. Uusimäki, S. Leppävuori and R. Rautioaho, “Effect of processing route on thermomechanical properties of low temperature firing ceramic for electronic packaging”, Brit. Ceram. T., 2002, 101 (1), 22-24.

69. US Patent, US4536535, “Castable ceramic compositions”.

70. C.L. Lo, J.G. Duh, B.S. Chiou and W.H. Lee, “Low-Temperature Sintering and Microwave Dielectric Properties of Anorthite-Based Glass-Ceramics”, J. Am. Ceram. Soc., 2002, 85 (9), 2230-2235.

71. Y.Q. Wang, M.B. Tian, D.F. Zheng, M. Suehiro and S.I. Ogura, “Influence of particle size on densification and abnormal expansion of LTCC multilayer substrate”, Brit. Ceram. T., 2002, 101 (2), 75-77.

72. S. Nishigaki and J. Fukuta, “Low-temperature, cofirable, multilayered ceramics bearing pure-Ag conductors and their sintering behavior”, Adv. Ceram., 1989, 26, 199-215.

73. C. Yong, et.al., International Publication Number of the patent, WO 03/101902 A1, “LTCC tape composition”.

74. “Materials Science and Technology, A Comprehensive Treatment, 17A, Processing of Ceramics”, Edited by R.J. Brook, John Wiley and Sons, 1996, “Tape casting”, by H. Hellebrand, 217-221.

75. L.S. Chen, S.L. Fu and W.K. Huang, “Effect of binder content on shrinkage behavior of a multilayered ceramic substarte”, Jpn. J. Appl. Phys., 2000, 39, 5209-5210.

76. D.H. Yoon and B.I. Lee, “Processing of barium titanate tapes with different binders for MLCC applications-Part I: Optimization using design of experiments”, J. Eur. Ceram. Soc., 2004, 24, 739-752.

77. S. Mei, J. Yang, X. Xu, S. Quaresma, S. Agathopoulos and J.M.F. Ferreira, “Aqueous tape casting of low dielectric cosntant cordierite-based glass ceramics-selection of binder”, J. Eur. Ceram. Soc., 2006, 26, 67-71.

78. R. Moreno, “The role of slip additives in tape-casting technology: Part I - Solvents and dispersants”, Am. Ceram. Soc. Bull., 1992, 71 (10), 1521-1531.

79. R. Moreno, “The role of slip additives in tape-casting technology: Part II – Binders and plasticizers”, Am. Ceram. Soc. Bull., 1992, 71 (11), 1647-1657.

80. K.S. Chou and L.J. Lee, “Effect of dispersants on the rheological properties and slip casting of concentrated alumina slurry”, J. Am. Ceram. Soc., 1989, 72 (9), 1622-1627.

81. “Thick-film Sensors”, Edited by M. Prudenziati, Elsevier, 1994, 3-32, 113-116.

82. “Ceramic Powder Science II”, Edited by G.L. Messing, Ceramic Transactions, 1988, 1 (A-B), “Basic requirements for tape casting of ceramic powders” by A. Roosen, 675-692.

83. J. Kiennemann, T. Chartier, C. Pagnoux, J.F. Baumard, M. Huger and J.M. Lamérant, “Drying mechanisms and stress development in aqueous alumina tape casting”, J. Eur. Ceram. Soc., 2005, 25, 1551-1564.

84. M. Schmidt, H. Münstedt, M. Svec, A. Roosen, T. Betz and F. Koppe, “Local flow behavior of ceramic slurries in tape casting,as investigated by laser-doppler velocimetry”, J. Am. Ceram. Soc., 2002, 85 (2), 314-320.

85. W.K. Jones, Y. Liu, B. Larsen, P. Wang and M. Zampino, “Chemical, structural and mechanical properties of LTCC tapes”, Internacional Symposium on Microelectronics, 2000, 669-674.

86. A. Dziedzic, L.J. Golonka, J. Kita, and J.M. Kozlowski, ‘‘Macro- and Microstructure of LTCC Tapes and Components,’’ Proceedings of the International Microelectronics and Packaging Society, IMAPS Poland, 2000, 163-168.

87. A.A. Shapiro, D.F. Elwell, P. Imamura and M.L. MeCartney, “Structure-Property relationships in low temperature co-fired ceramic2, ISHM Proceedings, 1994, 306-311.

88. http://www.ltcc.de/en/whatis_mat.php

89. 2004 IMAPS-CII / iNEMI Technology Roadmaps

90. “Thick-film Sensors”, Edited by M. Prudenziati, Elsevier, 1994, 73-84.

91. M. Prudenziati, B. Morten, P. Savigni and G. Guizzetti, “Influence of the preparing conditions on the physicochemical characteristics of glasses for thick-film hybrid microelectronics”, J. Mater. Res., 1994, 9 (9), 2304-2313.

92. B.E. Taylor, J.F. Felten and J.R. Larry, “Progress in and technology of low-cost silver containing thick-film conductors”, IEEE T Compon. Hybr., 1980, CHMT-3 (4), 504-517.

93. Y. Wang, Y. Liu, J. Ma, Z. Dong and M. Yin, „Preparation and sintering behavior of Au conductor pastes for LTCC substrate”, Mater. Sci. Forum., 475-479, 1763-1766.

94. Z. Liu and D.D.L. Chung, “Development of glass-gfree metal electrically conductive thick films”, Transactions of ASME, J. Electron. Packaging., 2001, 123 (3), 64-69.

95. C. Lopez, L. Chai, A. Shaikh and V. Stygar, “Wire bonding characteristics of gold conductors for low temperature co-fired ceramic applications”, Microelectron. Reliab., 2004, 44 (2), 287-294.

96. R. Rautioaho, O. Nousiainen, S. Leppävuori, J. Lenkkeri and T. Jaakola, “Thermal fatigue in solder joints of Ag-Pd and Ag-Pt metallized LTCC modules”, Microelectron. Reliab., 2001, 41, 1643-1648.

97. “Thick-film Sensors”, Edited by M. Prudenziati, Elsevier, 1994, 85-97.

98. A. Alessandrini, G. Valdre, B. Morten and M. Prudenziati, “Electric for ce microscopy investigation of the microstructure of thick-film resistors”, J. Appl. Phys., 2002, 92 (8), 4705-4711.

99. A. Dziedzic, L.J. Golonka, B.W. Licznerski and G. Hielscher, “Heaters for gas sesnors from thick conductive or resistive films”, Sensor. Actuat. B-Chem., 1994, 18-19, 535-539.

100. R. Schmidt, A. Stiegelschmitt, A. Roosen and A.W. Brinkman, “Preparation and Performance of thick film NTC thermistors”, Key Eng. Mat., 2002, 206-213, 1417-1420.

101. A. Dziedzic, L.J. Golonka, B.W. Licznerski, J. Kozlowski, B.W. Licnerski and K. Nitsch, “Thick-film resistive temperature sensors”, Meas. Sci. Technol., 1997, 8, 78-85.

102. K. Delaney, J. Barrett, J. Barton and R. Doyle, “Characterization and performance prediction for integral resistors in low temperature co-fired ceramic technology”, IEEE Tran. Adv. Pack., 1999, 22 (1), 78-85.

103. J. Zhong and H.H. Bau, “Thick-film thermistors printed on LTCC tapes”, A. Ceram. Soc. Bull., 80 (10), 39-42.

104. M. Hrovat, D. Belavic, A. Bencan, J. Bernard, J. Holc, J. Cilensek, W. Smetana, H. Homolka, R. Reicher, L. Golonka, A. Dziedzic and J. Kita, “Thick-film resistors on various

substrates as sensing elements for strain-gauge applications", Sensor. Actuat. A-Phys., 2003, 107, 261-272.

105. S. Vionnet-Menot, "Low firing temperature thick-film piezoresistive composites – properties and conduction mechanism", PhD thesis, Department of Micro- Engineering, Swiss Federal Institute of Technology, Lausanne (EPFL), Switzerland, 2005.

106. G.E. Pike and C.H. Seager, "Electrical properties and conduction mechanisms of Ru-based thick-film (cermet) resistors", J. Appl. Phys., 1977, 48 (12), 5152-5169.

107. C. Canali, D. Malavasi, B. Morten, M. Prudenziati and A. Taroni, "Piezoresistive effects in thick-film resistors", J. Appl. Phys., 1980, 51 (6), 3282-3288.

108. R.W. Vest, "A model for sheet resistivity of RuO2 thick-film resistors", IEEE T. Compon. Hybr., 1991, 14 (2), 396-406.

109. B. Morten, A. Masoero, M. Prudenziati and T. Manfredini, "Evolution of ruthenate-based thick film cermet resistors", J. Phys. D: Appl. Phys., 1994, 27 (10), 2227-2235.

110. Y.M. Chiang, L.A. Silverman, R.H. French and R.M. Cannon, "Thin glass film between ultrafine conductor particles in thick-film resistors", J. Am. Ceram. Soc., 1994, 77 (5), 1143-1152.

111. K. Adachi and H. Kuno, "Decomposition of ruthenium oxides in lead borosilicate glass", J. Am. Ceram. Soc., 1997, 80 (5), 1055-1064.

112. K. Adachi and H. Kuno, "Effect of glass composition on the electrical properties of thick-film resistors", J. Am. Ceram. Soc., 2000, 83 (10), 2441-2448.

113. J. Alexander, "Cofirable resistors for low temperature ceramic tape", ISHM Proceedings, 1993, 204-208.

114. http://www2.dupont.com/MCM/en_US/products/green_tape/green_tape_951.html.

115. J. Kita, A. Dziedzic, L.J. Golonka and T. Zawada, "Laser treatment of LTCC for 3D structures and elements fabrication", Microelectronics International, 2002, 19 (3), 14-18.

116. Y. Fournier, L.S. Bieri, T. Maeder and P. Ryser, "Influence of lamination parameters on LTCC shrinkage under unconstrained sintering", Proceedings of the 4th European Microelectronics and Packaging Symposium, 2006, 165-170.

117. "Thick-film Sensors", Edited by M. Prudenziati, Elsevier, 1994, 3-33.

118. "Ceramic Films and Coatings (Materials Science and Process Technology", Edited by J.B. Wachtman and R.A. Haber, Noyes Publications, 1993, "Electronic thick-film technology", by D.J. Shanefield, 284-299.

119. M. A. Piwonski and A. Roosen, “Low pressure lamination of ceramic green tapes by gluing at room temperature”, J. Europ. Ceram. Soc., 1999, 19, 263-270.

120. A. Roosen, “Low-temperature/low pressure lamination of green ceramic tapes”, Adv. Eng. Mater., 2000, 2 (6), 374-376.

121. A. Roosen, “New lamination technique to join ceramic green tapes for the manufacturing of multilayer devices”, J. Eur. Ceram. Soc., 2001, 21, 1993-1996.

122. A. Roosen and K. Schindler, “Cold low pressure lamination of ceramic green tapes”, Proceedings of the 2005 IMAPS Conference on Ceramic Interconnect Technology, June 2005.

123. D. Couto, L. Schwegler and A. Roosen, “Cold low pressure lamination of metallized ceramic green tapes”, Proceedings of the 2004 IMAPS Conference on Ceramic Interconnect Technology, June 2004, 238-242.

124. M.J. Cima, J.A. Lewis and A.D. Devoe, “Binder distribution in ceramic greenware during thermolysis”, J. Am. Ceram. Soc., 1989, 72 (7), 1192-1199.

125. P. Calvert and M. Cima, “Theoretical models for binder burnout”, J. Am. Ceram. Soc., 1990, 73 (3), 575-579.

126. D. Schultze and W.A. Schiller, “Burnout of organic components of glass ceramic composite tapes”, J. Thermal. Anal., 1998, 52, 211-219.

127. S.J. Lombardo and Z.C. Feng, “Determination of the minimum time for binder removal and optimum geometry for three-dimensional porous green bodies”, J. Am. Ceram. Soc., 2003, 86 (12), 2087-2092.

128. R.C. Sutterlin, G.O. Dayton and J.V. Biggers, “Thick-film resistor/dielectric interactions in a low temperature co-fired ceramic package”, IEEE T. Compon. Pack. B., 1995, 18 (2), 346-351.

129. K.B. Shim, N.T. Cho and S.W. Lee, “Silver diffusion and microstructure in LTCC multilayer couplers for high frequency applications”, J. Mater. Sci., 2000, 35 (4), 813-820.

130. J.H. Jean and C.R. Chang, “Cofiring kinetics of an Ag-metallized ceramic-filled glass electronic package”, J. Am. Ceram. Soc., 1997, 80 (12), 3084-3092.

131. S.F. Wang and W. Huebner, “Interaction of silver/palladium electrodes with lead-and bismuth-based electrocermaics”, J. Am. Ceram. Soc., 1993, 76 (2), 474-480.

132. R. Zuo, L. Ti, Z.Gui, X. Hu and C. Ji, “Effects of additives on the interfacial microstructure of cofired electrode-ceramic multilayer systems”, J. Am. Ceram. Soc., 2002, 85 (4), 787-793.

133. T. Martin and D. Schroeder, “Reliability analysis of LTCC MCM’s utilizing silver conductives”, ISHM’94 Proceedings, 1994, 295-300.

134. C.J. Ting, C.S. His and H.Y. Lu, “Interactions between ruthenia-based resistors and corderite-glass substrates in low-temperature co-fired ceramics”, J. Am. Ceram. Soc., 2000, 83 (12), 2945-2953.

135. T. Nakano, T. Iizuka, T. Takada and T. Yamaguchi, “Glass/substrate interaction in model RuO5-glass double layer thick films”, J. Am. Ceram. Soc., 1995, 78 (6), 1705-1707.

136. T. Yamaguchi and K. Iizuka, “Microstructure development in RuO2-glass thick-film resistors and its effect on the electrical resistivity”, J. Am. Ceram. Soc., 1990, 73 (7), 1953-1957.

137. C.S. Hsi and M.W. Lee, “Properties of ruthenia-based resistors embedded in low-temperature co-firable ceramic substrates”, Jpn. J. Appl. Phys., 2002, 41 (8), 5323-5328.

138. P.Yang, M.A.Rodriguez, P.Kotula, B.K.Miera and D.Dimos, “Processing, microstructure and electric properties of buried resistors in low-temperature co-fired ceramics”, J. Appl. Phys., 2001, 89 (7), 4175-4182.

139. M.A. Rodriguez, P. Yang, P. Kotula and D. Dimos, “Microstructure and phase development of buried resistors in low temperatura co-fired ceramic”, J. Electroceram., 2000, 5 (3), 217-223.

140. C.S. His, D.F. Chen, F.M. Shieh and S.L. Fu, “Processing of LTCC with embedded RuO_2-based resistors”, Mater. Chem. Phys., 2002, 78, 67-72.

141. H. Thust, K.H. Drüe, T. Kirchner, T. Thelemann and E.K. Polzer, “Behavior and performance of buried resistors in green tape”, Applied Microwave and Wireless, 1999, 11 (10), 30-36.

142. H. Birol, T. Maeder, C. Jacq and P. Ryser, “Investigation of interactions between co-fired LTCC components”, J. Eur. Ceram. Soc., 2005, 25, 2065-2069.

143. H. Birol, T. Maeder and P. Ryser, “Influence of processing and conduction materials on properties of co-fired resistors in LTCC structures”, J. Eur. Ceram. Soc., 2006, 26, 1937-1941.

144. H. Birol, T. Maeder and P. Ryser, "Materials compatibility issues in ltcc technology and their effects on structural and electrical properties", Proceedings of the 1st CICMT Conference on Ceramic Interconnect Technology, April 2005, Baltimore, 300-309.

145. A. Dziedzic, “Electrical and structural investigations in reliability characterization of modern passives and passive integrated components”, Microelectron. Reliab., 2002, 42 (4-5), 709-719.

146. A. Dziedzic, L.J. Golonka, J. Kita, H. Thust, K.H. Drüe, R. Bauer, L. Rebenklau and K.J. Wolter, “Electrical and and stability properties and ultrasonic microscope characterization of low temperature co-fired ceramics resistors”, Microelectron. Relaib., 2001, 41 (5), 669-676.

147. G.Q. Lu, R.C. Sutterlin and T.K. Gupta, “Effect of mismatched sintering kinetics on camber in a low-temperature cofired ceramic package”, J. Am. Ceram. Soc., 1993, 76 (8), 1907-1914.

148. M. Wagner, A. Roosen, A. Stiegelschmitt, D. Schwanke and F. Bechtold, “In-situ shrinkage measurements of LTCC multilayers by means of an optical dilatometer”, Key Eng. Mater., 2002, 206-213, 1281-1284.

149. S.H. Lee, G.L. Messing and D.J. Green, “Warpage evolution of screen printed multilayer ceramics during co-firing”, Key Eng. Mater., 2004, 264-268, 321-330.

150. A. Roosen and M. Wagner, “Characterization of the shrinkage behavior of pure, screen printed thick film pastes and LTCC green tapes”, Proceedings of the International Microelectronics and Packaging Society (IMAPS-CTI) Meeting, 2004, Denver.

151. M. Valant and D. Suvorov, “Glass-free low-temperature cofired ceramics: calcium germanates, silicates and tellurates”, J. Eur. Cer. Soc., 2004, 24, 1715-1719.

152. M. Valant and D. Suvorov, “Microstructural phenomana in low-firing ceramic”, Mater. Chem. Phys., 2002, 9528, 1-7.

153. A. Roosen, “Materials process and manufacturing: current and future directions”, Proceedings of the 1st CICMT Conference, 2005, Baltimore.

154. P.C. Donohue, B.E. Taylor, D.I. Amey, R.R. Draudt, M.A. Smith, S.J. Horowitz and J.R. Larry, “A new low loss lead free LTCC system for wireless and RF applications”, Proceedings of the IEEE International Conference on Multichip Modules and High Density Packaging, 1998, 196-199.

155. Y.S. Cho, K.W. Hang, M.F. Barker, P.J. Olivier, C.B. Wang, D.I. Amey, K. Souders and C.R. Needes, “New Pb-free system for automotive and telecommunication applications”, Proceedings of the Ceramic Interconnect Technology Conference, Denver, 2004.

156. US Patent, US6844278, “Dense lead-free glass ceramic for electronic devices”.

157. M. Fukaya, T. Matsuo, S. Nishigaki and C. Higuchi, “Highly reliable and lead (Pb) free thick film resistor paste system for low thermal expansion LTCC application”, Proceedings of the 1997 International Symposium on Microelectronics, 1997, 65-71.

158. http://www.wc-heraeus.com/wch2/dach/e_wch_home.nsf/$pages/news_heralock

159. Heraeus, Design Guidelines for LTCC, HeraLock HL2000 Materials System.

160. F. Lautzenhiser and E. Amaya, “HeraLockTM 2000 self-constrained LTCC tape”, Proceedings of the IMAPS 2002 Meeting, 2002, Rhode Island.

161. T. Rabe, W.A. Schiller, T. Hochheimer, C. Modes and A. Kipka, “Zero shrinkage of LTCC by self-constrained sintering”, Int. J. Appl. Ceram. Technol., 2005, 2 (5), 374-382.

162. A. Kipka, C. Modes, Q. Reynolds, M. Neidert, S. Malkmus and F. Gora, „Self-constrianed sintering LTCC – A reliable solution for automative electronic application“, Proceedings of the 1st CICMT Conference, 2005, Baltimore.

163. J.C. Chang ad J.H. Jean, “Self-constrained sintering of mixed low-temperature-cofired ceramic laminates”, J. Am. Ceram. Soc., 2006, 89 (3), 829-835.

164. A. Mohanram, S.H. Lee, G.L. Messing and D.J. Green, “Constrained sintering of mixed low-temperature co-fired ceramic”, J. Am. Ceram. Soc., 2006, 89 (6), 1923-1929.

165. M. Itagaki, K. Miura, Y. Hakotani, S. Yuhaku, Y. Bessho, S. Nakatani, M. Tsukamoto, T. Ishida and H. Nishikawa, “Zero X-Y shrinkage multilayered ceramic substrate”, Proceedings of the ISHM’93 Conference, 1993, 221-225.

166. M. Hintz, R. Perrone and H. thust, “Bulk materials in LTCC multilayers”, Proceedings of the 1st CICMT Conference, 2005, Baltimore.

167. T. Tick, J. Mähönen and H. Jantunen, “Ongoing developments in the LTCC technology beneficial for high-frequency components with advanced performance”, Proceedings of the 2004 Annual Meeting of the Chinese Materials Society, Multilayer Ceramic Devices Section, 2004, Hsin-Chu, Taiwan.

168. L. Devlin, G. Pearson and J. Pittock, “RF and microwave component development in LTCC”, http://www.cmac.com/mt/LTCC_IMN.pdf.

169. D.L. Wilcox, R.F. Huang and D. Anderson, “The multilayer ceramic integrated circuit (MCIC) technology: Opportunities and challenges”, Proceedings of the 1997 ISHM Meeting, 1997, 17-23.

170. C.L. Lo, J.G. Duh, B.S. Chiou and W.H. Lee, “Low-temperature sintering and microwave dielectric properties of anorthite-based glass-ceramics”, J. Am. Ceram. Soc., 2002, 85 (9), 2230-2235.

171. J.H. Jean and T.K. Gupta, “Design of low dielectric glass+ceramics for multilayer ceramic substarte”, IEEE T. Compon. Pack. B, 1994, 17 (2), 228-233.

172. S.J. Horowitz, “Ceramic technologies for multigigabit opto-electronic packaging”, Presented at Multi-GigaBit Opto Electronics Meeting, 2001.

173. D. Anderson, “Trends in LTCC Processing”, Proceedings of the 2003 Ceramic Interconnect Technology Conference, 2003, 165-170.

174. S. Nishigaki, U. Goebel and W. Roethlingshoefer, “LTCC (LFC) material systems and its application in automotive ECU’s”, Proceedings of the IMAPS 2004 Meeting, 2004, Denver, 1-7.

175. U. Schmid, H. Seidel and T. Becker, “Miniaturized sensor elements based on LTCC technology for automotive and airborne applications”, Proceedings of the Ceramic Interconnect Technology Conference, 2005, Denver.

176. P.K. Khanna, B. Hornbostel, T. Jäger and W. Schäfer, “MEMS and Microsystems based on low-temperature cofired ceramics: A cost analysis”, VDI/VDE- Technologiezentrum Informationstechnik, MST News (Germany), 2004, 4, 40-41.

177. K.A. Peterson, K.D. Patel, C.K. Ho, S.B. Rohde, C.D. Nordquist, C.A. Walker, B.D. Wroblewski and M. Okandan, “Novel microsystem applications with new techniques in LTCC”, Proceedings of the Ceramic Interconnect Technology Conference, 2005, Denver.

178. Y. Lai, “Eddy current displacement sensor with LTCC technology” PhD thesis, Department of Materials Sciences, Albert-Ludwigs University, Freiburg, Germany, 2005.

179. P.K. Khanna, B. Hornbostel, R. Grimme, W. Schäfer and J. Dorner, “Miniature pressure sensor and micromachined actuator structure based on low-temperature co-fired ceramics and piezoelectric material”, Mater. Chem. Phys., 2004, 87, 173-178.

180. J. Li and G.K. Ananthasuresh, “Three-dimensional low-temperature co-fired ceramic shells for miniature systems applications”, J. Micromech. Microeng., 2002, 12, 198-203.

181. M.R. Gongora-Rubio, S.T. Kofuji, A.C. Seabra, E.M. Hernandez, E.W. Simoes, M.B.A. Fontes and P.B. Verdonck, “LTCC sensors for environmental monitoring system”, Proceedings of the Ceramic Interconnect Technology Conference, 2005, Denver.

182. T. Voss, P. Gründler, A. Kribs and G.U. Flechsig, „Temperature pulse voltammetry: hot layer electrodes made by LTCC technology", Electrochem. Commun., 1999, 1, 383-388.

183. M. Hrovat, D. Belavic, A. Bencan, J. Kita, J. Holc, J. Cilensek, L. Golonka and A. Dziedzic, "Thick-film temperature sensors on alumina and LTCC substrates", J. Eur. Ceram. Soc., 2005, 25, 3443-3450.

184. R. Bauer, K.J. Wolter and W. Sauer, "Three-dimensionally formed thick film devices with low temperature cofiring ceramic multilayer technology", ISHM'95 Proceedings, 1995, 481-486.

185. R.E.B. Leminski, E.W. Simoes, R. Furlan, M.R. Gongora-Rubio, Z.M. Rocha, M.R. Cunha, I. Ramos, N.I. Norimoto and J.J. Santiago-Aviles, "Development of microfluidic devices using LTCC substrates", Proceedings of the IMAPS 2004 Meeting, 2004, Denver.

186. L.J. Golonka, T. Zawada, J. Radojewski, H. Roguszczak and M. Stefanow, "LTCC microfluidic system", Proceedings of the IMAPS 2004 Meeting, 2004, Denver.

187. J. Youngsman, A. Moll, D.G. Plumlee and M. Schimpf, "Mini- and micro-channel devices in LTCC", Proceedings of the IMAPS 2004 Meeting, 2004, Denver.

188. L. Rebenklau, K.J. Wolter and S. Howitz, "Realization of microfluidic modules using standard LTCC process", Proceedings of the IEEE Electronic Components and Technology Conference, 2000, 1696-1700.

189. P.K. Khanna, B. Hornbostel, M. Burgard, W. Schäfer and J. Dorner, "Studies on three-dimensional moulding, bonding and assembling of low-temperature cofired ceramics for MEMS and MSt applications", Mater. Chem. Phys., 2005, 89, 72-79.

190. R. Bauer, M. Luniak, L. Rebenklau, K.J. Wolter and W. Sauer, "Realization of LTCC-multilayer with special cavity applications", Proceedings of the 1997 International Symposium on Microelectronics, 1997, 659-664.

191. E.G. Palmer and C.M. Newton, "3-D Packaging using low-temperature cofired ceramic (LTCC)", The International Journal of Microcircuits and Electronic Packaging, 1993, 16 (4), 279-284.

192. H. Birol, T. Maeder and P. Ryser, "Low temperature co-fired ceramic (LTCC) technology: General processing aspects and 3-D structuration for fabrication of micro-fluidic devices", Proceedings of the 4th International Conference on Science, Technology and Applications of Sintering, 2005, 216-219.

193. US Patent, US5683535, “Method and apparatus of producing cavities in LTCC substartes”.

194. US Patent, International Publication No, “Method of producing an LTCC substrate with cavities having improved bondability”.

195. P.E. Vallejos, J. Zhong, M. Góngora-Rubio, L.S. Laguna and J.J.S. Aviles, “Meso (intermediate)-scale electromechanical systems for the measurement and control of sagging in LTCC structures”, Mat. Res. Soc. Symp. Proc., 1998, 518, 73-79.

196. US Patent, US5601673, “Method of making ceramic article with cavity using LTCC tape”.

197. H. Birol, T. Maeder and P. Ryser, “Preparation and application of minerals-based sacrificial pastes for fabrication nof LTCC structures”, EMPS 2006, 4th European Microelectronics and Packaging Symposium, 2006, Slovenia, 57-60.

198. Manufacturer’s web-site, Harmonics, Inc. : http://www.hmnx.com/

199. W.K. Jones, S. Kappagantula and J. Wang, “Micro channel fabrication in LTCC substarte”, Proceedings of the Ceramic Interconnect Technology Conference, 2005, Denver.

200. H. Birol, T. Maeder, C. Jacq, S. Straessler and P. Ryser, "Fabrication of LTCC Micro-fluidic Devices Using Sacrificial Carbon Layers", Int. J. Appl. Ceram. Technol., 2005, 2 (5)], 345-354.

201. H. Birol, T. Maeder and P. Ryser, "Processing of Graphite-Based Sacrificial Layer for Microfabrication of Low Temperature Co-fired Ceramics (LTCC)", Sens. Actuat.A- Phys., 2006, 130-131, 560-567.

202. J. Park, P.E. Vallejos, L.S. Laguna and J.S. Aviles, “Etching and exfoliation techniques for the fabrication of 3-D meso-scales structures on LTCC tapes”, Proceedings of the IMAPS 1998 Meeting, 1998, 142-147.

2 SCIENTIFIC APPROACH:

Preparation of graphite-based sacrificial paste

2.1 The basis of the developed technique

The graphite-based sacrificial paste (referred to as "sacrificial paste" hereafter), which is prepared for fabrication of flat and well-integrated cavities in LTCC multi-layer structures, is composed of two main ingredients: graphite powder and organic vehicle. The former is the functional element of the sacrificial paste and it supports LTCC laminates up to its full oxidation temperature (~ 800-850 °C), which is much higher than that of the organics both in LTCC and in the sacrificial paste (~ 450 and 300 °C, respectively). The organic vehicle, on the other hand, is based on a mixture of binder-solvent-dispersant system, which determines the rheology of the sacrificial paste and facilitates screen-printing.

Fabricating cavities in LTCC using sacrificial paste requires determination of the temperature ranges of LTCC open pore elimination and graphite oxidation. This is of particular importance as the open porosity in LTCC facilitates degassing of the oxidized paste. The LTCC open pore elimination temperature, which was qualitatively determined by using a specially-developed closed chamber system, was found to be around 790 °C and thus, well comparable to the sacrificial paste oxidation temperature. Therefore, the basic requirement for paste oxidation and degassing processes was satisfied.

There are numerous motives for selection of graphite as the sacrificial material [1]: its oxidation temperature ideally close to the onset of LTCC densification temperature, its ease of removal and chemical inertness, etc. Moreover, once mixed with an organic vehicle, it can be screen-printed on LTCC tape in the desired form (determined by the layout), laminated with additional layers and fired.

Cavities within the bulk of such multi-layer structures using sacrificial paste are formed by oxidation of the paste, a process which consists of a series of physical and chemical steps that can be listed as follows [2]:

- Transport of oxidant (air) to the graphite layer: through the ports which are in direct contact to air and also through the pores in LTCC,

- Adsorption of air onto graphite surface (physisorption): the larger the surface area, the higher the amount of oxidant adsorbed on the graphite.
- Formation of carbon-oxygen bonds (chemisorption),
- Breaking of carbon-carbon bonds,
- Desorption of products following the oxidation reactions (ΔH: standard formation enthalpy of the substance)

$C + O_2 \rightarrow CO_2$	$\Delta H = -393.5$ kJ/mol	→ full oxidation	(1)
$C + ½\ O_2 \rightarrow CO$	$\Delta H = -110.5$ kJ/mol	→ partial oxidation	(2)
$CO + ½\ O_2 \rightarrow CO_2$	$\Delta H = -283.0$ kJ/mol	→ completed	(3)

- Transport of reaction product from the graphite surface.

Although it is not the scope of this work to get into details, it should be emphasized here that the oxidation of graphite is a quite complex process and only partly understood [3]. The overall process is driven by the dominant oxidation mechanism and as a function of temperature, particle shape, environment and location of the graphite powder: either on the inert planar surface or on the reactive edge surfaces, the latter known to provide active sites for binding of oxygen molecules and thus, having the major influence on oxidation [3, 4].

The oxidation mechanism of sacrificial paste, which is buried in LTCC layers and with inlet and outlet channels open to air, can be seen in figure 2.1. Paste oxidation, which is enhanced by the air intake through the ports and the porous LTCC, and is followed by countercurrent oxidized products degassing. Therefore, the kinetic competition between the two events; the graphite oxidation and the LTCC open porosity elimination process (sintering), play the major role in determining the cavity features: incomplete paste oxidation following LTCC densification (elimination of open porosity) results in deformation. This is a consequence of the increased gas pressure upon oxidation, which exerts force on the non-porous LTCC environment.

In light of these discussions, the critical materials and processing parameters can be summarized as:

- Size (d_{50}) and oxidation temperature of the graphite powder: the smaller the particle size, the larger the surface area, which hosts increased amount of air and thus, facilitates sacrificial paste removal.
- Air intake facility (volume and flow rate): the higher the air intake, the faster the oxidation and degassing, which is related to the dimensions of the structure, amount of sacrificial paste deposited (screen type) and the ease of access to the air source.
- Composition of the paste: although it does not affect the kinetics of the oxidation process, it determines the rheology and thus screen-printability of the paste, and thus has an indirect but important influence in the final structure.
- Heating rate: it influences oxidation and LTCC densification processes simultaneously and therefore has to be investigated with utmost care. Higher heating rates shift both oxidation and LTCC open porosity elimination to higher temperatures, where the former is more affected by it compared to the latter that occurs at a relatively narrow temperature range.

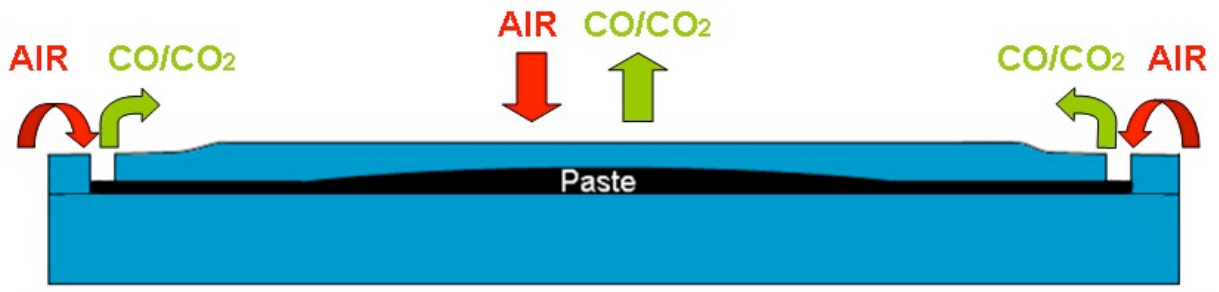

Figure 2.1. Mechanism of buried paste oxidation and degassing. Note that air and/or degassed gas transport through LTCC occurs only at temperatures below LTCC open-porosity elimination temperature.

2.1.1 Preparation of the sacrificial paste

Sacrificial paste preparation is a multi-step process based on consecutive mixing of ingredients, which are presented in table 2.1. The procedure followed can be summarized as:

- Dissolving binder in solvent at 80 °C (~ 15 minutes),
- Adding graphite (TIMREX KS5-25 and TIMREX KS5-44 of TIMCAL, Switzerland were used) at small quantities over the mixture, a process that is accompanied by dispersant addition gradually,
- Mixing the materials and transferring the mixture in the 3-roll mill (figure 2.2.),

- Homogenizing the sacrificial paste for 30 minutes,
- Recovering the paste and transferring it into plastic jars.

Material losses, at the end of processing, were found to be in the 18-24 % (by weight) range, which are estimated to occur mainly during the recovery from the three-roll mill.

Table 2.1. Sacrificial paste ingredients

Product	Function	Specification	Product commercial Name
Graphite	Sacrificial	Type I - d_{50} : 1-2 µm Type II - d_{50} : 11 µm Type III - d_{50} : 15. 3 µm Type IV - d_{50} : 27 µm	Aldrich, 28,286-3 KS25 KS5-25 KS5-44
Ethyl cellulose	Binder	- attaches particles in the paste - decomposition temperature ~ 120 °C	Aldrich, 43,383-7
Terpineol	Solvent	- lowers slurry viscosity - boiling point ~ 215 °C	Fluka, 86480
Acetyl acetone	Dispersant	- dispersing additive - boiling point ~ 140 °C	Sigma-Aldrich, P775-4

d_{50}: particle size (indicates 50% of the overall powder below this size)

The morphology and the size of the graphite powders (type II, III and IV) were analyzed using SEM (Philips XLF-30) by dispersing uncoated graphite powders on alumina sample holders at 5 keV. It is evidently seen in figure 2.3 that the particles are flake-like, exhibiting a high aspect ratio (diameter or length to thickness ratio). Oxidation of such particles occurs mainly on the edge sites of the powder, which provide sites for oxygen adsorption [4].

SEM images also demonstrate that the observed particle sizes are comparable to those provided by the supplier data sheets, in spite of a slightly higher particle size reported for type IV powder (ca. 10%).

Considering the number of initial materials in addition to their interactions and effects on the sacrificial paste properties, design of experiments (DoE) was used to determine the

necessary number of experiments and to study the influence of each parameter on paste characteristics qualitatively [5].

Therefore, 5 factors were determined, which were estimated to have an influence on the sacrificial paste produced: particle size of graphite, weight percentage of graphite, binder (ethyl cellulose), solvent (terpineol) and dispersant (acetyl acetone). Among those, the first three were selected as the independent factors of the experiments, while the other two (solvent and dispersant amounts) as the dependent variables determined by the following relations:

$$G + B + S + D = 100 \quad (1)$$

$$D \approx 1/5 * G \quad (2)$$

where, G, B, S and D stand for graphite, binder, solvent and dispersant ratios of the paste by weight percentage, yielding a total of 100%. This gives an experimental design with 3 factors and 2 responses (variants) per factor, yielding 8 experiments (table 2.2). The ranges of the factors and equation (2) were determined according to preliminary findings in optimizing viscosity and miscibility of pastes and recipes used in slurry preparation for tape casting [6, 7].

The sacrificial pastes in table 2.2. were prepared in random order to reduce the effects of environmental conditions on the experiments. The batches were 15 grams for each paste and table 2.3. shows the exact experimental order carried and the compositions used.

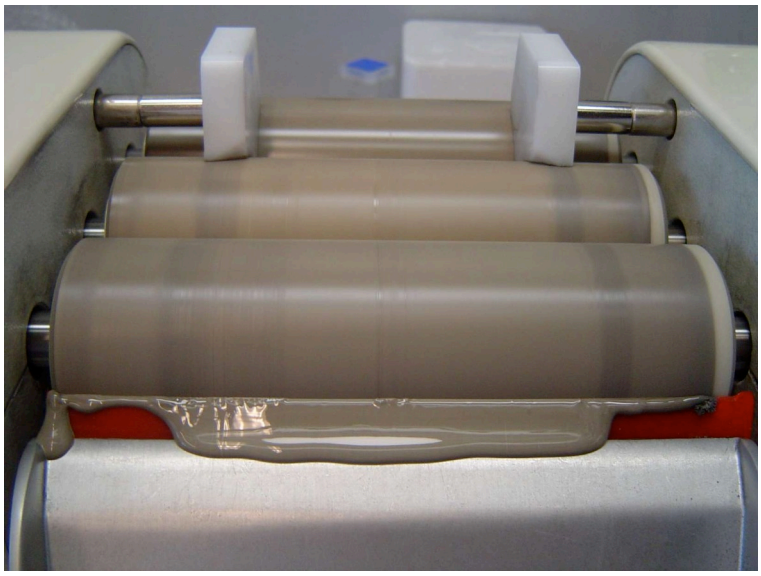

Figure 2.2. Mixing and homogenizing the paste mixture on three-roll mill.

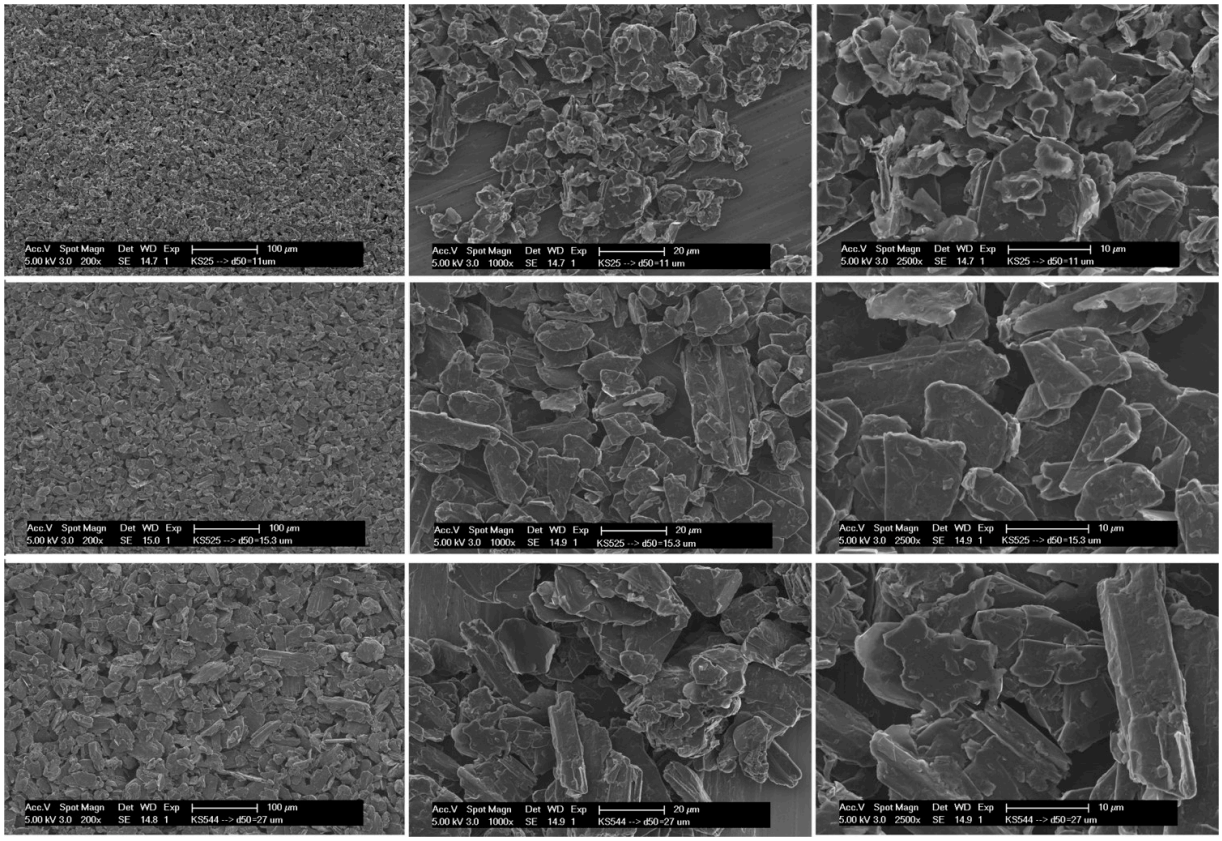

Figure 2.3. SEM images of graphite powders: each row shows images of different graphite powders used (type II, III and IV) at magnifications of 200, 1000, 2500 for comparison.

Table 2.2. DoE for paste preparation

Paste	G-d_{50}[a]	G[b]	B[b]	D[b] = 1/5* G[b]	S[b] → rest
KS5-25-1	15.3	20	3	4	73
KS5-25-2	15.3	20	5	4	71
KS5-25-3	15.3	35	3	7	55
KS5-25-4	15.3	35	5	7	53
KS5-44-1	27.0	20	3	4	73
KS5-44-2	27.0	20	5	4	71
KS5-44-3	27.0	35	3	7	55
KS5-44-4	27.0	35	5	7	53

G: graphite, B: binder, D: dispersant, S: solvent
[a] Graphite particle size in µm.
[b] Percentages of ingredients (by weight) given in equations (1) and (2).

Table 2.3. Experimental order of paste preparation

Paste	Paste code	G-d_{50}[a]	G[c]	B[c]	D[c]	S[c]
KS5-44-2	P1	27.0	3.00	0.75	0.60	10.65
KS5-25-3	P2	15.3	5.25	0.45	1.05	8.25
KS5-44-4	P3	27.0	5.25	0.75	1.05	7.95
KS5-25-1	P4	15.3	3.00	0.45	0.60	10.95
KS5-44-3	P5	27.0	5.25	0.45	1.05	8.25
KS5-25-4	P6	15.3	5.25	0.75	1.05	7.95
KS5-44-1	P7	27.0	3.00	0.45	0.60	10.95
KS5-25-2	P8	15.3	3.00	0.75	0.60	10.65

G: graphite, B: binder, D: dispersant, S: solvent
[a] Graphite particle size in μm.
[c] Weight (g) of ingredients given in equations (1) and (2).

2.1.2 Characterization of the paste

2.1.2.1 TGA

Thermogravimetry analysis was carried out to measure the mass change of sacrificial material as a function of temperature at different heating rates (Mettler-Toledo TGA/SDTA 851 [8]). Thus, the kinetics of the oxidation process was determined, which was then compared to that of the LTCC densification process.

Within this perspective first the functional element of the paste, the graphite powder in different sizes (Type I, III and IV: 1-2, 15.3 and 27 μm, respectively) was heated at three rates: 2, 5 and 8 °C/minute (figure 2.4.). As expected, the powder with the smallest particle size was oxidized at a much earlier stage at all heating rates than the other two, as a consequence of its larger surface area hosting increased amount of air. This powder was not considered for application, as it was found to provide insufficient cavity spacing due to excessively fast oxidation [9], which will be discussed in detail in the following chapters.

The amount of un-oxidized powder at 790 °C (approximate temperature at which LTCC open porosity is eliminated – discussion in the next section) and the temperature for full oxidation of the other two graphite powders are summarized in table 2.4. It is clearly seen that

increased heating rates shift full oxidation of the graphite powder to higher temperatures. Consequently, the graphite, which is not oxidized prior to the porous LTCC elimination temperature, remains either entrapped within the cavity or is oxidized through the ports only (figure 2.1.).

According to the results of table 2.4., the prepared pastes were analyzed by TGA at a heating rate of 2 °C/min only to avoid excessive accumulation of unreacted/entrapped products. Figure 2.5. gives the corresponding results in terms of remaining weight versus temperature. The analysis was performed by heating ca. 5 mg of paste at a rate of 2 °C/min. It is seen that the organic vehicle is fully consumed by 330 °C and the onset of graphite oxidation temperature is around 600 °C. This yields a very comfortable processing window for preparation of structures given typical LTCC binder burnout temperatures of ca. 450 °C [10]. The remaining weight fraction between these temperatures agrees well with the relative amount of graphite in the paste.

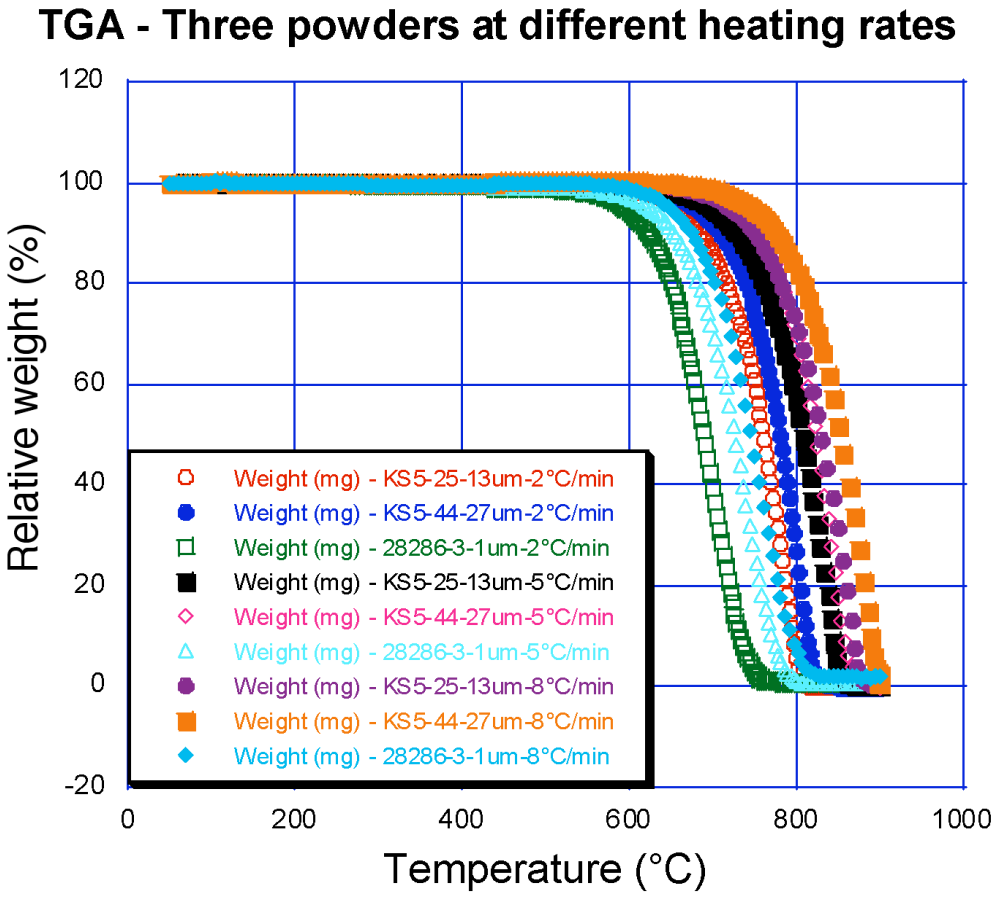

Figure 2.4. TGA of three graphite powders, varying in d_{50}, at three different heating rates (2, 5, 8 °C/min).

Table 2.4. Remaining powder amount at 790 °C and full oxidation temperature

Powder	Powder remaining at 790 °C (%)			Full oxidation temperature (°C)		
	At different heating rates (°C/min)			At different heating rates (°C/min)		
	2	5	8	2	5	8
KS5-25	17	61	75	815	877	>900
KS5-44	40	73	85	846	895	>>900

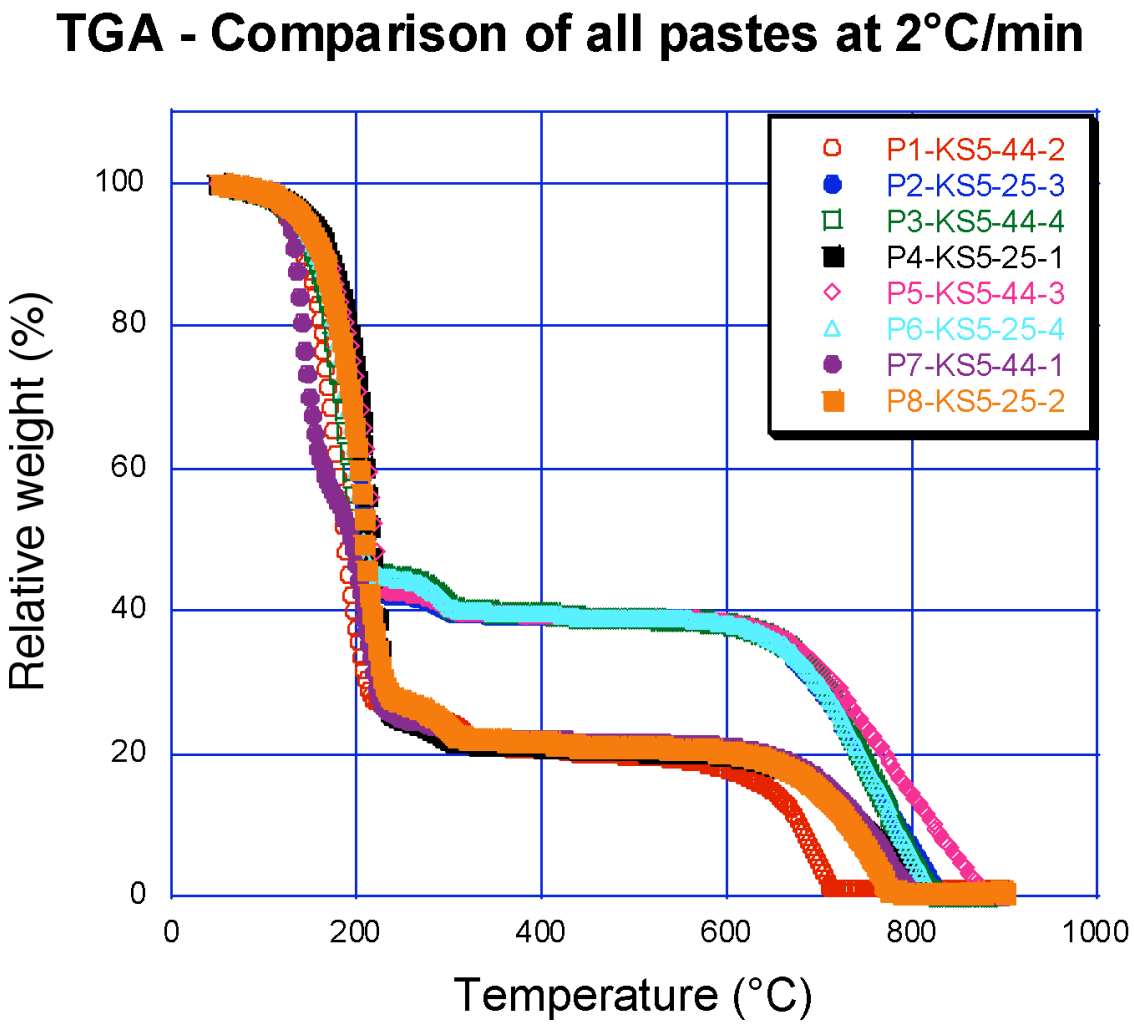

Figure 2.5. TGA of selected pastes at 2 °C/min heating rate.

2.1.2.2 Viscosity

The viscosity of pastes was measured using a cup and cone type, controlled stress rheometer (Bohlin Reologi). The samples were placed between the upper cone (4° inclination) and the fixed lower plate (40 mm diameter), following calibration with standard viscosity oils that yielded an error of 3 %. The viscosity values upon applied shear stress were accepted and recorded with the sole condition that they remained in the reliable measuring range defined by the viscosity – shear rate – shear stress diagram [11].

Table 2.5. shows the applied shear stress range and the instant viscosities at 10 or 100 Pa, depending on the rheological properties of pastes. In case of low solid (graphite) content, the pastes possessed low viscosities and apparent viscosity was measured using 10 Pa. In a similar manner viscosity of pastes with higher solids loading was measured at 100 Pa.

Table 2.5. Viscosity of pastes

Paste	Paste code	G[c]	Stress-range (Pa)	Apparent viscosity (Pa.s) at *10* [d] & 100[e] Pa
KS5-44-2	P1	3.00	10-100	*13.4*
KS5-25-3	P2	5.25	80-160	442
KS5-44-4	P3	5.25	100-200	721
KS5-25-1	P4	3.00	2-100	*3.7*
KS5-44-3	P5	5.25	10-100	123
KS5-25-4	P6	5.25	100-200	1055
KS5-44-1	P7	3.00	5-20	*4.1*
KS5-25-2	P8	3.00	1-20	*18.5*

G: graphite
[c] Amount of graphite in grams
[d, e] Apparent viscosity measured at 10 Pa (text written in italics) and 100 Pa, respectively.

2.1.2.3 Sedimentation

The pastes were also visually checked to determine the extent of sedimentation one month after processing. This simple process provides a quick idea on the quality of dispersion of particles in the paste, thus giving information on the stability of the produced paste in the

long term. It was observed that pastes with higher viscosities showed almost no sedimentation, whereas graphite in the others sedimented.

2.2 Evaluation and selection of the paste

The results are summarized in table 2.6. Apparent viscosity and extent of sedimentation, which are the responses of the experimental design, cannot be used in order to analyze the influence of factors quantitatively. This is due to different test conditions used for the responses; i.e. apparent viscosity of pastes measured at two different stresses due to different rheology of pastes, which don't fulfill the requirement (orthogonality) for quantitative description. Therefore we preferred to make a list of the most important findings and the conclusions for selection of the paste for future applications:

I. Viscosity of pastes is a strong function of the solvent content, as expected. However it is seen that for similar solvent content, the binder percentage has a more direct influence on the apparent viscosity of the pastes.
II. Moreover, the finer particles result in higher viscosities compared to coarser particles, except at high solvent and low binder contents (P4 and P7), where viscosity is very low.
III. Pastes with minimum viscosities were prone to extreme sedimentation of graphite particles in the solvent-excess environment, contrary to stable compositions with higher viscosity.
IV. The least viscous pastes, P1, P4, P7 and P8 show excessive sedimentation and thus insufficient stability, P4 and P7 could not be screen printed, even immediately after thorough mixing. On the other extreme, P6 is too viscous, and is found to be excessively sensitive to solvent loss.

According to the factors and ranges selected, 35 % by weight of graphite is estimated to be the upper limit of the graphite-based sacrificial paste so far. In addition to this, P2, P3 and P5 have the best compatibility with screen printing and show resistance to sedimentation (stable) so that they are considered to be the candidate pastes for future applications, with P2

(20% by volume), being preferred as it lies in the middle of the optimal range (shown as bold in table 2.6.).

Table 2.6. Overall results

Paste code	G-d_{50}[a]	G[c]	B[c]	S[c]	Apparent viscosity (Pa.s) at *10*[d] & 100[e] Pa	Extent of sedimentation
P6	15.3	5.25	0.75	7.95	1055	None
P3	27	5.25	0.75	7.95	721	None
P2	**15.3**	**5.25**	**0.45**	**8.25**	**442**	**None**
P5	27	5.25	0.45	8.25	123	None
P8	15.3	3.00	0.75	10.65	*18.5*	Extreme
P1	27	3.00	0.75	10.65	*13.4*	Extreme
P7	27	3.00	0.45	10.95	*4.1*	Extreme
P4	15.3	3.00	0.45	10.95	*3.7*	Extreme

G: graphite, B: binder, D: dispersant, S: solvent
[a] Graphite particle size in μm.
[c] Weight (g) of ingredients given in equations (1) and (2).
[d, e] Apparent viscosity measured at 10 Pa (text written in italics) and 100 Pa, respectively.

References

1. H. Birol, T. Maeder, C. Jacq and P. Ryser, "3-D structuration of LTCC for Sensor Micro-fluidic Applications", Proceedings, European Microelectronics and Packaging Symposium, Prague-Czech Republic, 2004, 366-371.

2. IAEA, “Irradiation damage in graphite due to fast neutrons in fission and fusion systems”, IAES-TECDOC-1154, 2000, Vienna, 207-213.

3. R. Backreedy, J.M. Jones, M. Pourkashanian and A. Williams, “A study of the reaction of oxygen with graphite: Model chemistry”, Royal Soc. Chem., 2001, 119, 385-39.

4. W. Jiang, G. Nadeau, K. Zaghib and K. Kinoshita, “Thermal analysis of the oxidation of natural graphite: effect of particle size”, Thermochim. acta., 2000, 351, [1-2], 85-93.

5. B.H. Gunter, “How statistical design concepts can improve experimentation in the physical sciences”, Comput. Phys., 1993, 7 (3), 262-272.

6. H. Hellebrand, “Tape Casting, Materials Science and Technology”, Vol. 17A, Processing of Ceramics, ed. R. J. Brook, VCH, Weinheim, Germany, 1996, 189-265.

7. R.E. Mistler, “Tape casting: past, present, potential”, Am. Ceram. Soc. Bull., 1998, 82-86.

8. http://ch.mt.com/mt/productUpdates/ta_booster_promotion_06_Editorial-News_1137071318828.jsp

9. H. Birol, T. Maeder, C. Jacq, S. Sträessler and P. Ryser, “Fabrication of LTCC micro-fluidic devices using sacrificial carbon layers”, Int. J. Appl. Ceram. Technol., 2005, 2 (5), 345-354.

10. http://www2.dupont.com/MCM/en_US/PDF/datasheets/951.pdf.

11. Datasheet, The Bohlin Controlled Stress Rheometer, Cone/plate CP 4/40, Measuring range: AS8810JB BRI: 100 126/134.

3 FABRICATION OF MICRO-FLUIDIC STRUCTURES

3.1 Determination of the model structure

The membrane structure was selected as a model for fabrication of cavities in the multi-layer LTCC structure. It was realized simply by laminating a layer of LTCC sheet that is screen-printed with sacrificial paste with another layer (figure 3.1).

It is an ideal structure for testing the functionality of the prepared sacrificial pastes for fabrication of cavities in addition to other benefits, some of which are listed in the following:

- It has micro-fluidic channels opening to oxidizing source (via ports) on one side and to the large membrane area on the other (figure 3.1),
- It is an ideal structure to study the effects of processing and device parameters on the final device dimensions and performance (membrane diameter, channel width/height, etc.),
- It can be used for various applications such as pressure sensing, heat conductivity measurement, micro-fluidic pumping, etc.

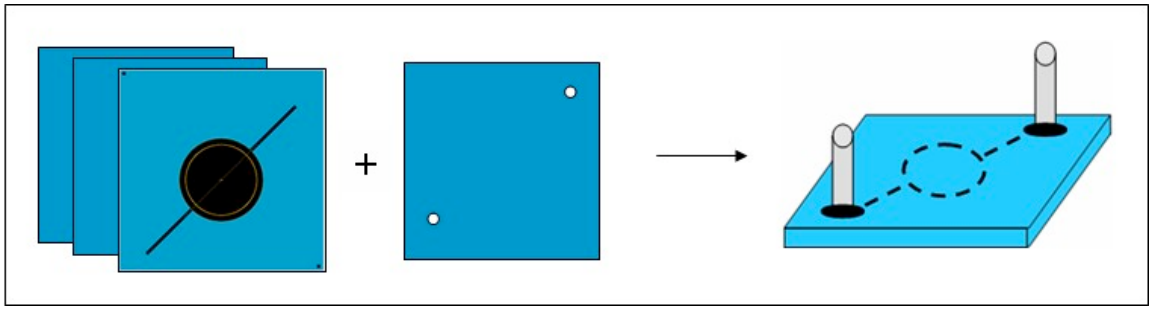

Figure 3.1. Fabrication of membrane: completion by integration of inlet and outlet ports (far right).

3.2 Processing

Membranes were fabricated from thick and thin LTCC sheets, which were used for the base and the membrane layer, respectively (all from DuPont 951 series). The graphite paste, which is selected as optimal in the previous chapter (table 3.1.) was used throughout the whole study.

Table 3.1. Paste properties

Graphite-d_{50}[a]	Graphite[b]	Ethyl cellulose[c]	Acetyl acetone[d]	Terpineol[e]	Apparent viscosity at 100 Pa (Pa.s)	Sedimentation[f]
15.3	5.25	0.45	1.05	8.25	441.85	Not detected

[a] Graphite particle size in µm
[b] amount of graphite in g.
[c] amount of binder in g.
[d] amount of dispersant in g.
[e] amount of solvent in g.
[f] by visual observation

3.2.1 Layout

The graphite paste was screen-printed on the thicker (254 µm) LTCC sheet of 60x60 mm^2 LTCC layer according to the layout shown in figure 3.2. There are a total of four membranes, each on a 30x30 mm^2 and having a diameter of 25 mm for batch production.

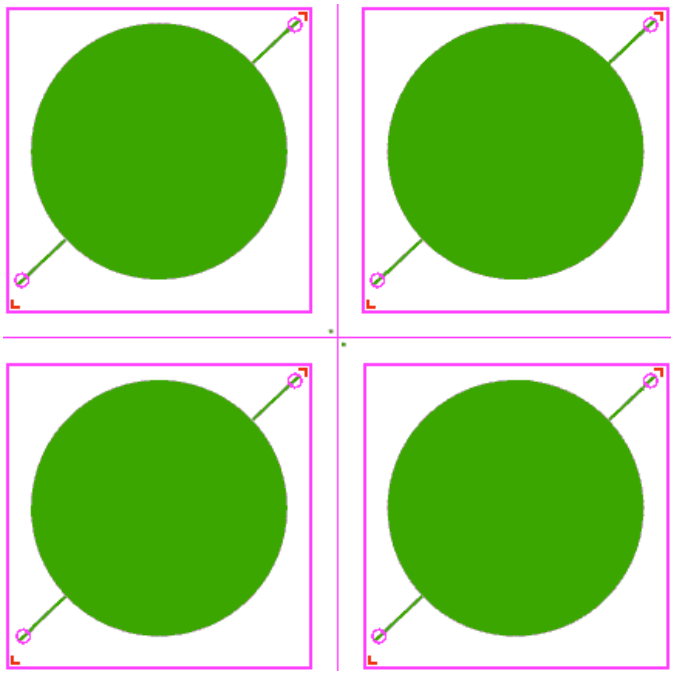

Figure 3.2. Layout for batch production of the membranes.

3.2.2 Screen-printing

Sacrificial paste deposition on LTCC tape was conducted by screen-printing, a process, in which a squeegee forces the paste through the screen (figure 3.3.). The printed tape was leveled at room temperature, and then dried at 120 °C, each for 10 minutes. The printed thickness was measured using a surface profiler (UBM), which operates by laser reflection.

The thickness varied as a function of the screen used for printing, which is designated by two numbers: number of wires per inch (1 inch=25.4 mm) and emulsion thickness in µm [1-3]. The screen with coarser mesh and thicker emulsion (i.e. 165/80 for this study) permitted increased passage of paste, yielding a higher printed thickness, around 70 µm, whereas the screen with finer mesh and finer emulsion (325/40) resulted in a thickness of ca. 27 µm. This data represents the average of a wide range of values, where the screen with coarser mesh provided a better reproducibility of printed thickness.

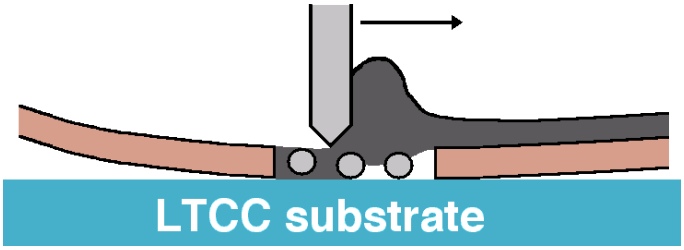

Figure 3.3. Screen-printing sacrificial paste onto LTCC.

3.2.3 Stacking and lamination

Following this step, the printed LTCC sheet was collated with two other thick layers from the bottom (254 µm-thick DuPont 951-AX) and one 50 µm-thick LTCC sheet (DuPont 951-C2) from the top, which is actually the membrane (figure 3.4.). The layers were carefully aligned by using optical microscopy to avoid mismatch. The base thickness was considerably increased by additional bottom layers in order to enhance its mechanical stability and stiffness, thus providing cleaner boundary conditions for the membrane. This structure was then laminated at 25 MPa with a uni-axial press having a heating plate that is kept at 70°C during pressing. A rubber layer was inserted between the moving bottom part of the die and the LTCC layers, in order to enhance the efficiency of lamination and preserve the shape of the membrane.

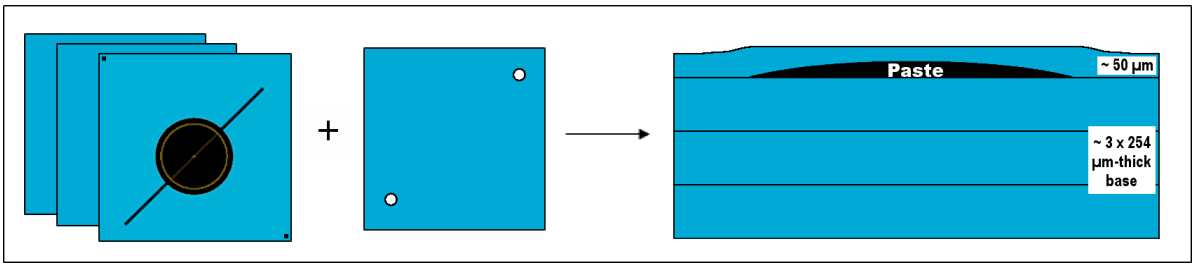

Figure 3.4. Individual LTCC layers laminated to build up the membrane.

3.2.4 Sintering and integration of device components

The laminated piece was then fired in an LTCC oven (ATV PEO-601) according to a two-step firing profile (figure 3.5.) with two dwell temperatures: ca. 440 °C for LTCC organics burnout (2 hours) and 875 °C for densification of LTCC (25 minutes) according to manufacturer's processing guidelines [4]. For the graphite paste, 440 °C conveniently lies above the organics vehicle burnout (~ 330 °C) and well below the onset of graphite oxidation (~ 600 °C), which were discussed in the previous section.

The thick-film components were screen-printed and post-fired (details in the devices section) and finally the inlet and outlet tubes were glued on the membrane using an epoxy resin to complete the fluidic circuit and characterize the membrane displacement (figure 3.6.).

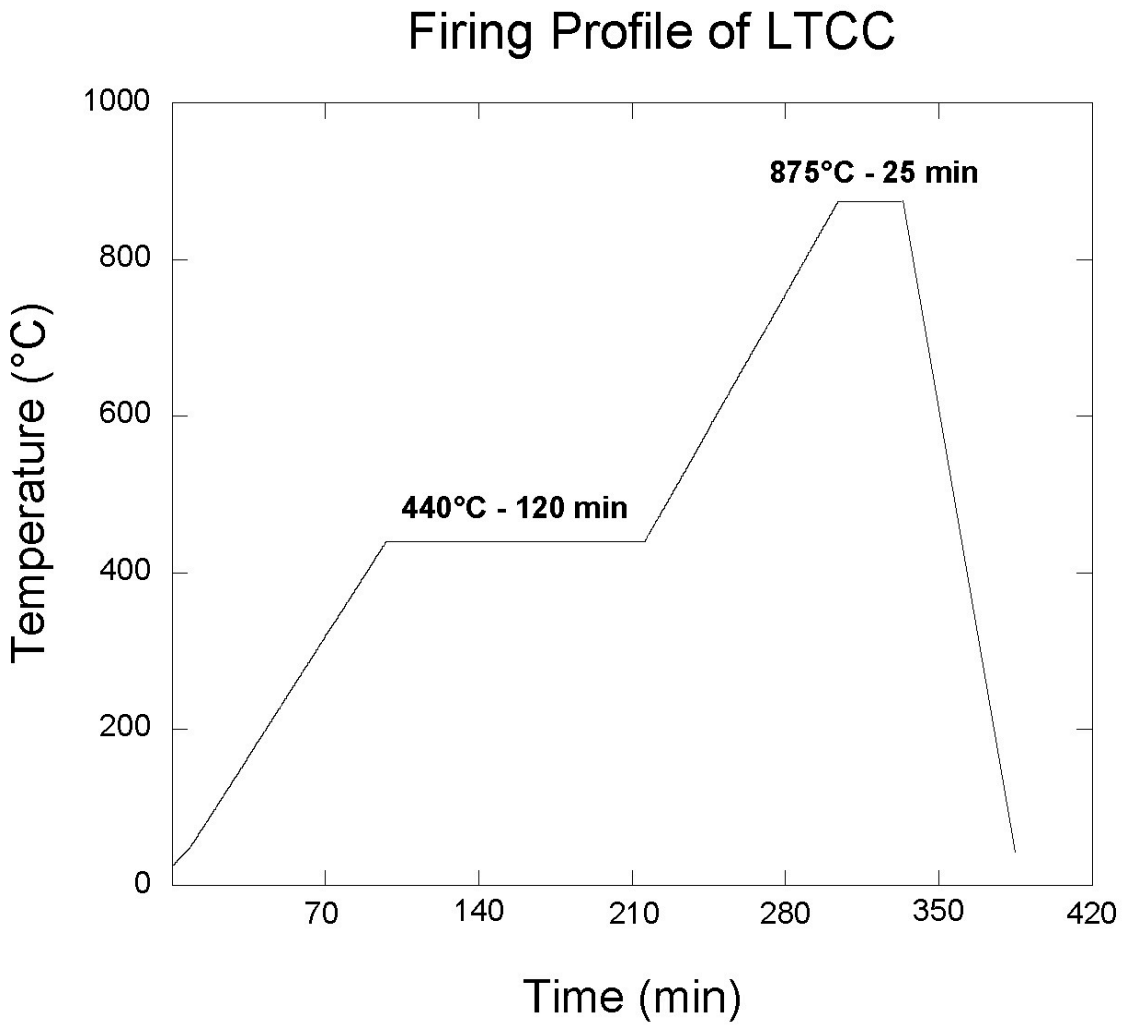

Figure 3.5. Heating profile for the multilayer LTCC.

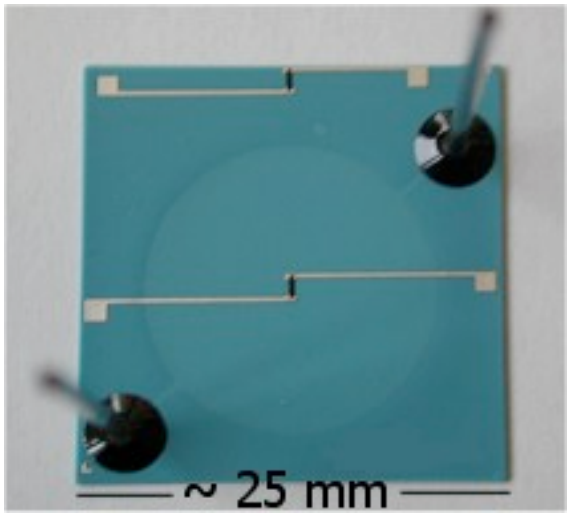

Figure 3.6. Complete 18mm-diamater membrane: ports-glued, PTC thick-film integrated and singulated.

3.3 Critical materials and processing parameters

In this sub-section, the important processing parameters having a direct effect on the final device properties are listed and discussed.

3.3.1 Sacrificial paste

As discussed previously, graphite powder is the functional element of the sacrificial paste and it is the material which supports LTCC layers at elevated temperatures, up to its full oxidation. It was found, as expected, that fine graphite particles were oxidized very fast, thus being inefficient in supporting LTCC. Therefore, we worked with relatively coarser particles ($d_{50} \geq 15$ µm), which were well dispersed in optimized paste media that is stable and printable with ease. For the appropriate rheology of the paste, on the other hand, the paste composition was optimized and preliminary tests prior to real experiments were conducted. It was found that the burnout process did not either cause a chemical interaction with LTCC or an early stage deformation due to organics burnout in the sacrificial paste.

3.3.2 Heating rate

The heating rate has a direct influence both on sacrificial paste oxidation and on LTCC densification processes. Therefore, it directly affects the structural and thus, the functional properties of the final device. Influence of faster rates on sacrificial paste oxidation was previously discussed and the consequence was reported as a shift in the oxidation to higher

temperatures. However, the effect of heating rate on LTCC open porosity elimination process was not shown, and will be discussed hereafter.

3.3.2.1 Heating rate versus LTCC open pore elimination temperature

It has already been shown that increased heating rates shift the full-densification temperature of LTCC to higher values [5]. This is mainly ascribed to the sintering mechanism of LTCC, which is based on combination of glass redistribution, grain rearrangement and viscous flow [5]. These processes are strongly time dependent and consequently they are affected at high heating rates due to limited material interactions.

The effect of heating rate on LTCC open pore elimination was analyzed by using a closed-chamber system (figure 3.7.). LTCC substrates, which were fired in the 750-810 °C range and varying in thickness (254 and 50 μm-thick tapes from DuPont 951-AX and 951-C2 series, respectively), were used in this analysis. The essence of this system is to detect the leakage through the fired LTCC substrate, which is placed between the two O-rings, by exerting air pressure on the surface by the piston. The air leak, which is quantified by the pressure relaxation time, is actually a qualitative assessment of the open porosity. The measuring system is composed of a power supply, a multimeter, which reads the current coming from the pressure sensor and the PC system.

The response of the instrument for a porous substrate is shown in figure 3.8., where one can see two peaks indicating pressure application and release immediately after, due to porosity. On the other hand, figure 3.9. shows the overall results for both substrates fired at 2, 5 and 8 °C/min. Determination of the open porosity closure temperature on a 50 μm-thick LTCC tape that is heated at 2 °C/min is illustrated in figure 3.10. It is seen that open porosity elimination occurs in the 780 to 790 °C range and we interpret the exact temperature as 785 °C within ± 2.5 °C deviation. The criterion for closure of open porosity in this study is for the pressure drop to remain below 10% of the initial overpressure in a time interval of 900 seconds and observed in the figure as a flat line parallel to the x-axis.

The open porosity closure temperature for the other samples is determined through the same procedure, and the results are compiled in table 3.2. Despite the shift to higher temperatures, which is observed at faster heating rates, open porosity elimination is mainly confined to a narrow temperature range. This indicates low sensitivity of LTCC densification process to heating rate, compared to the graphite oxidation, which occurs over a wider temperature range (table 3.3. – data from table 2.4.).

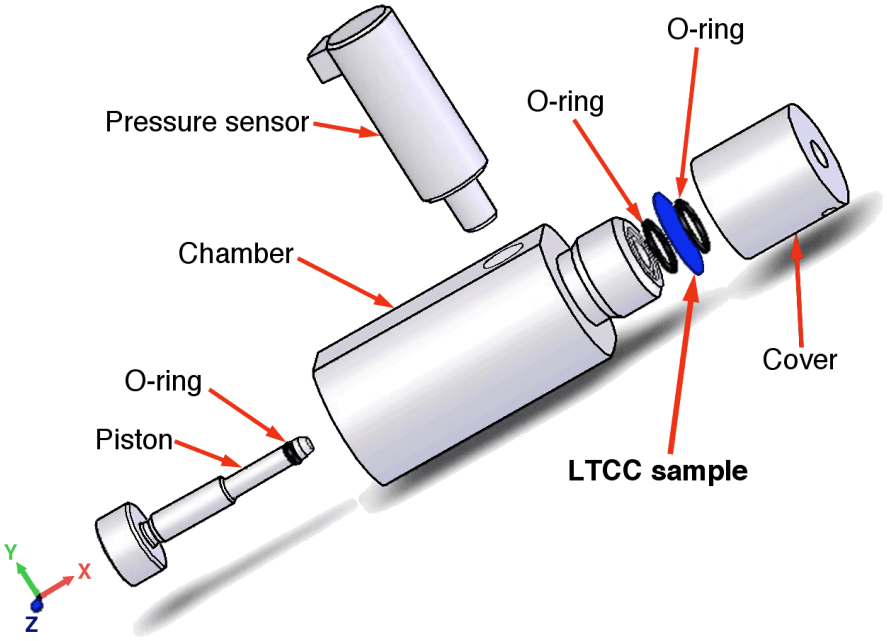

Figure 3.7. Closed chamber system for detection of LTCC permeability.

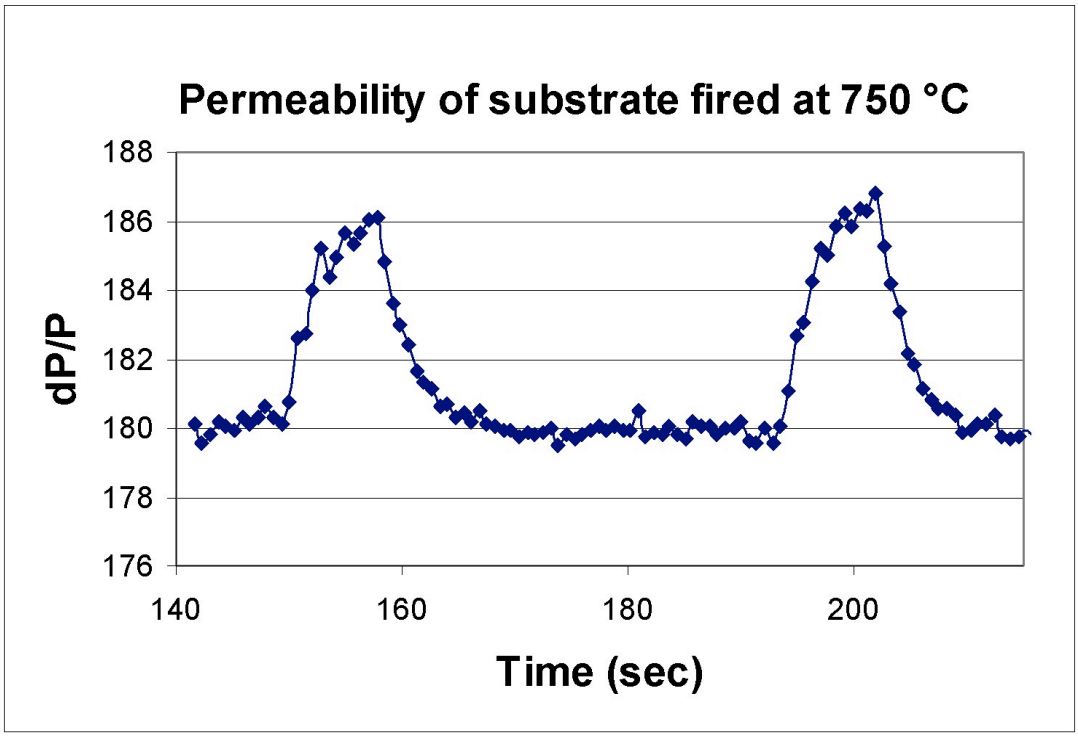

Figure 3.8. Decay of pressure on the permeable substrate: two peaks indicate application of pressure on the membrane (direct dP/P values read from the measurement, not normalized).

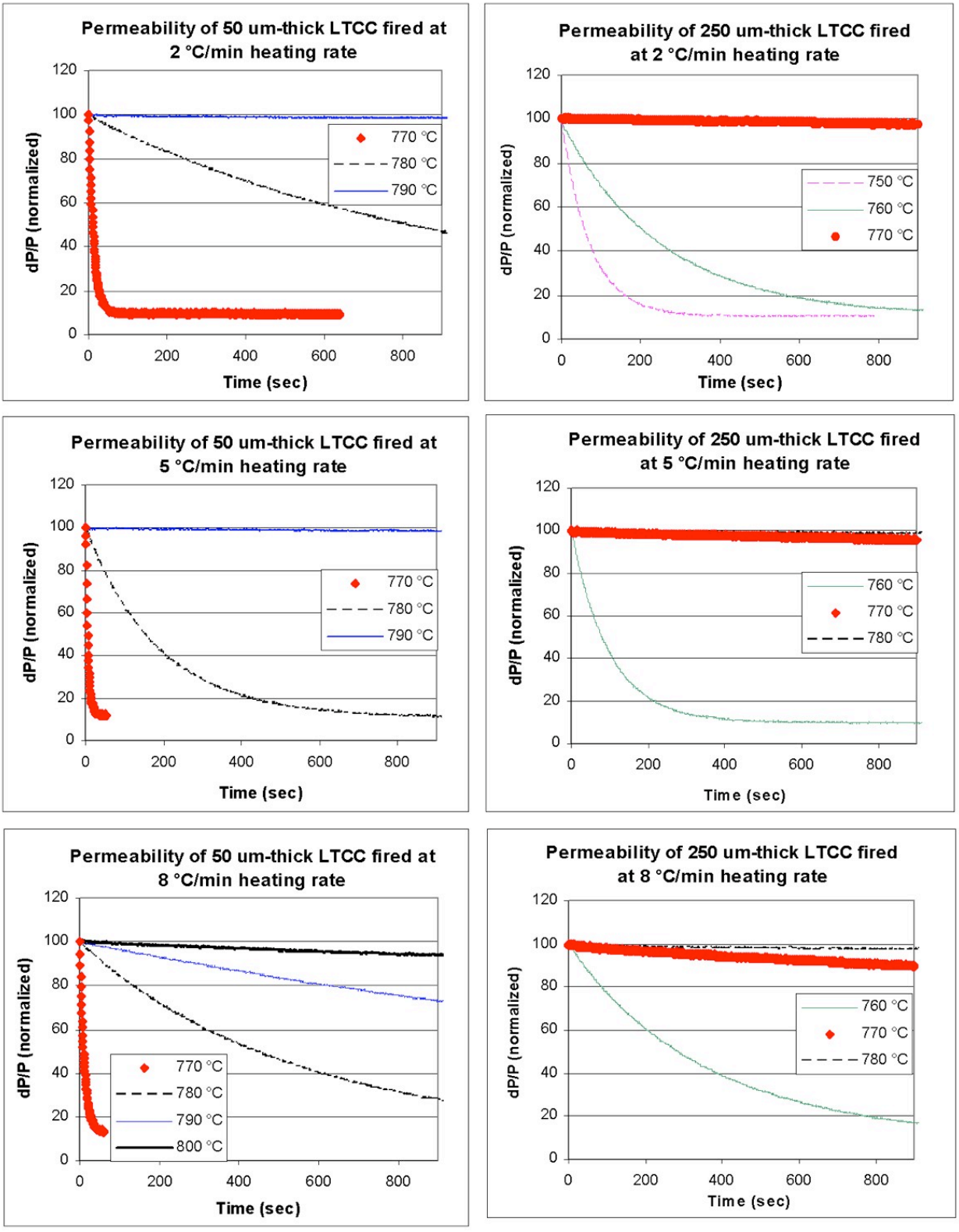

Figure 3.9. Qualitative permeability analysis of LTCC as a function of heating rate for 254 and 50 µm-thick LTCC substrates.

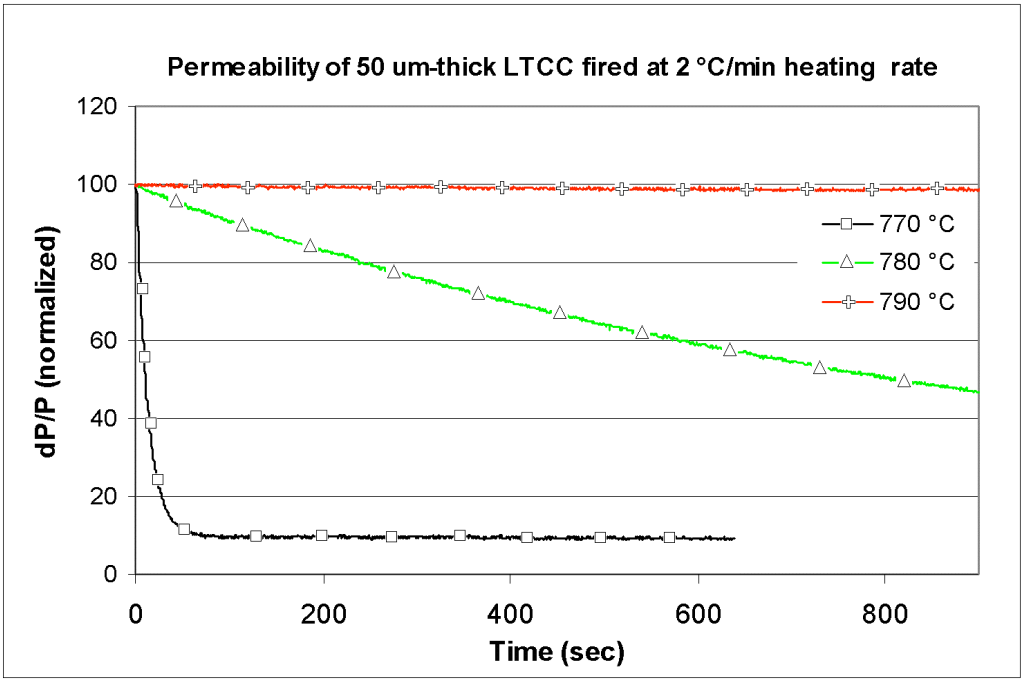

Figure 3.10. Evolution of open porosity of a 50 µm-thick LTCC substrates fired at different temperatures (heating rate: 2 °C/min).

Table 3.2. Heating rate versus LTCC open pore elimination temperature (± 2.5 °C)

LTCC (µm)	Heating rate (°C/min)		
	2	**5**	**8**
50	785	785	795
254	765	765	775

Table 3.3. Oxidation temperature of graphite powders used at different heating rates

Powder	T-full oxidation (°C)		
	At different heating rates (°C/min)		
	2	**5**	**8**
KS5-25	815	877	>900
KS5-44	846	895	>>900

3.3.3 Graphite layer thickness (screens used)

The type of the screen plays an indirect, but a significant role in facilitating oxidation process: it determines the amount of paste deposition and the height of the channel. Higher cavity provides increased air intake, which leads to increased sacrificial paste oxidation. Therefore, the effect of screen size is an important parameter for further study, as the consequences brought about by it can result in a broad range of cavity thickness/membrane spacing.

3.3.4 Device dimensions

Device dimensions such as the diameter of the membrane, width of the channel, etc. can considerably affect final device features by influencing the oxidation process. Similar to the height of the cavity, which is a function of the screen used, width of the channel also changes the oxygen intake capacity, influencing the sacrificial paste oxidation. In this case the dimensions can easily be changed by modifying the layout.

3.4 Processing parameters selected

In light of above discussions, heating rate, screen type and channel width were selected as processing parameters, as they were estimated to have the highest impact on final device properties. Therefore, their effects were studied systematically, using design of experiments (DoE).

Table 4 lists the experimental conditions with 8 experiments (2 responses, 3 factors), including an additional section of 4 experiments shown in italics, which were arranged to study low heating rate effects as well. The heating rates were selected as 2.50, 2.00 and 1.75 °C/min, in order to avoid retarded oxidation of sacrificial paste, which was observed at higher rates during TGA (the experimental parameters selected for the heating rate of 1.75 °C/min are shown in italics in table 3.4. in order to determine the lowest possible rate yielding acceptable membrane features). On the other hand, the effects of printed thickness and channel width were studied using different screens (325/40 and 165/80, as explained previously) and channel width (200 or 400 μm), respectively.

Channel dimensions have an influence both on diffusion (of oxidant/gas) and fluidics (flow). The ease of the former process is proportional to the channel cross-section, whereas the

ease of the latter is related to the multiplication of width with the cube of the height, where width is much higher than the height [6].

The following chapter will discuss the effects of these parameters on membrane morphology, spacing and displacement as a function of pressure.

Table 3.4. Experiments to study effects of selected processing parameters

Series 18mm	HR (°C/min)	Screen (mesh/emulsion)	Channel width (mm)
S1	2.50	325/40*	0.20
S2	2.50	325/40	0.40
S3	2.50	165/80°	0.20
S4	2.50	165/80	0.40
S5	2.00	325/40	0.20
S6	2.00	325/40	0.40
S7	2.00	165/80	0.20
S8	2.00	165/80	0.40
S9	*1.75*	*325/40*	*0.20*
S10	*1.75*	*325/40*	*0.40*
S11	*1.75*	*165/80*	*0.20*
S12	*1.75*	*165/80*	*0.40*

* Typical thickness of printed layer ~ 27 μm
° Typical thickness of printed layer ~ 70 μm

References

1. M. Prudenziati, “Thick-film Sensors”, Elsevier, 1994, 6-15.

2. K. Pitt, Handbook of Thick Film Technology, 2nd ed., British Isles, 2005, pp. 43-62.

3. L.F. Miller, “Paste transfer in the screening process”, Solid State Technology., vol. 12 (6), 1969, pp. 46-52.

4. http://www2.dupont.com/MCM/en_US/PDF/datasheets/951.pdf.

5. A. Mohanram, “Co-sintering of integrated ceramics: fundamentals, observations and design guidelines” PhD thesis, Department of Materials Science and Engineering, The Pennsylvania State University, Pennsylvania, 2005, 113-116, 16-21.

6. J.A. Frank and A.P. Pisano, “Low-leakage micro gate valves”, Transducers, 2003, 143-146.

4 STRUCTURAL & FUNCTIONAL CHARACTERISTICS OF MEMBRANES

4.1 Thickness of the cavity (membrane spacing)

The physical appearance of fabricated structures as a function of heating rate is schematically depicted in figure 4.1. As expected and in light of previous discussions, faster heating rates lead to increased swelling as a consequence of retarded graphite paste oxidation: burnout products were entrapped in the cavity exerting pressure on the non-porous membrane and deforming it. Although this seems to be a correct approach from the first look, swelling can further be ascribed to other phenomena such as a reaction in the form:

$$2C + O_2(g) \rightarrow 2CO(g) \quad (1)$$

which explains the volume increase. Moreover, sacrificial layer forced into the porous LTCC during lamination can also be expected to give rise to delayed oxidation, following the oxidation and removal of the bulk layer at elevated temperatures (> 850 °C).

The extent of swelling was characterized by using SEM and surface profilometer to determine membrane spacing and surface profile, respectively. Spacing analysis of samples, which were fabricated using different processing conditions and cut across their cross-section, is presented in figure 4.2. It is seen that screens providing lower sacrificial paste deposition (325/40) lead to extended swelling particularly at higher heating rates. The extended information on spacing is presented in table 4.1., which shows average values for 5-6 membranes per experimental condition.

Surface profiles of membranes were plotted by a laser profilometer (UBM), which is used for measuring thickness of films screen-printed on substrates. Figure 4.3. shows the surface profile of membranes fired at 2.5 °C/min heating rate using different experimental conditions (screen and channel width).

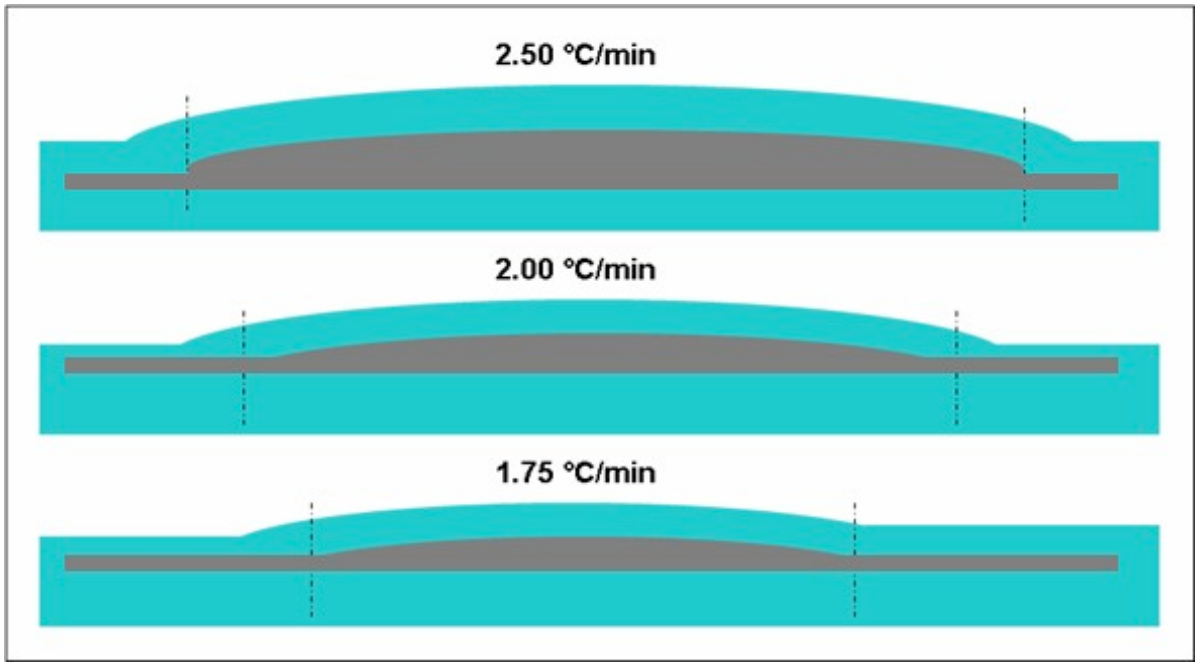

Figure 4.1. Qualitative description of membranes with identical screen and channel width, at high heating rates (2 and 2.5 °C/min). The regions out of the dashes are apparently closed.

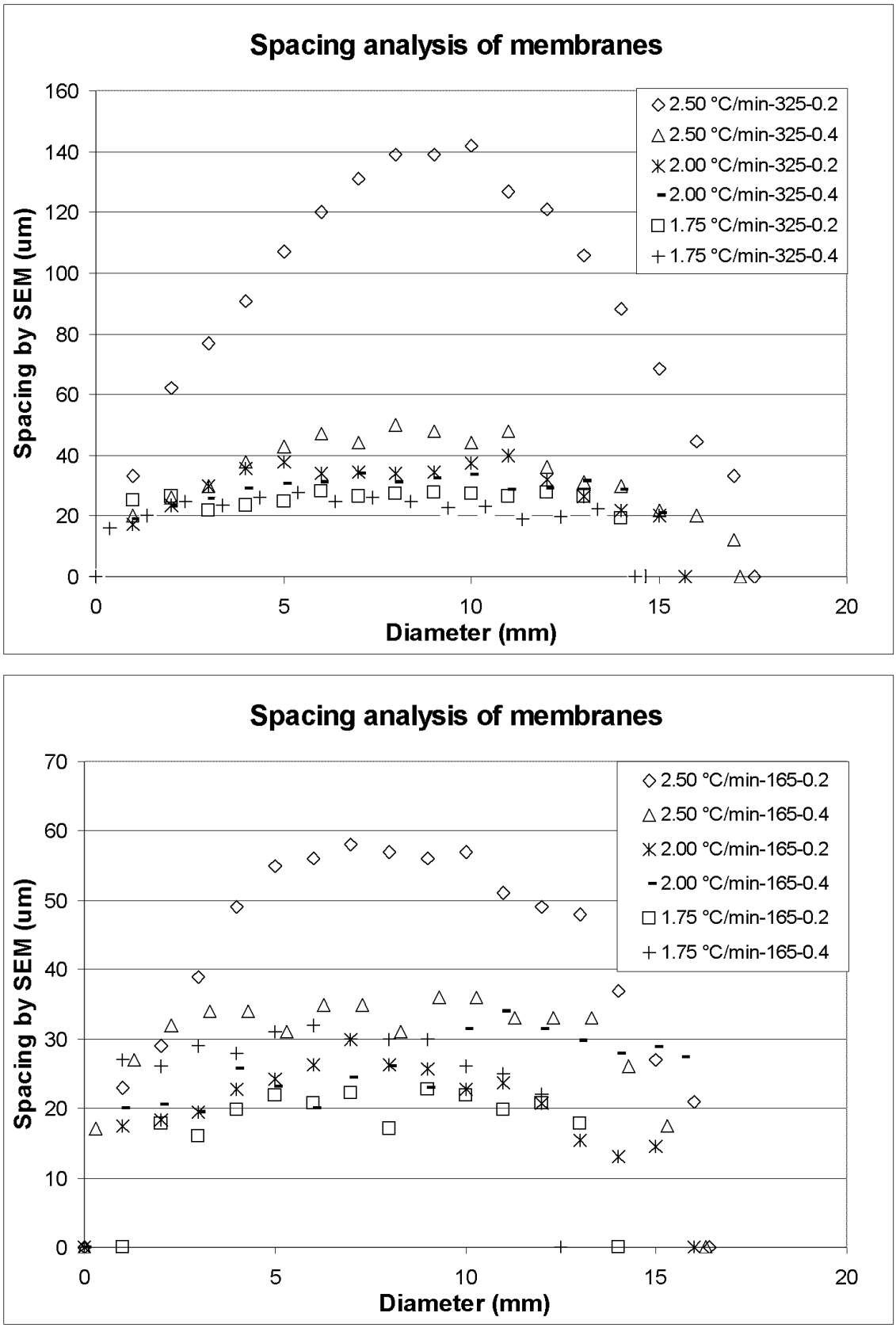

Figure 4.2. Membrane spacing in terms of heating rate for membranes those prepared with a) 325/40 (top) and b) 165/80 screens. Note the different scale in both figures.

Table 4.1. Results of the membrane spacing analysis

Screen-channel (mm)	Heating rates (°C/min)		
	2.50	**2.00**	**1.75**
	Representative spacing at the center of the membrane (µm)		
325/40 – 0.20	140	35	24
325/40 – 0.40	50	32	27
165/80 – 0.20	57	31	21
165/80 – 0.40	37	25	30

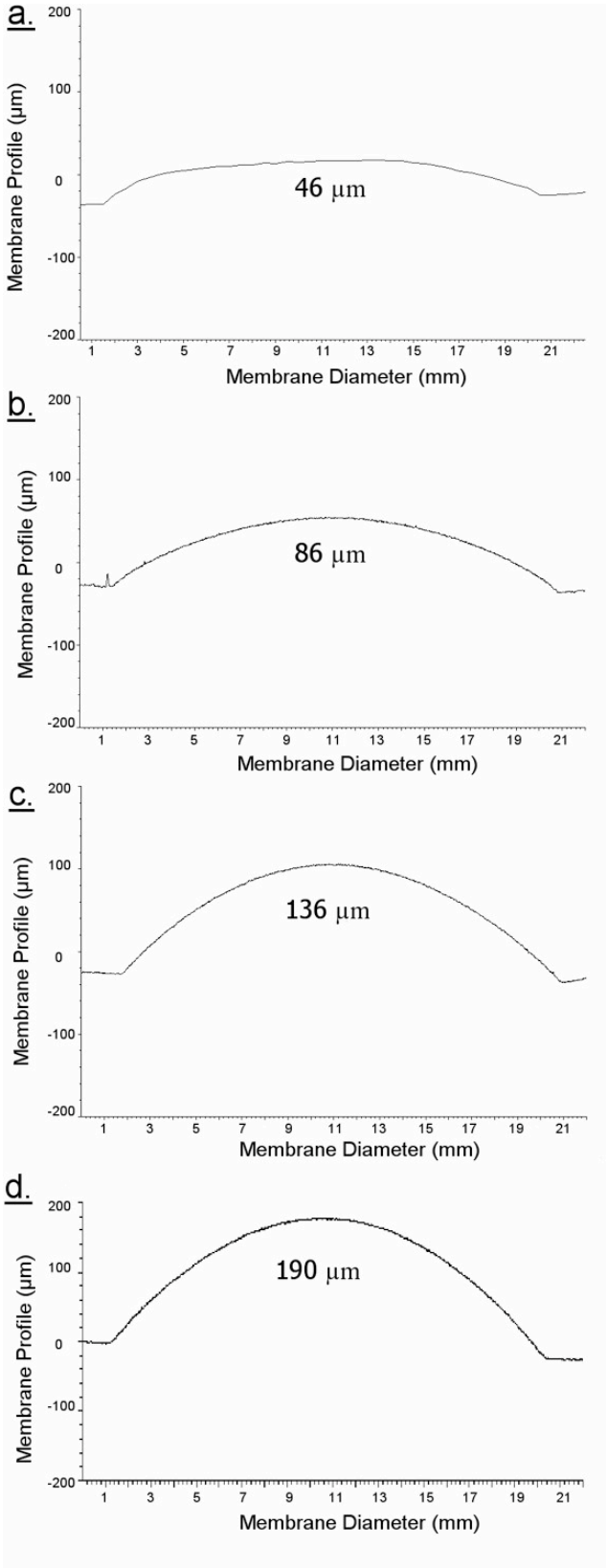

Figure 4.3. Membrane surface profiles at fixed heating rate of 2.5 °C/min. a) high depositing screen (HDS, 165/80) and wide channel (WC, 0.40 mm), b) HDS and narrow channel (NC, 0.20 mm), c) low depositing screen (LDS, 325/40) and WC, d) LD and NC.

The results also indicate that the edges of the membranes tend to fuse to the base due to glass softening in LTCC induced by laser-cutting of samples for SEM analysis (figure 4.4.). These two effects increase the extent of collation for membranes those fired at lower rates, reducing their detectable length and thickness. This decreases the apparent diameter especially for membranes fired at lower heating rates.

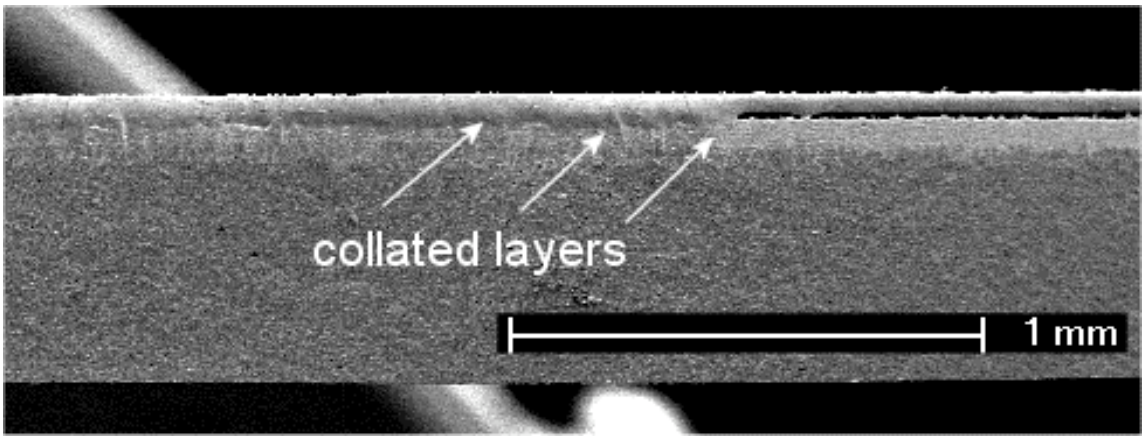

Figure 4.4. SEM image showing the increased extent of collation of layers at the edge (arrows) due to lowest heating rate and laser cutting.

The overall results of this sub-section can be summarized as in the following:

- Heating rate has a more direct effect on the paste oxidation than on the closure of LTCC porosity: faster rates, under the same experimental conditions, lead to swelling of the membranes, confirming the results of the preceding part,
- Changing the channel width allows to control the degree of swelling independently of other parameters, by affecting the ease of oxidation of graphite and degassing of CO/CO_2 (it is also expected that the number of channels and the channel length have the same effect.),
- The facilitation of burnout brought about by large paste thickness has a stronger effect than the increased amount of graphite: overall swelling is reduced. In practice, selecting large graphite thickness leads to more reproducible membrane geometries.

4.2 Membrane displacement and swelling

In light of previous observations, the membranes fired at 2.50 °C/min were used in order to analyze the effect of screen and channel width on functional properties of membranes.

The most interesting feature of samples was found to be the hysteretic behavior of membrane displacement as a function of pressure. The dependence and extent of hysteresis, therefore, was studied in order to determine the relation between the processing conditions and properties of fabricated membranes. The procedure of hysteresis analysis can be listed as follows:

1. The data, which consists of displacement values as a function of pressure, is represented by two terms: origin and the sign. The former one is defined as the displacement value that is equal to zero (z=0), when the membrane touches the base, whereas the latter is positive for increasing membrane–base distance (figure 4.5.).
2. To determine the hysteresis that is representative for each membrane, the derivative of displacement as a function of pressure (dz/dP) is calculated to find the switching pressures defined as the positions of the peaks in dz/dP (figure 4.6.a.). The corresponding displacements are then taken at the center of this switching range (figure 4.6.b.). For this, the data is treated as follows:

P: average pressure over 12 points (ca. ±2 mbar, 3 values/mbar),
dz/dP: slope of the least square linear regression fit of z versus P, over the same 12 points,
P^+: upper switching pressure = peak of dz/dP with increasing P,
P^-: lower switching pressure = peak of dz/dP with decreasing P (figure 4.6.a.),
Pressure hysteresis is defined as $\Delta P=P^+-P^-$,
Center of pressure hysteresis: $P_c=(P^+-P^-)/2$,
z^+: displacement at P_c with decreasing P,
z^-: displacement at P_c with increasing P (figure 4.6.b.),
Displacement hysteresis is defined as $\Delta z=z^+-z^-$

The extent of hysteresis in terms of processing conditions is demonstrated in table 4.2. It is seen that swollen membranes (high spacing) lead to pronounced hysteretic behavior.

Moreover, increased thickness provided by appropriate screens (165/80) in addition to wider channels results in reduced spacing, which will be further discussed in the conclusions.

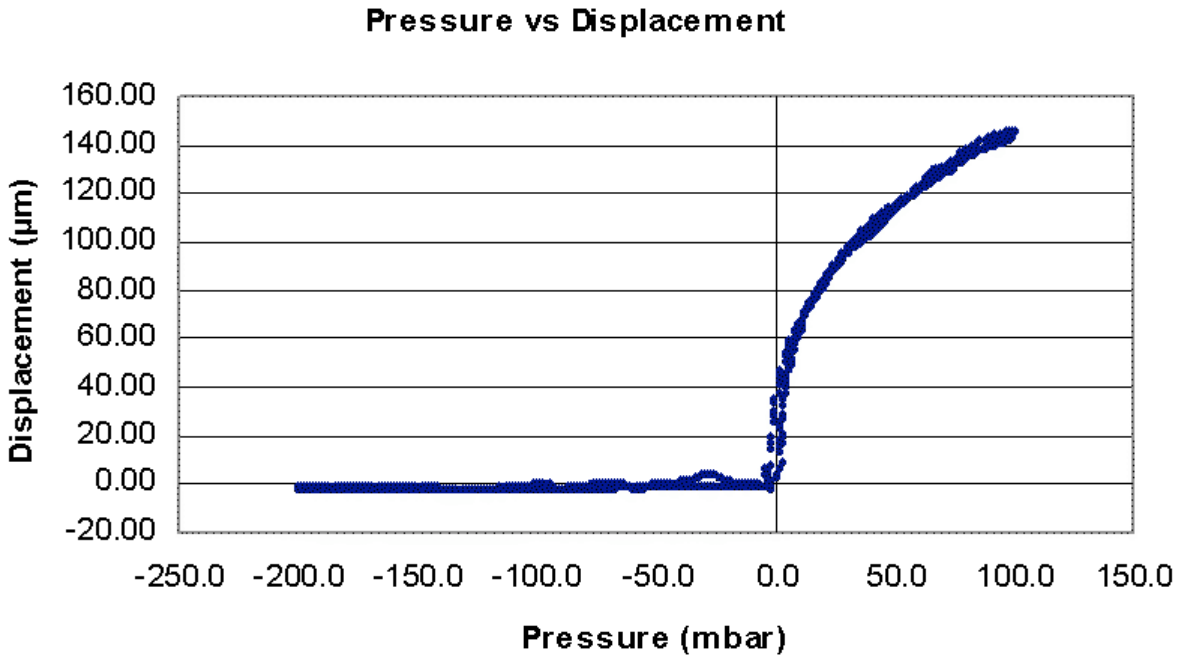

Figure 4.5. Displacement versus pressure (at 2.5 °C/min heating rate and using 165/80 screen with 400 µm-wide channels).

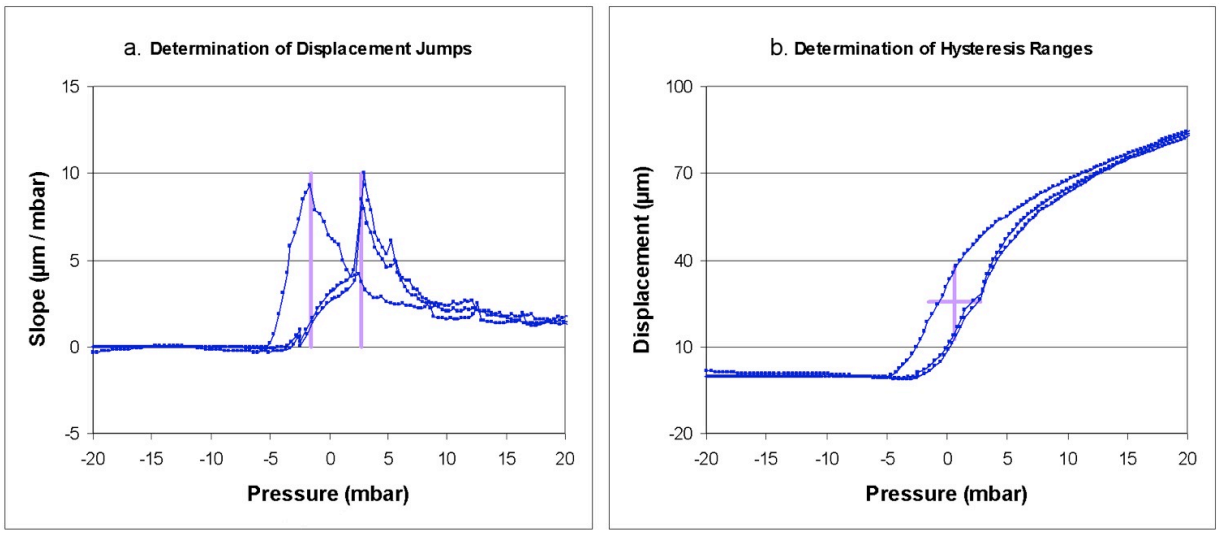

Figure 4.6. Determination of hysteresis parameters of a selected membrane (prepared by 165/80 screen with 400 µm channel width and fired at 2.5 °C/min); a) displacement jumps (left) and b) hysteresis area (3 half cycles: 2 increasing and 1 decreasing).

From the point of view of swelling, on the other hand, membranes with wider channels fabricated from screens providing thicker paste deposition, exhibit reduced swelling. This indicates that the characteristics of the channels, which become the dominant mechanism of degassing upon closure of LTCC porosity, are the most important factors controlling the extent of swelling at a given heating rate. Thus, wider channels promote easy degassing. In the case of paste thickness, our results indicate that the increased channel height brought about by thicker paste more than compensates for the increased amount of carbon to oxidize.

The relation between the membrane displacement and swelling is demonstrated in figure 4.7. and in table 4.2. It is clearly seen that the hysteresis increases with increased swelling, which is observed in membranes fabricated with narrow channels and thin paste. From a general perspective, hysteresis can originate from compressive stresses or deformation of the structure [1-3]. The former effect is thought to be less likely in our application since internal stresses are not expected considering the homogenous structure of LTCC material. Therefore the hysteretic behavior of membrane displacement as a function of pressure is ascribed to swelling.

In conclusion, such swollen fabricated structures, although not favorable for accurate pressure sensing, can be used to achieve a bistable effect in some other micro devices (relays, pressure switches, etc.).

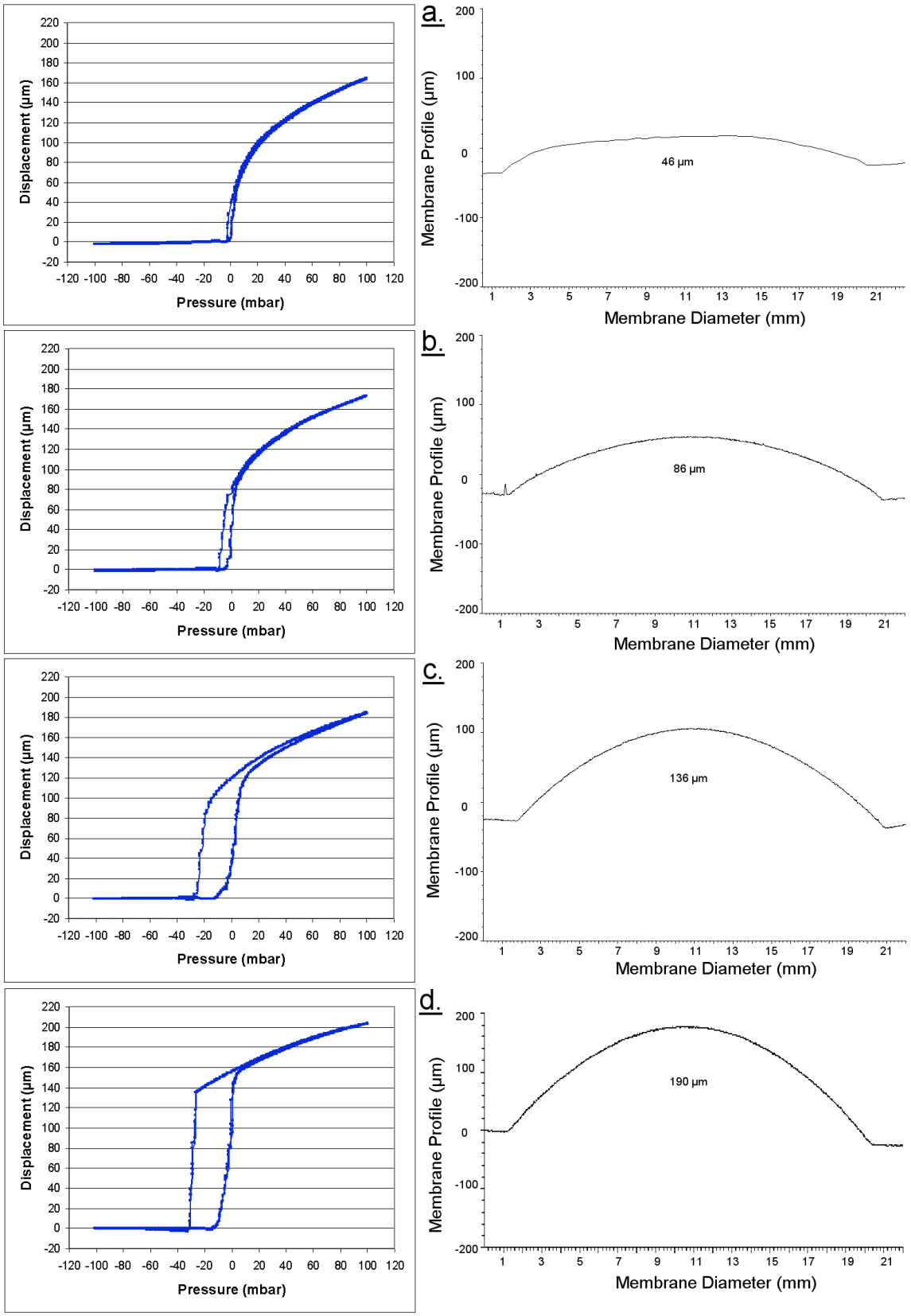

Figure 4.7. Displacement (left column) and surface profile of membranes fired at 2.5 °C/min in terms of screen and channel width: a-b) Screen: 165/80, Channel width: 400 and 200 µm, respectively, c-d) Screen: 325/40, Channel width: 400 and 200 µm, respectively.

Table 2. Hysteresis ranges

Processing parameters	Width of hysteresis P (mbar)	Height of hysteresis Z (µm)	Spacing at the center d (µm)
165/80-0.40	3.8	36.5	37
165/80-0.20	7.1	58.4	57
325/40-0.40	24.1	110	50
325/40-0.20	28.8	148.3	140

4.3 Fabricated structures

The extreme case of swelling, which occurs at relatively higher heating rates, is demonstrated in figure 4.8. Images shown in figure 4.9. on the other hand, represent membranes with smaller spacing, free of swelling or sagging. It is clearly seen that the technique is very efficient and suitable for fabrication of well-integrated LTCC structures with controlled geometry.

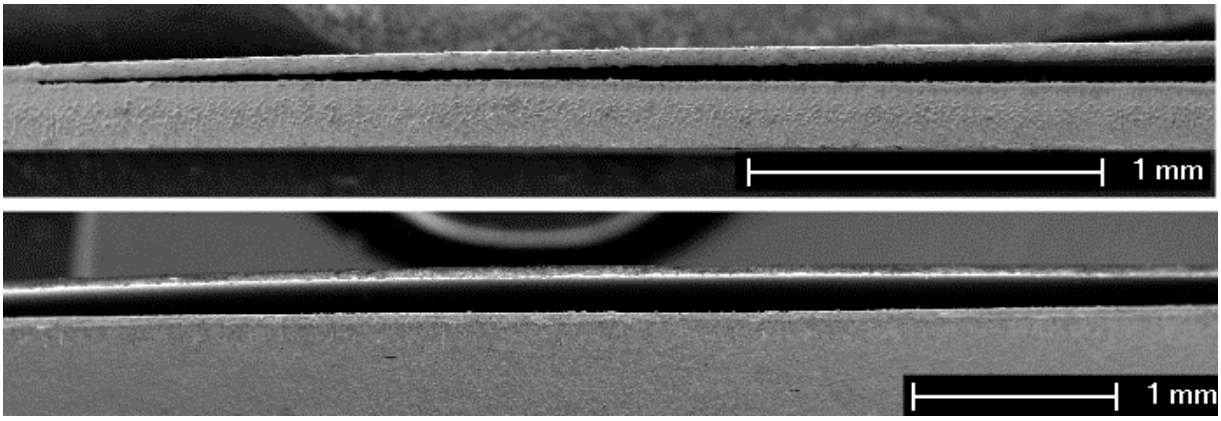

Figure 4.8. a) edge (on the top) and b) middle section of the membranes produced by using 325/40 screens (200 µm-wide channels and 2.5 °C/min heating rate).

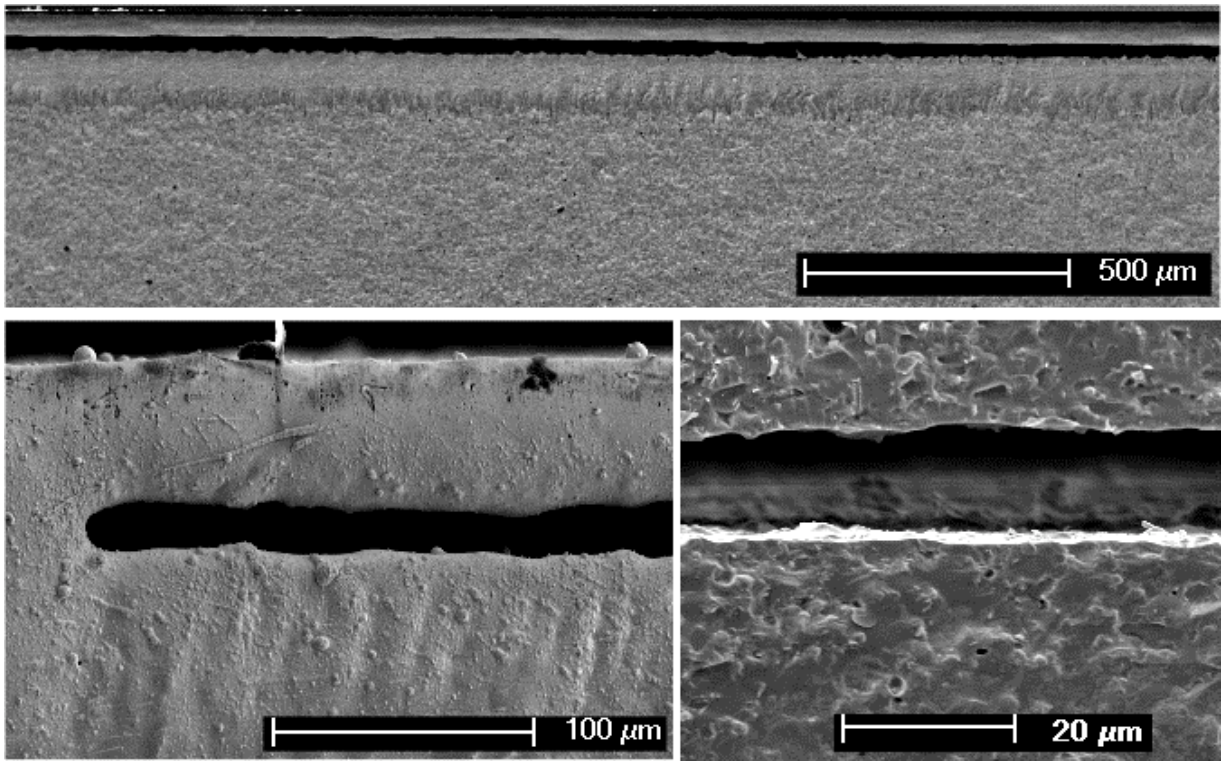

Figure 4.9. Well-integrated and sag-free membranes produced by using 165/80 screens and 400 μm-wide channels (1.75 °C/min heating rate).

By selecting the right parameters (heating rate, large channels and thick paste deposition), sag-free, flat membranes in fully-integrated LTCC layers may be fabricated. They can be used for fabrication of pressure sensors, micro-fluidic devices, etc.

References

1. M. A. Huff, A. D. Nikolich, and M. A. Schmidt, “A threshold pressure switch utilizing plastic deformation of silicon,” in Proc. 6th Int. Conf. Solid State Sensors Actuators, 1991, 177–180.

2. B.Wagner, H.J. Quenzer, S. Hoerschelmann, T. Lisec, M. Juerss, “Bistable microvalve with pneumatically coupled membranes”, in Proc. MEMS '96, 1996, 384-388.

3. R. Arya, M.M. Rashid, D. Howard, S.D. Collins and R.L. Smith, “Thermally actuated, bistable, oxide/silicon/metal membranes”, J. Micromech. Microeng., 2006, vol. 16, 40–47.

5 NOVEL LTCC SENSORS AS ALTERNATIVE TO Al_2O_3-BASED SENSORS

5.1 LTCC as an alternative to alumina

Various substrate materials have been employed in thick-film in addition to electronics, interconnect and packaging technologies [1]. The selection criteria of the ideal substrate are determined by a set of parameters, which can be summarized as in the following:

- Application area: whether intrinsic features of the substrate respond sufficiently to the environmental conditions during operation. Major engineering concerns are related to dielectric constant and strength, dissipation factor, thermal conductivity, thermal expansion of coefficient, Young's modulus, flexural strength, etc…
- Processability: the ease of substrate fabrication, shaping, integration to other functional components such as passive or active electronics.
- Compatibility: whether the substarte exhibits chemical, thermo-mechanical, physical compatibility with the functional components during processing (sintering, soldering, etc).
- Feasibility: cost calculation and optimization.

It is evident that no single material possesses all the requirements for the full range of applications. Alumina among all, however, should be appointed as the most suitable and widely used material for thick-film applications since it combines desirable physical and chemical properties with economical advantages [1].

A recently developing alternative to alumina, within the perspective of the factors mentioned above, is LTCC. Although most of the alumina features seem superior to LTCC substrates at a first glance, novel LTCC applications turn this handicap into otherwise-hard to achieve-advantages in many applications: the lower Young's modulus of LTCC being ideal for force detection [2], and poor thermal conductivity serving as an ideal platform for hot-spot applications [3]. Moreover, the fine and easily machinable LTCC sheets provide the basis for versatile and smart concepts for packaging, sensors and micro-fluidic structures [3, 4]. The

examples will be explained in more details following the LTCC materials compatibility issues section, where details of substrate-integrated element relations will be highlighted and further discussed.

5.2 Definition of drawbacks and solutions

Although LTCC technology is an attractive solution for smart-packaging of micro-electronic devices, numerous studies are still underway to overcome the difficulties encountered during processing and application. These difficulties center on chemical and physical issues occurring between the LTCC components during firing. The chemical issues arise from the interaction of the glass phase(s) in the tape and the thick-films, whereas the physical issues are usually due to the shrinkage mismatch of the tape and the screen-printed pastes. This is observed both microscopically and macroscopically in the form of chemical diffusion (by microscopy and spectroscopy analysis) and deformed structures (warpage, delamination, curling etc.), respectively.

Therefore, the objective of this section is primarily to highlight the importance of control on processing conditions, which have a direct influence on the performance of fabricated devices. This is studied by measuring the TCR (temperature coefficient of resistance) and sheet resistance (R_{sq}) values of a PTC resistor that is screen-printed on commercial electrodes and fired at different temperatures (chemical issues). Next, the origin of apparent defects such as warpage, swelling, etc. will be discussed and solutions developed to reduce these defects will be presented (physical issues).

Experimental

The samples for TCR and R_{sq} measurements were prepared according to the test pattern shown in figure 5.1. As can be seen on the figure, it consists of different resistor lengths, which is ideal to study the effects of interactions near to and away from the terminations on the electrical properties. For this study, the selected thick-film materials (table 5.1.) were screen-printed either on (surface) or within (buried) the LTCC layers according to this layout.

Buried samples were prepared by uni-axial lamination of the screen-printed layer with a blank layer having openings at the contact points (squares on the edge) at 70 °C and under 25 MPa. This was followed by firing the surface-printed and buried samples. Although both

set of samples were co-fired, we would rather, for convenience, call the former as co-fired and the latter as buried.

Firing was carried according to a 2-step profile in an LTCC-oven (ATV-PEO 601) in air atmosphere. Heating rate of 5°C/min was applied until the first dwell time of 120 minutes at 440 °C, which was followed by keeping the same rate until the peak dwell time of 25 minutes at 850, 875 and 900 °C separately. Finally 3 conductor-resistor pairs were prepared in two processing variants as co-fired and buried.

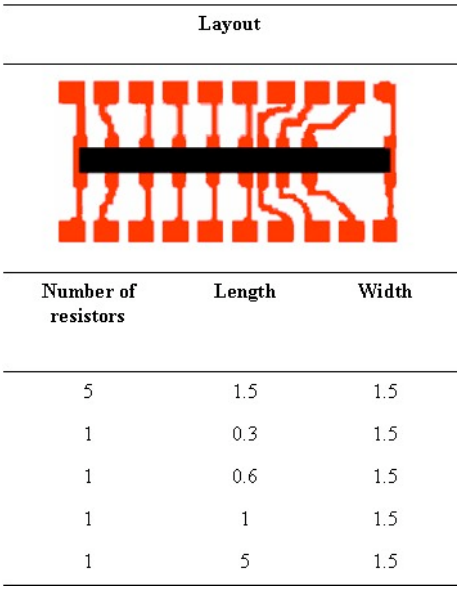

Layout		
Number of resistors	**Length**	**Width**
5	1.5	1.5
1	0.3	1.5
1	0.6	1.5
1	1	1.5
1	5	1.5

Figure 5.1. Test pattern for electrical measurements using PTC resistors. Long rectangle in the middle represents the resistor.

Table 5.1. Materials used for the test patterns

Function	Product	Specification
Substrate	DuPont 951-AX LTCC	Glass-ceramic/ Ca-Al-Si-O
Resistor	ESL 2612	PTC resistor/ Ru-based
Conductor	DP 9473	Classical / Ag/Pd
	DP 5744	Classical / Au
	ESL 8837	Organometallic/Au

Four-wire electrical resistance measurements were performed by a Keithley 2000 and 7000 series multimeter and scanner respectively, while a Pt-1000 PTC resistor recorded the temperature. R_{sq} was measured at 30, 65 and 100 °C and the TCR and standard deviation (SD) was calculated according to

$$TCR = (R_T - R_{25}) / R_{25} (T-25) \quad (1)$$

$$SD = \sqrt{\frac{n\sum y^2 - \left(\sum y\right)}{n(n-1)}} \quad (2)$$

where, R is the resistance at temperature T and n is the number of values (R_{sq} or TCR) measured. It should be remembered that the geometry yielding one for the length to width ratio (width=length) is used to present the TCR and R_{sq} versus processing conditions data (figure 5.2.), as it corresponds to 5 nominally equivalent resistors, which gives sufficient statistical information.

The dilatometry analysis, on the other hand, was carried out on thick-film pellets to study the shrinkage behavior of the electrodes and the LTCC tape. This was made by separating the organics of the pastes in acetone by applying ultrasound and drying the mixture up to 250 °C gradually. The dried product was then crushed in a mortar to prepare the powders. Obtained powders were uni-axially pressed under 25 MPa for 5 minutes. The pellets were then placed into the dilatometer (Setaram), which was operated by the same firing profile described for that of test patterns.

Micro-structural and EDXS analysis were performed using SEM (Philips XLF-30), which is simultaneously operated with an EDXS detector. The cross-sectional areas of both the pellets of single components and the multilayers (tape-conductor-resistor interface) were polished using pastes films of various grain size (from 30 to 0.1 μm). The analysis with the pellets of single components was used as a reference, to explain the materials interaction in the multilayer.

The prepared surfaces were then electroded with carbon, which is the optimum alternative concerning the Au conductors used in this study. The images were taken in back-scattered electron (BSE) mode at 20 keV. On the other hand the oxygen percentage was

calculated by stoichiometry after the atomic percentages of the other elements are normalized to 100.

5.2.1 Chemical issues: processing conditions vs TCR & R_{sq}

TCR and R_{sq} values are presented in figures 2 and 3 respectively, where standard deviation (SD) is shown at the tip of the columns. One can see the firing temperatures as a series of 850, 875 and 900 °C directly under the columns and the 2 processing variants (co-fired and buried) in the x-axis. On the other hand, the y-axis presents the TCR (figure 5.2.) and R_{sq} (figure 5.3.) values. Each triple column in one processing variant represents a commercial thick-film conductor that is fired with the PTC resistor (same resistor for all conductors).

It is evident from figure 5.2. that the buried samples demonstrate a high deviation from the specified TCR range, which is illustrated with red spots around 2400 ppm/K (a value corresponding to the alumina substrate that is fired at 850 °C for 10 minutes with an overall firing period of 45 minutes). Moreover SD reaches to extremely high values, indicating a considerable amount of unreliability.

On the other hand, the dependence of TCR on the selected conductors for co-fired samples is negligible. Although the values do not exactly match the specified range, they are close to it, with small standard deviation.

The irreproducibility and unreliability of the buried samples can be best seen in figure 5.3., where R_{sq} can be an order of magnitude higher compared to the specified R_{sq} of 100 ohm. As a result of this, R_{sq} of the buried samples is represented on a separate y-axis on the right hand side of the co-fired samples for convenience.

It can also be seen from the figure that the R_{sq} of the co-fired samples varies among each other for different conductors, which may be attributed to their different metallurgy and glass phase composition. This will be discussed in more detail in the following sections.

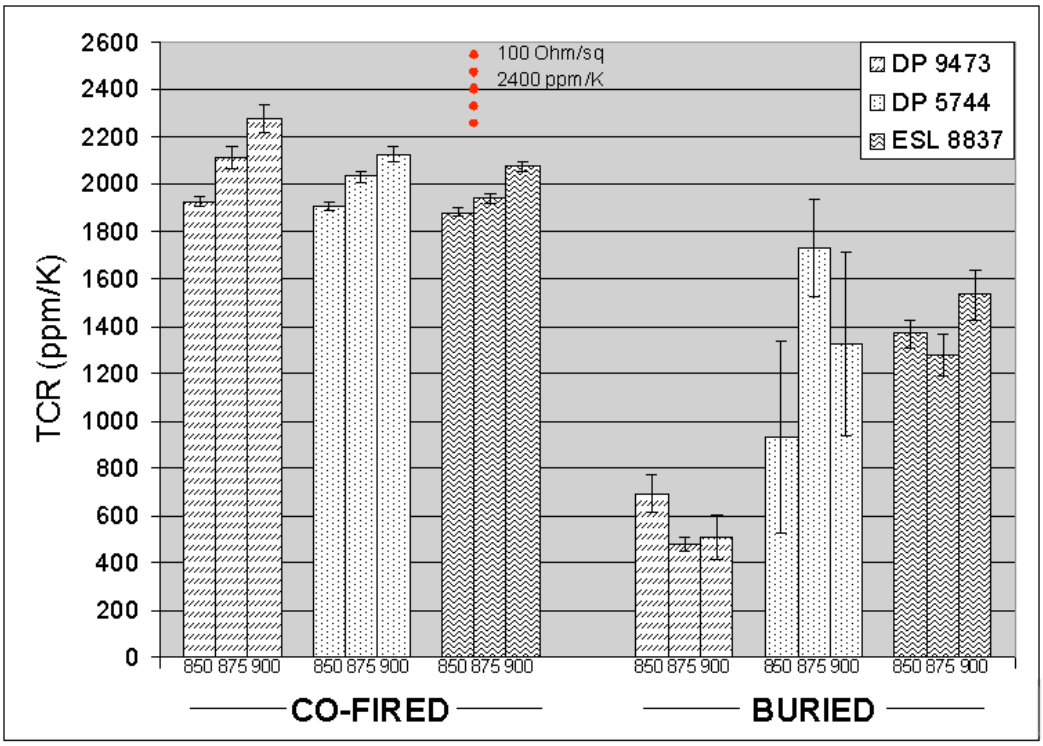

Figure 5.2. TCR versus processing parameters. Buried samples show a strong deviation from the expected values (shown in red spots).

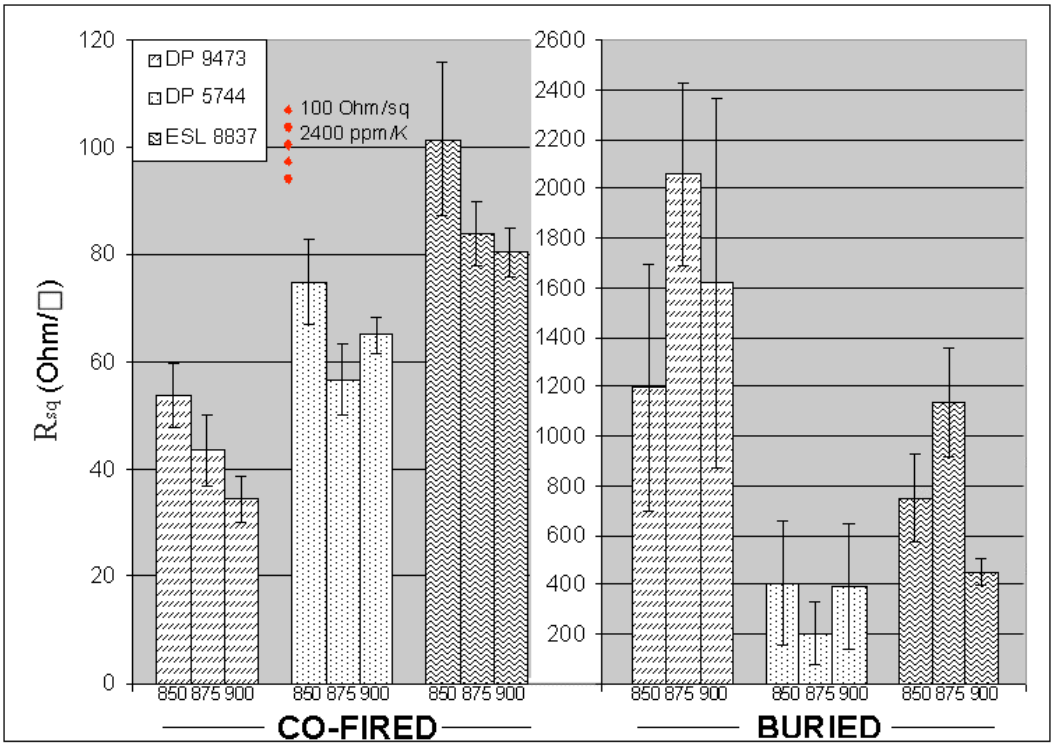

Figure 5.3. R_{sq} versus processing parameters. R_{sq} of buried samples are presented on the second y-axis on the right-hand side of the co-fired samples.

The presented data for buried samples in figures 5.2. and 5.3. were selected from a broad range of values, which varied from very low to very high. The reasons behind this result are mainly ascribed to the chemical interactions between the co-fired components [5-7], which are due to the constituents - especially the glass phase in their compositions - and also diffusion of some species, both of which are directly affected by the processing conditions [8-10].

In this study, this is investigated by analyzing the relation between the TCR and R_{sq} values of the co-fired (surface) samples and the resistor length, which is cited to be a classical approach to check the existence of conductor – resistor chemical reactions [11]. Figure 5.4. shows this relation for the different conductors, which are fired at 850, 875 and 900 °C. Au conductors exhibit an expected stability of TCR with varying resistor length, whereas Ag/Pd shows visible changes. This variation between two metallurgies is also observed in the R_{sq} versus resistor length relation. It is seen from the figure (graphs in the second row) that the samples co-fired with Ag/Pd composition has a R_{sq} value that is less than with the Au conductors and it shows a relatively higher change upon changing resistor length. Among all, samples co-fired with ESL 8837 conductor exhibit the best length dependence and are closest to the specified R_{sq} value of 100 ohm. These results point to a chemical interaction between the Ag/Pd conductor and the resistor, which is stronger than for Au conductors. Thus we focused our attention to the chemical composition of the conductors in order to reveal the origin of this difference between the Ag/Pd and the Au conductors using SEM and EDXS. One must note that screen printing effects (thickness increase near the terminations and ink spreading) also influence R_{sq}.

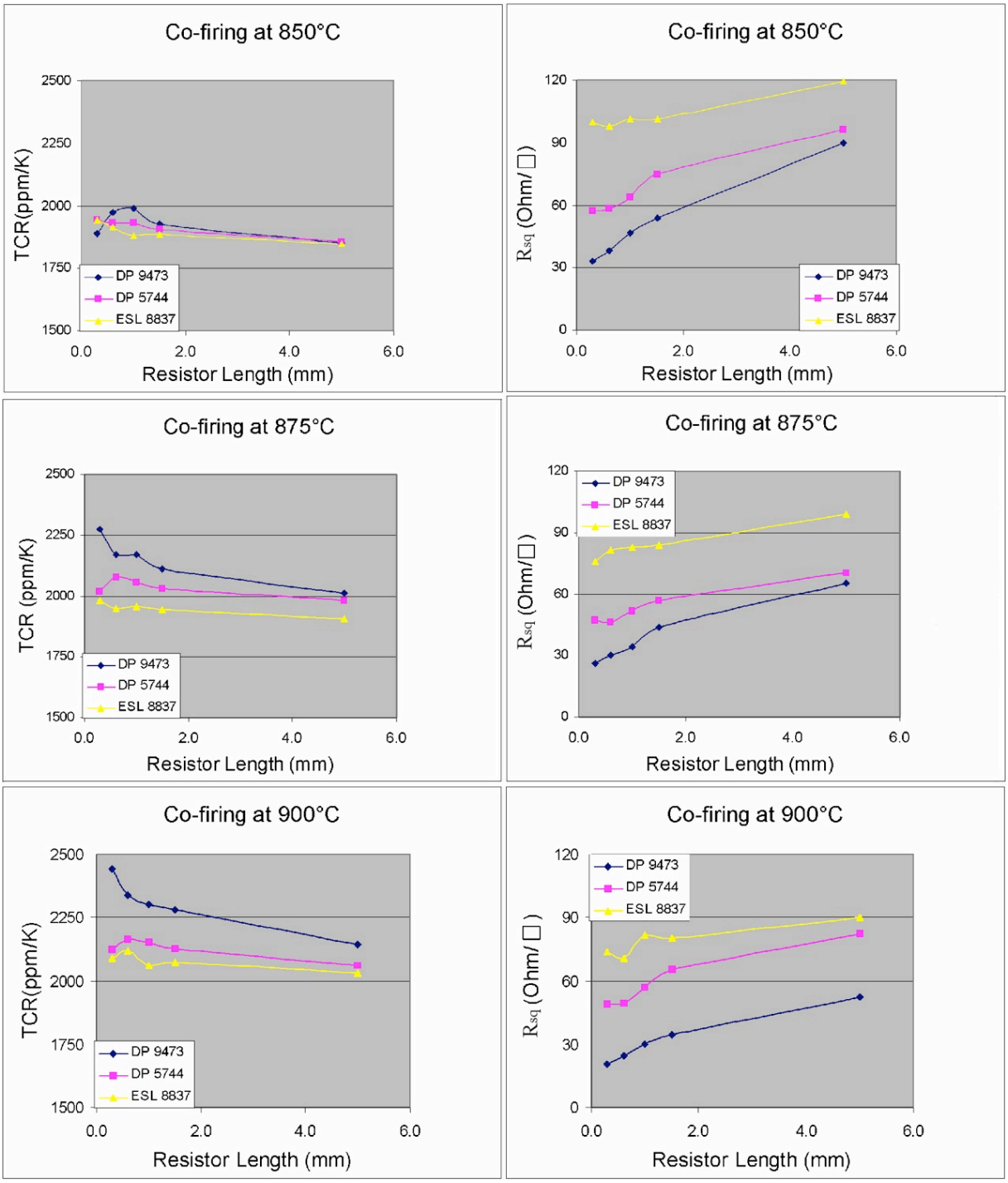

Figure 5.4. TCR (first row) and R_{sq} versus resistor length for conductors fired at 850, 875 and 900°C.

The SEM images, which belong to the pellets of individual conductors, are shown in figure 5.5. It is seen from the images that all the conductors contain two major phases, the ratio of which differs significantly. This is clearly observed in the case of the Ag/Pd conductor (the first picture). Its microstructure shows large, glassy regions between the metallic phase. It is confirmed by the EDXS analysis that it is Bi-Zn-Si-rich glass, whereas the metal is Ag/Pd

phase at 76/24 atomic ratio, which agrees well with the nominal 3:1 value. The distribution of both phases is very uniform in the overall structure.

The second and third pictures correspond to the Au conductors (DP 5744 and ESL 8837 respectively). One can observe local scratches on the surfaces, which are due to the softness of Au making it harder to prepare. Both conductors are composed of 2 major phases similar to the Ag/Pd. However, in this case, the metal (Au) covers by far the largest area in the structure and only a limited portion is formed by the glass phase (large, black particles). In the former one the glass is based on Bi-Pb-Si system whereas it is Pb-Si-Zn in the latter one. It is also observed that the size and distribution of the glass particles are random in both conductors. According to our understanding in light of these microstructures, the glass in the Au conductors is mainly used for adhesion to the substrate. This differs from the fritted-Ag/Pd conductor, where a much larger amount of glass also strongly aids densification. For a better understanding, the elemental analysis of the glass content of the thick-film materials and LTCC tape is presented in figure 5.6. It is clearly seen that Si-Pb-Zn and partially Bi are the main elements used to form the glass phase. It should be noted that boron, which is expected to be in the chemistry of the glass, could not be detected by EDXS system and thus was excluded from the elemental analysis results.

In light of these results (figures 5.4-6.), further SEM and EDXS analysis were performed on the cross-section of the conductor-resistor-tape interface. The focus was made on the Ag/Pd and Au (DP 9473) conductors those co-fired with PTC resistor (figure 5.7).

The first microstructure, which shows 4 different regions, belongs to the sample co-fired with the Ag/Pd conductor. One can see the resistor, the conductor (white), a reaction zone denoted by RZ (light grey area with black, needle-like particles) and the LTCC substrate. Among all, RZ and conductor are the most interesting features of this microstructure.

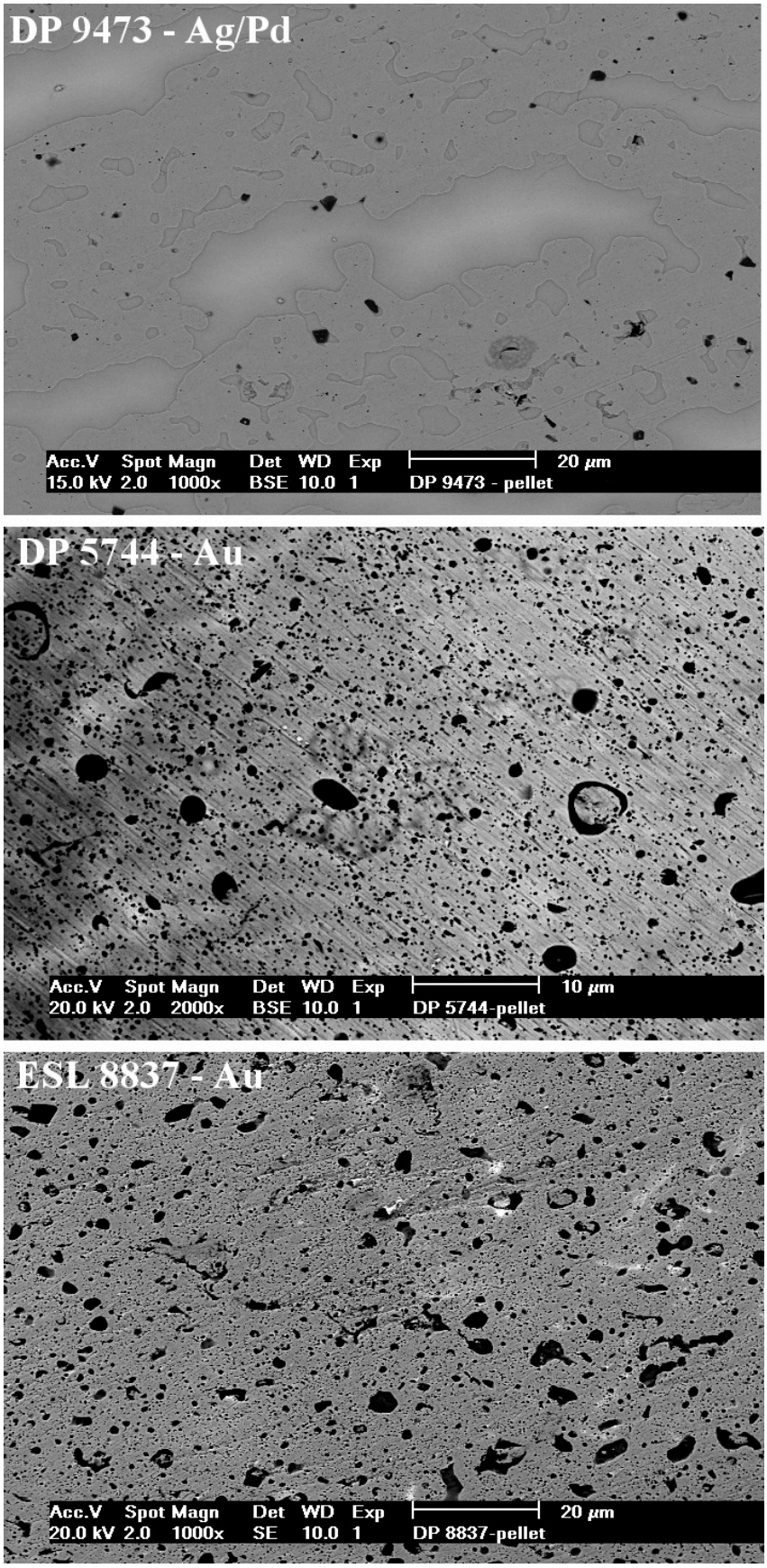

Figure 5.5. Microstructures of conductor pellets (2nd image has a different magnification).

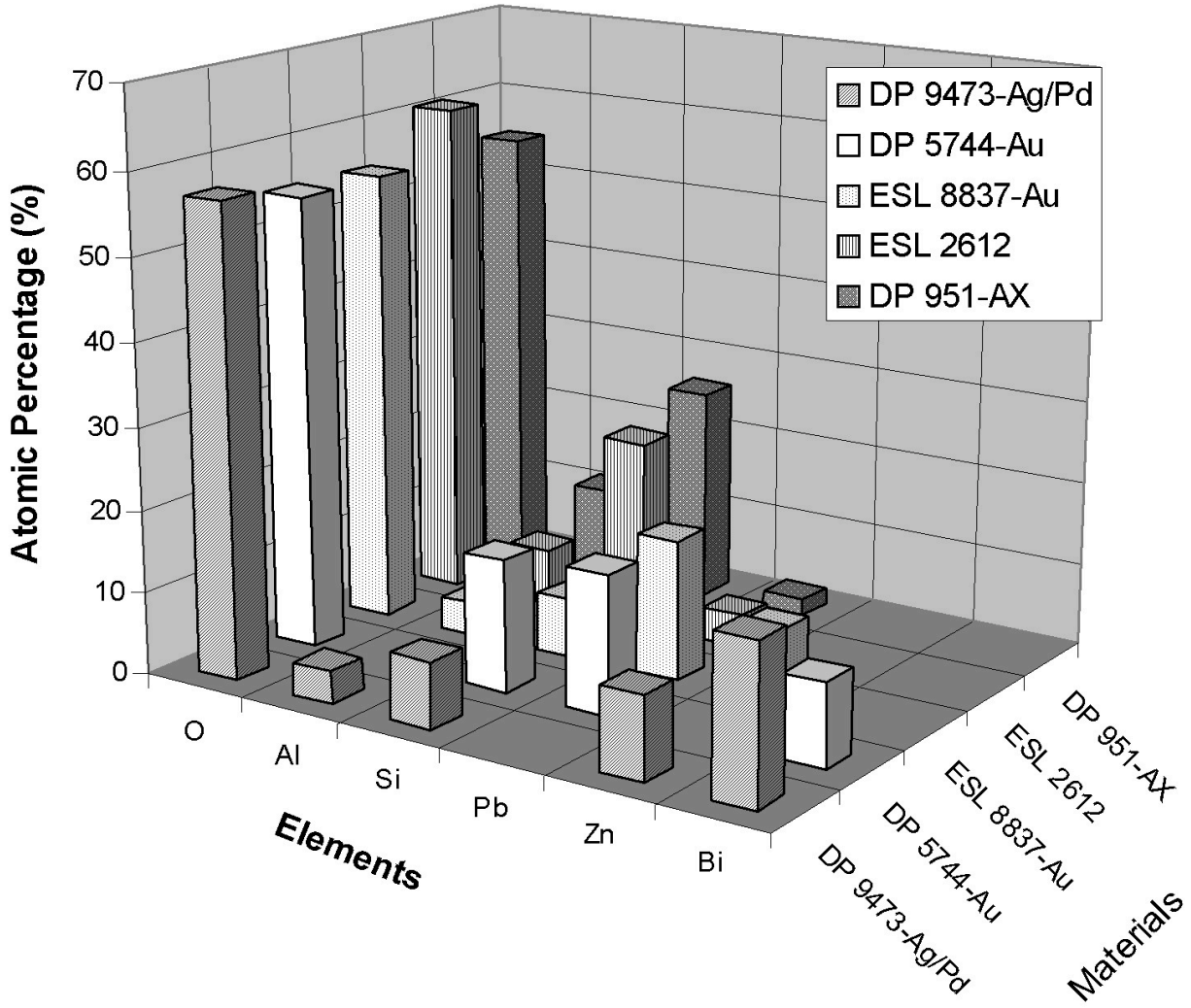

Figure 5.6. EDXS analysis of the glass phase of thick-film material and LTCC tape. Note that only elements those exceeding a certain limit are shown.

The reaction zone, which is observed in a different contrast, is located between the LTCC substrate and the Ag/Pd conductor. An understanding of this region can well be based on the interaction of the glass phases of the LTCC substrate and the conductor, which clearly influences the properties. The extent and the nature of this interaction is best seen in figure 5.8., which shows the EDXS analysis of the Ag/Pd pellet, LTCC and the reaction zone. According to the EDXS results, the reaction zone contains a high amount of Bi that can only originate from the conductor. In a similar manner, Pb (originally absent in the conductor) is found in the close neighborhood of it. On the other hand, the sample co-fired with the Au conductor does not exhibit a visible reaction zone and the conductor line is not significantly altered by any kind of penetration or diffusion.

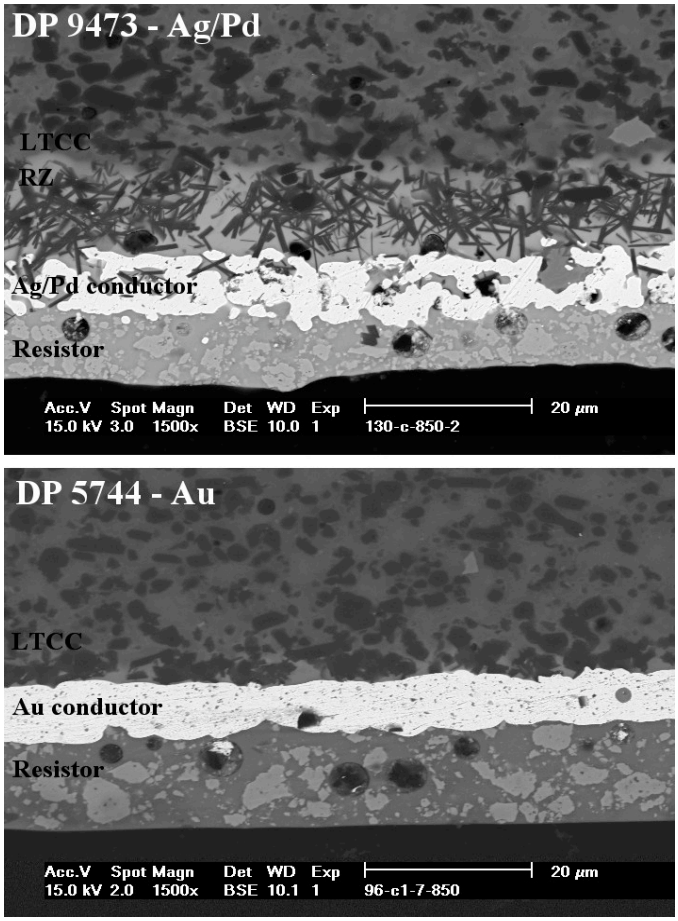

Figure 5.7. Microstructures of Ag/Pd (above) and DP 5744-Au co-fired samples.

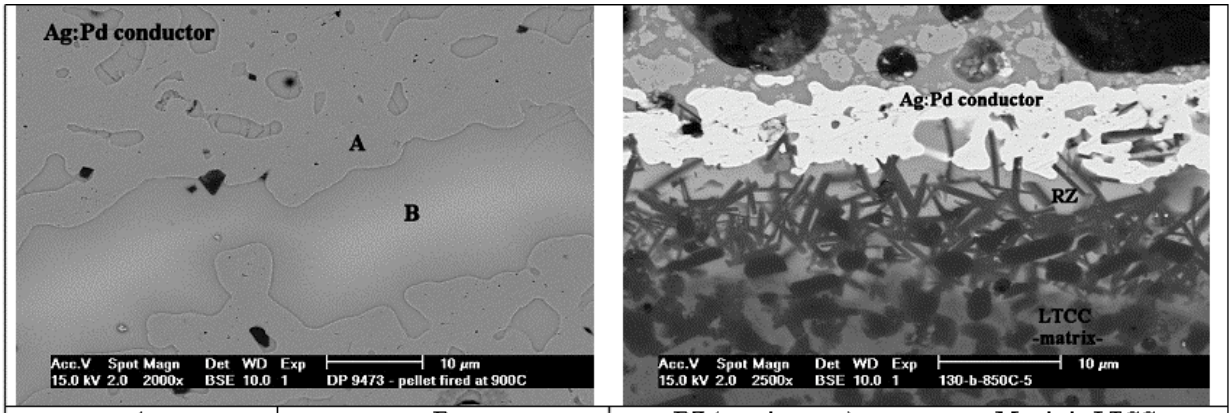

A		B		RZ (reaction zone)		Matrix in LTCC	
Element	Atomic %	Element	Atomic %	Element	Atomic %	Element	Atomic %
Ag	76	O	57	O	59	O	55
Pd	24	Zn	10	Na	4	Al	10
		Al	4	Al	10	Si	26
		Si	8	Si	15	Pb	2
		Bi	18	Pb	4	Ca	3
		Others	3	Bi	6	Na	2
				Others	2	Others	2

Figure 5.8. EDXS analysis of the reaction zone (RZ), located between the conductor and the LTCC.

Therefore, the relation obtained in the TCR/ R_{sq} versus resistor length analysis (figure 5.4.), which demonstrated a less favorable result for the Ag/Pd conductor, is explained using the SEM and EDXS. It is observed that the glass content of the Ag/Pd conductor reacted strongly with that of the LTCC, which accordingly influenced the electrical properties.

5.2.2 Physical issues: swelling in buried samples and warpage

As explained previously, physical issues arise mainly from the shrinkage mismatch of the tape and the thick-film pastes [12-13], which can in the most severe cases, destroy the fired structure. This will later be discussed in detail with solutions developed to reduce it. However, another defect, which turned out to be the major cause for unreliable electrical properties presented in the previous part, will be treated primarily: swelling inside the buried structures (Figure 5.9.). Formation of cavities at the conductor-resistor intersection was interestingly observed only in samples with buried Au conductors (classical and organometallic) and not with the Ag/Pd.

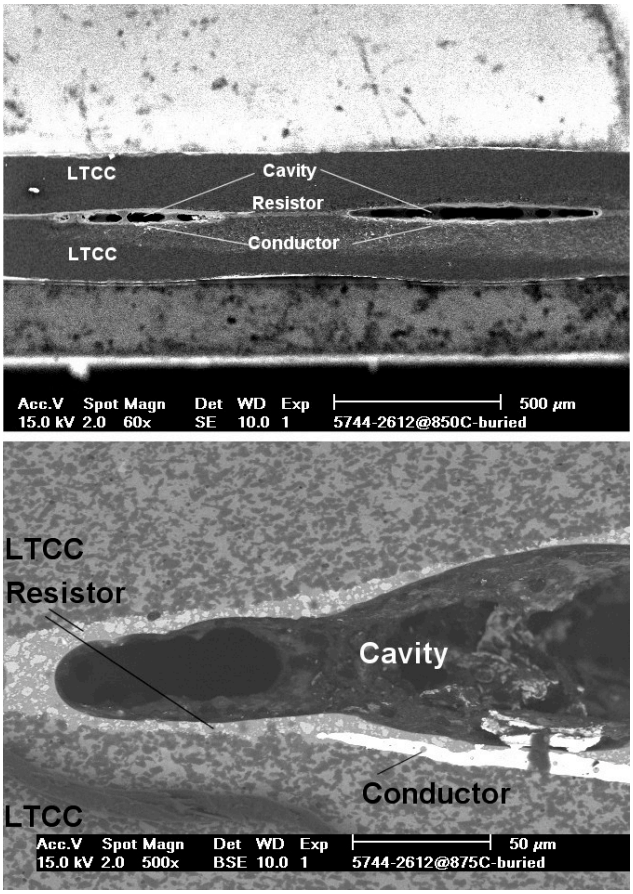

Figure 5.9. Cavities in the DP 5744 buried sample.

It is strongly supposed that cavity formation is either due to a high temperature oxidation-reduction reaction or organics burnout as a result of which gas evolution occurs. It is previously shown that the porosity is eliminated around 785 °C. Thus any reaction that leads to gas liberation (reduction, organic burn-out, etc…) after this temperature increases the gas pressure between the LTCC sheets of the buried sample and deforms the structure.

To check the validity of this statement, we fired buried samples with Au (DP 5744) conductor at different temperatures. A series of SEM images, which shows the corresponding structures, is shown in figure 5.10.

According to our current understanding, the formation of the gas, which probably arises from elemental interaction above 785 °C or reduction of an oxide, is estimated to cause the observed effects shown in figures 5.9. and 5.10. Another interesting result is that the samples buried with Ag/Pd conductors did not show this type of deformation at resistor-conductor contact.

In order to better understand the origin of this deformation, we buried the individual pastes by screen-printing them on LTCC sheets. Upon firing, we observed that ESL 2612 resistor paste only resulted in swelling-type deformation, whereas neither Au nor the Ag/Pd conductors alone caused swelling in the buried structure. Thus, the Ag/Pd conductor apparently suppresses the occurrence of swelling, through the large amount of chemical interaction it exhibits. However, the exact mechanism of cavity formation and suppression thereof remains unclear.

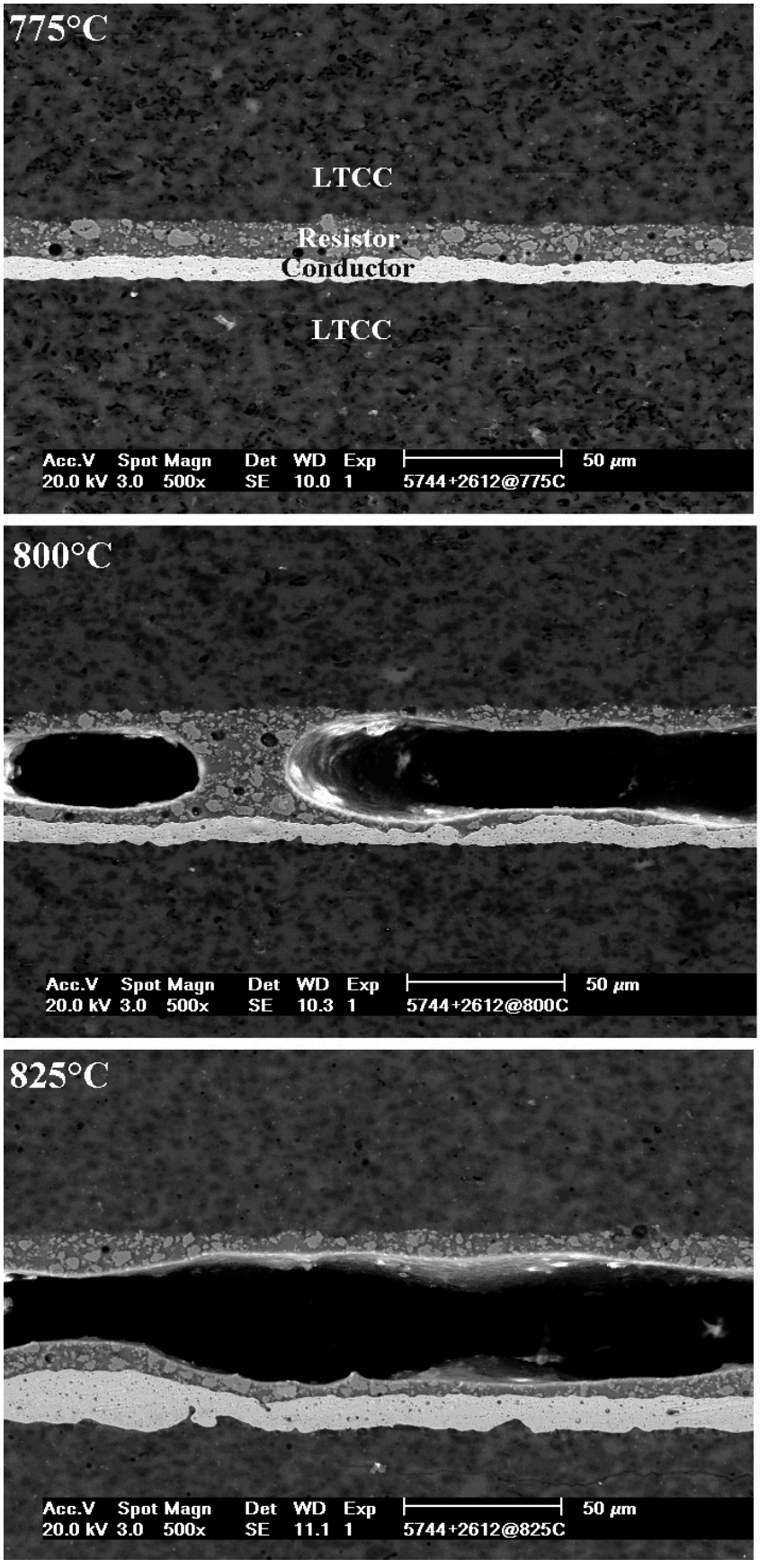

Figure 5.10. Extent of deformation in buried samples, fired at different temperatures.

Differential shrinkage between the components of an LTCC module is the main origin of deformation such as warpage, curling, etc (figure 5.11.), which is an undesired consequence in applications (membranes, channels, etc.), but it is an interesting topic in science. Thus, in this section we propose a method to match the shrinkage rates of the tape and the conductor to reduce deformation.

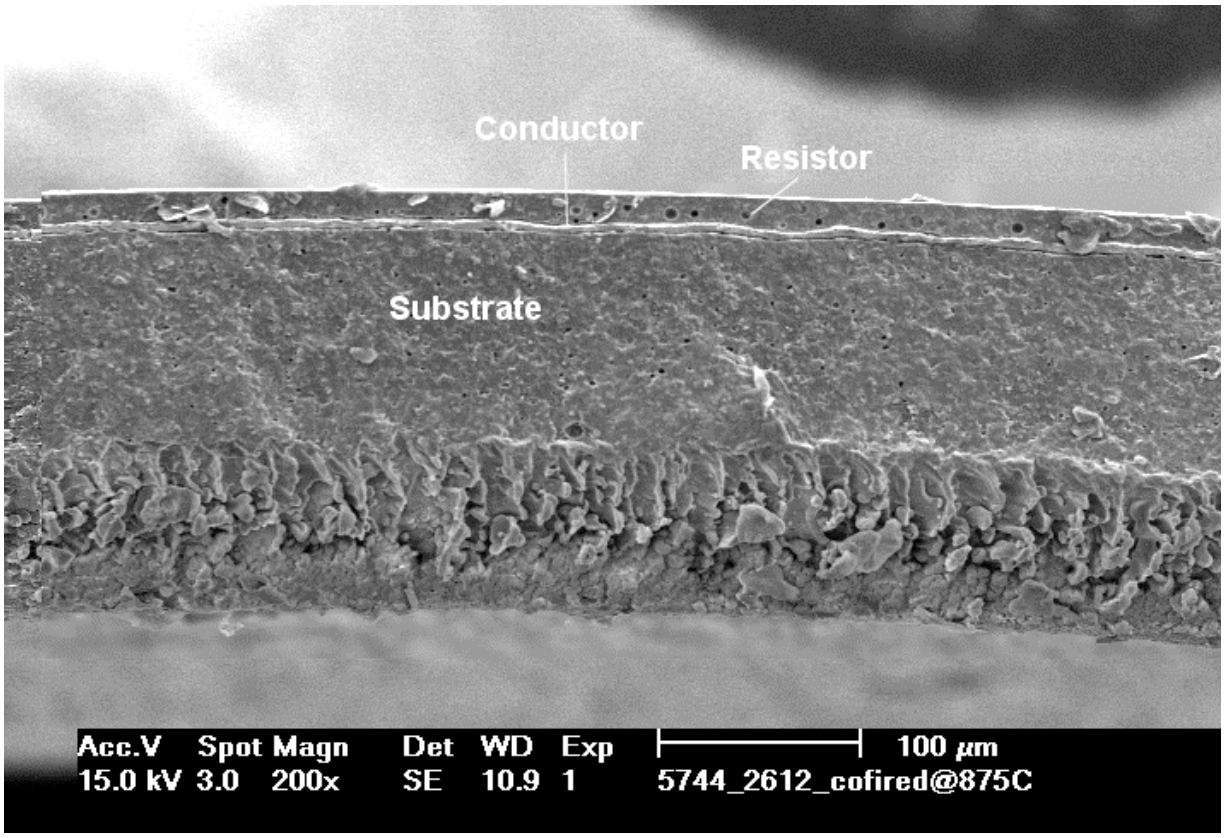

Figure 5.11. Warpage on the LTCC tape due to unmatched shrinkage between the conductor and the LTCC tape.

In order to match the shrinkage behavior of the conductor to that of the LTCC tape, we basically mixed the commercial conductors - DP 9473 Ag/Pd used in this study and ESL 9562 Ag/Pd/Pt – with selected additives. The exact description of the used materials is presented in table 5.2. Mixtures were prepared with to 10 or 20% of additive (prepared from SiO_2 powder –commercial- and LTCC tape according to the method described previously) to paste ratio by weight, which was followed by homogenization in the three-roll mill. Part of the prepared paste was then dried to make the dilatometry analysis, and the rest was screen-printed on the LTCC sheets for co-firing with the PTC resistor used in this study.

Table 5.2. Materials used for modification of pastes

Paste	Specification	Additive	
		SiO_2*	LTCC
DP 9473	Ag/Pd	10%	10%
		20%	20%
ESL 9562**	Ag/Pd/Pt	10%	10%
		20%	20%

**SiO_2: Sihelco, Sikron B 600*
*** Fritless conductor with Cu additions (Ag/Pd~16)*

The results of the dilatometry analysis, being the method used for figure of merit – shrinkage, are presented in figure 5.12. It is seen in both graphs that the additives play different roles on the shrinkage behavior of the pastes. For instance, addition of LTCC powder, which was aimed to establish a shrinkage behavior similar to that of the tape, results in expansion starting from 700 °C. On the other hand addition of SiO_2, which is known to increase the glass transition temperature by promoting network formation [13], leads to a shrinkage behavior that is similar to the tape.

The effects of the more favorable additive - SiO_2 - is presented in table 5.3., which is derived from figure 5.12. The onset temperature of the paste shrinkage can be effectively pushed up to that of the LTCC tape. In case of the modified DP 9473 paste, this is seen as a considerable shift of both sintering temperature range and the amount of shrinkage.

Thus, we prepared new samples by screen-printing the commercial DP 9473, its doped versions with 20% SiO_2 and 10% LTCC on the tapes and checked the deformation on the surface of the co-fired samples (figure 5.13.). We used the LTCC powder-added paste in order to check the final deformation on the structure, although its dilatometry data follows a different trend.

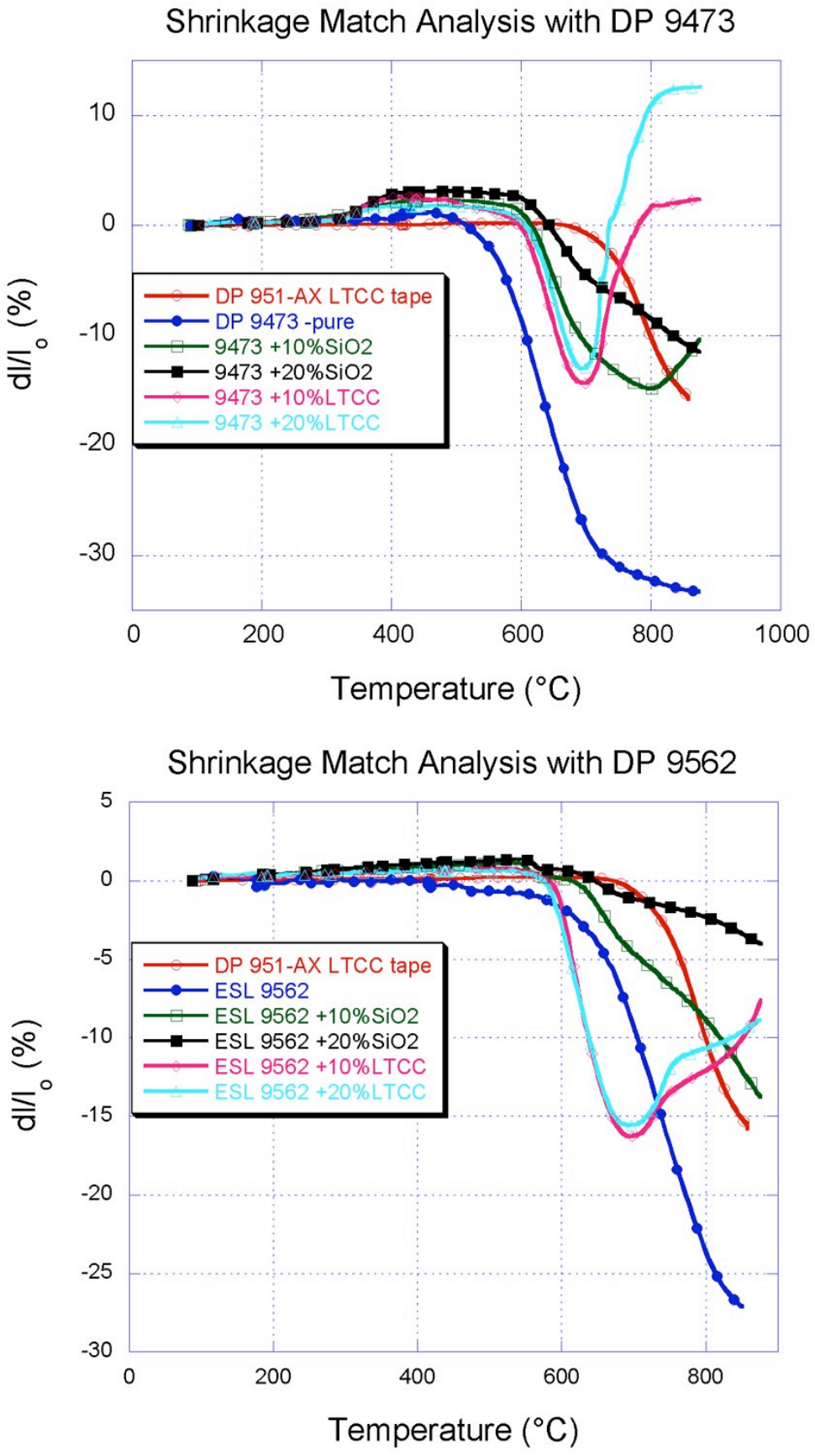

Figure 5.12. Dilatometry analysis for the modified pastes.

Table 5.3. Effect of SiO_2 addition on pastes

Paste (ratio of additive)	$T_{shr.}^{+}$ (°C)	%Shrinkage^{++} (-)
DP 9473	516	23
DP 9473 + 10%	618	7.7
DP 9473 + 20%	644	2.3
ESL 9562	430	5.5
ESL 9562 + 10%	615	3
ESL 9562 + 20%	646	0.7

$T_{shr.}^{+}$:Onset temperature of shrinkage of the paste($\Delta l/l<0$)
%Shrinkage^{++}: Amount of paste shrinkage at the onset temperature of the tape shrinkage (670°C).

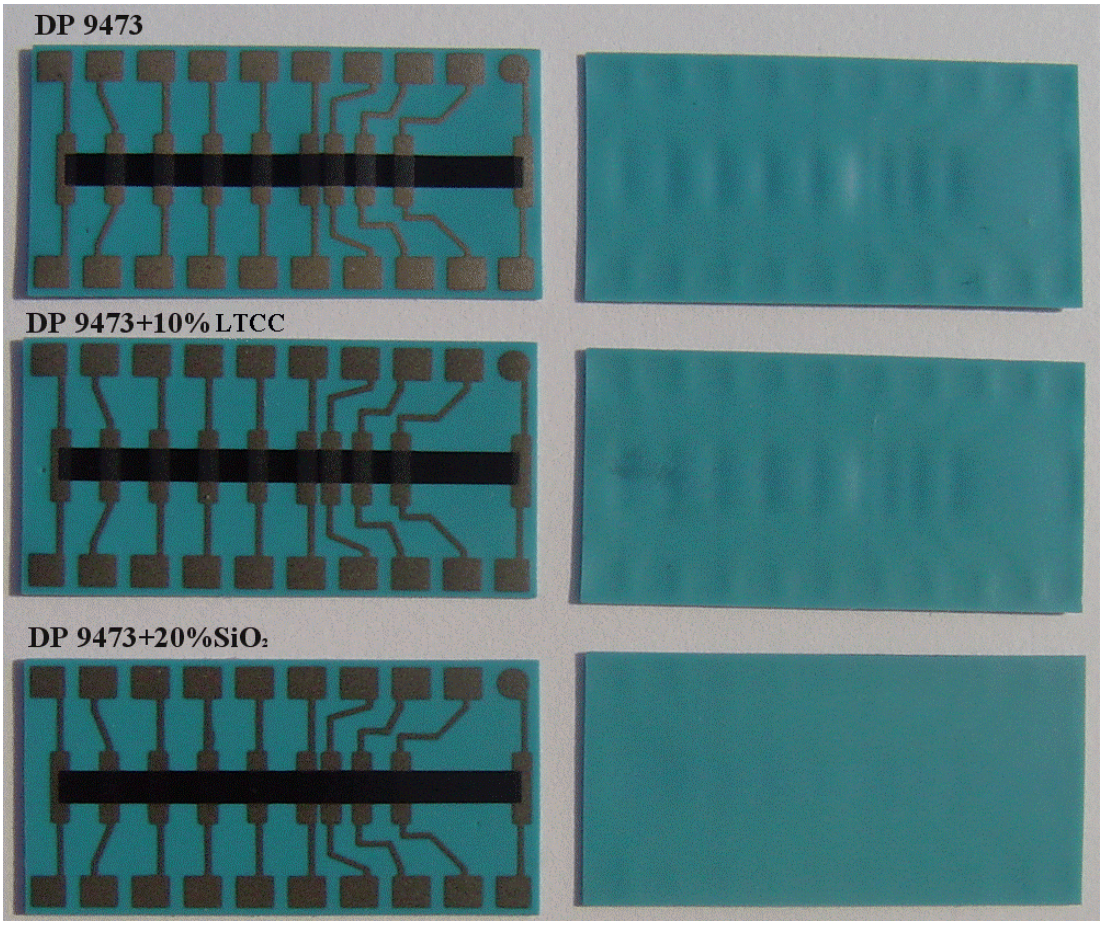

Figure 5.13. Pure (first row) and doped DP 9473 pastes co-fired on the LTCC tapes. Column on the right hand side shows the back-sides of the samples.

Doping with 20% SiO_2 addition clearly yielded almost no deformation on the tape. Moreover firing this paste on 114 μm-thick LTCC tape (Du Pont 951-AT) also resulted in limited deformation.

Following this result, we made SEM analysis to see the effects of modification on the microstructure. Figures 5.14. and 5.15. compare the microstructures of the pure and the 20% SiO_2-added DP 9473 pellets and tape-conductor-resistor interface, respectively.

In figure 5.14., the effect of SiO_2 powder addition can be observed clearly by the modified microstructure. They are seen as black particles homogeneously dispersed in the matrix (Ag/Pd seen in white) in different size and morphology, which have not reacted with the glass in the conductor as confirmed by the EDXS analysis. It is believed that the addition of SiO_2 powder has increased the viscosity of the glass as a result of which the shrinkage rate of the modified conductor paste is delayed. Thus, the onset of shrinkage temperatures of LTCC and the conductor are matched, resulting in reduced deformation related to differential shrinkage.

In figure 5.15., on the other hand, it is remarkable that the conductor line in the modified (second image) version is mostly discontinuous. This is observed to be due to the SiO_2, which is seen as longitudinal black particles located in the conductor line (large, black circles in the resistor are pores).

We finally checked the electrical properties of the new pastes with 20% SiO_2 and 10% LTCC. The TCR and R_{sq} values of the pastes those co-fired at 875 °C are shown in figure 5.16. The influence of SiO_2 and LTCC powder addition is directly observed as an increase of R_{sq}. It is evident that these species increase the resistance considerably - by a factor of 2. However the value of TCR did not deviate significantly from that of the pure paste. It is interesting that the modified pastes reach a R_{sq} value that is expected for the commercial paste by specification.

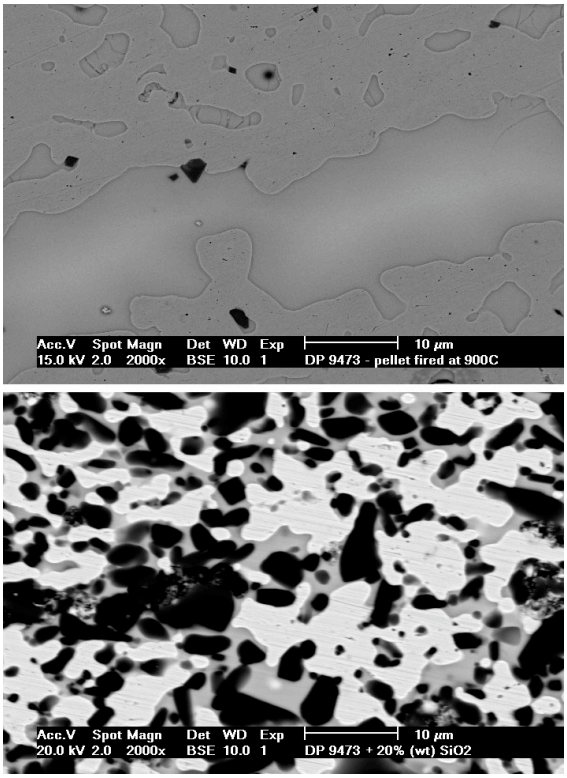

Figure 5.14. Pure (first) and 20% (wt) SiO_2 added DP 9473 pellets. The microstructure changes upon addition of SiO_2.

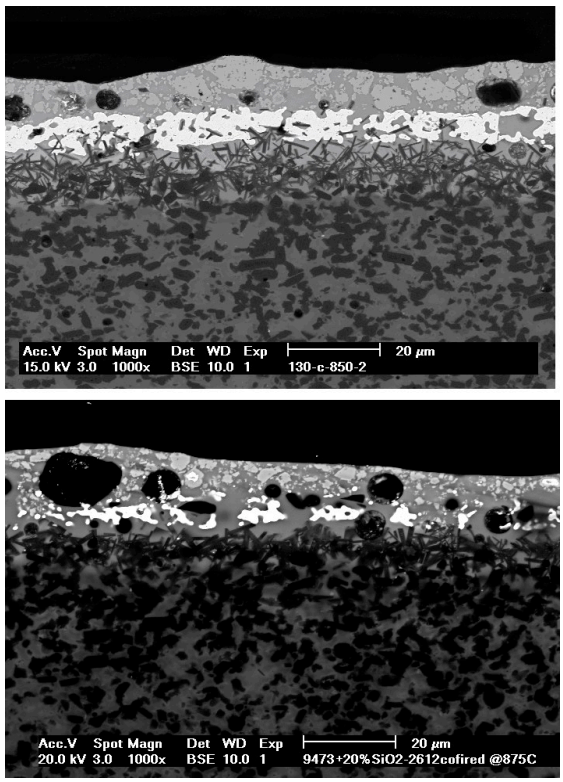

Figure 5.15. Cross-section of the tape-conductor-resistor interface co-fired. Pure (first) and 20% SiO_2-added DP 9473 conductors.

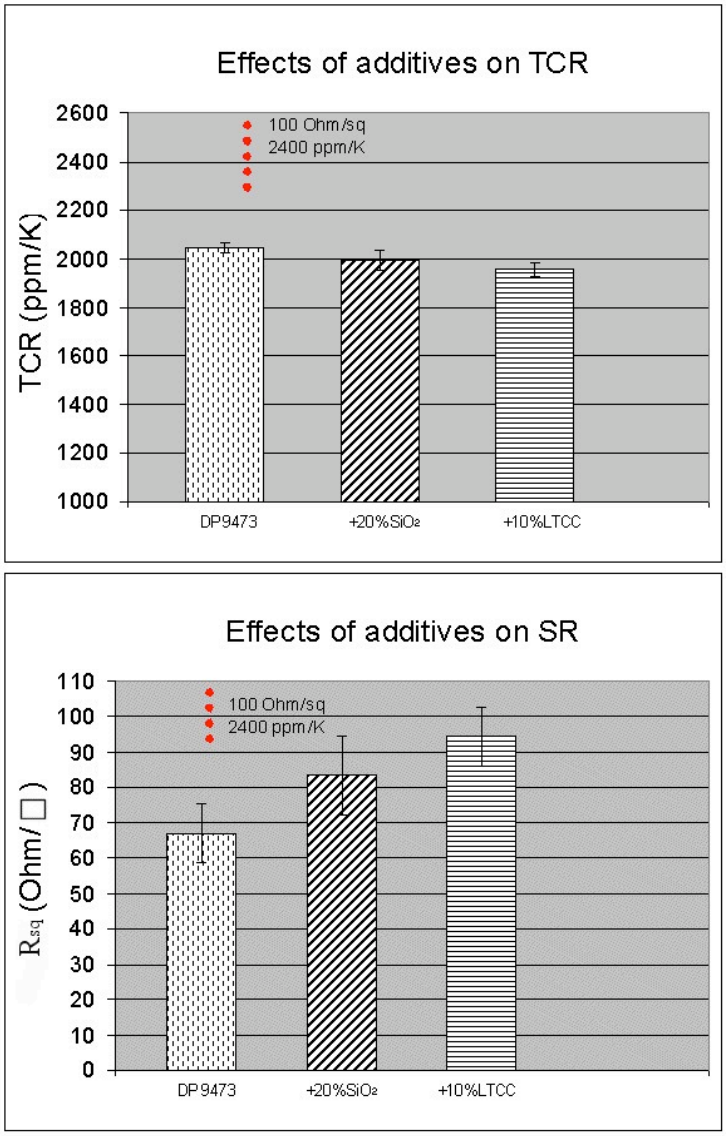

Figure 5.16. Effect of additives on TCR (above) and R_{sq} of PTC resistor.

As summarized, processing conditions have a major influence on the properties of the selected thick-film compositions, particularly PTC resistors. The results are grouped as chemical and physical issues, which are discussed according to the important observations made.

The chemical issues are classified as those, which are provoked by the glass content of the thick-film composition. It is shown in details that the composition and the quantity of the glass phase in the selected thick-film paste is prone to chemical interactions with the surroundings, the extent of which can alter the final electrical properties.

Deformations such as warpage, swollen buried structures (partially) are treated in the physical issues section. Swelling is attributed to the imprisoned burnout products of the pastes

in the buried LTCC upon porosity elimination around 785 °C. The latter defect on the other hand, stems from the densification of the thick-film pastes much prior to the tape and thus deforming the whole structure. A method is proposed with the aim of overcoming this problem, which is based on doping the paste. The results show that the selected additive yields satisfactory results both in physical and electrical properties, by almost eliminating the deformation on the tape and not altering the value of TCR considerably.

In light and as a result of these results, some of the fabricated sensors are demonstrated in the following section.

5.3 Fabrication and characterization of LTCC sensors

5.3.1 Viscosity sensor

Natural gas is an environment-friendly energy source that is reliable and feasible. Current trends indicate an increase in its application in the next 20 years [14-18] and thus, further optimization of its combustion is required for increased benefits. The major challenge at this point arises in determination of the composition of the natural gas, which is actually a mixture of various gases [19]. This feature is also known as the gas quality and the variations in it leads to inaccuracy in the amount of oxidant by which the fuel has to be mixed in the burner. This ratio of fuel to air is called the equivalence ratio and it determines the efficiency of the combustion process. Variations in the gas quality, thus, pushes this ratio out of the high efficiency range and results in poor burner performance in addition to many other undesired effects such as high emissions of NO_x, CO and CH, ignition and thermoacoustic problems [20].

Therefore, to maintain stable, safe and efficient combustion, the gas quality, which is expressed by Wobbe number (the link to the equivalence ratio of a gas), W_o must be taken into consideration [19-20]. W_o in addition to the calorific value of a gas is correlated with its viscosity, which has been the starting point of our study: fabrication of a LTCC-based gas viscosity sensor to determine W_o.

The principle of the sensor is based on capillary viscosimetry: the pressure drop of a gas through an orifice is expressed by its density and viscosity, which is in our case measured by analyzing the relaxation behavior of a pressurized volume of gas through a capillary (fluidic resistor) [21]. The sensor is fabricated using DuPont 951 LTCC green tapes and

commercial thick-film components integrated with the corresponding major units of the sensor (table 5.4.): heater module, pressure-sensing membrane and the meander (fluidic resistor) (figure 17).

The chamber (heated volume) is periodically heated by a thick film resistor that is screen-printed on a thin LTCC sheet suspended in the heating chamber. The heater module is fabricated by laser cutting green tape (for membrane opening and lateral slits aside the membrane to reduce heat losses) and laminating the support and the membrane layers between the two flat plates (Figure 5.18.a.). The heater cavity is completed by gluing a heat conducting lid on the top using Dow Corning Q5-8401 silicone adhesive (Figure 5.18.a.). The completed heater and membrane modules are finally assembled onto base using the silicone adhesive and the electrical connections to the base were realized by Au wire bonding and conductive epoxy adhesive, respectively. The membrane and the meander are fabricated using carbon sacrificial paste technique as explained previously in detail.

Turning on the heater causes an increase of average gas temperature in the cavity, thermal equilibrium in the membrane being established fast due to the small thermal mass and enhanced cooling of outer walls. The resulting pressure is measured by the membrane (figure 5.18.b.), and its relaxation is limited by the meander that acts as a fluidic resistor.

The viscosity of the gas is finally measured by its characteristic relaxation time in the meander. The relaxation behaviors of thick (viscous) and thin gases in terms of temperature cycles in addition to sensor principle are schematized in figures 5.19-20. The performance of the completed sensor by the time of thesis submission was under investigation.

Table 5.4. Parts of the sensor

Part	**Base and meander**	**Membrane**	**Heater**
Basic method	Sacrificial C	Sacrificial C	Cutting
LTCC tapes	2A+B	2A+B	A+B
AgPd	DuPont 7484	DuPont 7484	DuPont 7484
Au	-	ESL 8837	DuPont 5744
Resistor	-	DuPont 5092 D	DuPont 5092 D
Thick-film firing	Post-fired	Post-fired	Post-fired

A = thick tape, 254 µm green → 210 µm fired
B = thin tape, 50 µm green → 40 µm fired
C = sacrificial paste

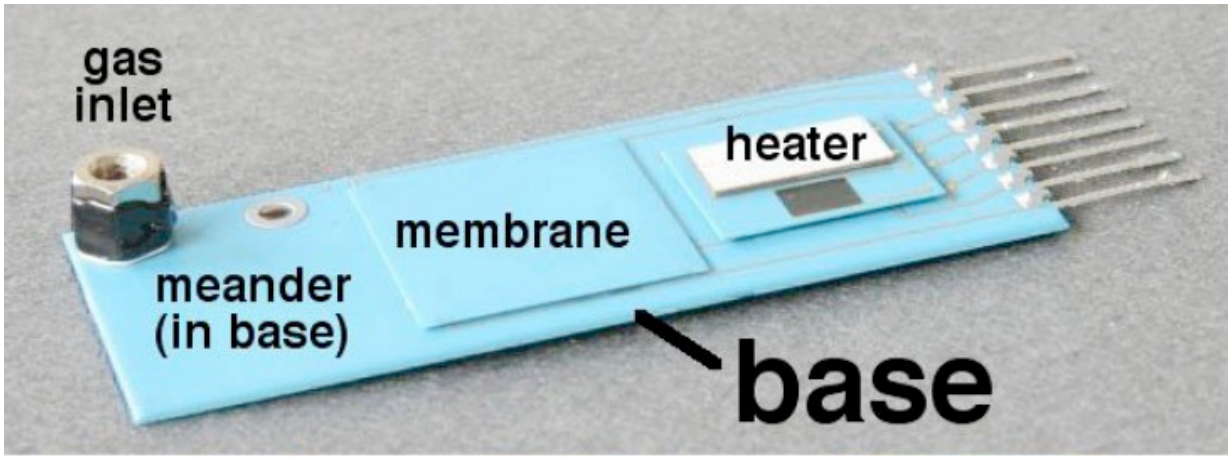

Figure 5.17. The complete viscosity sensor.

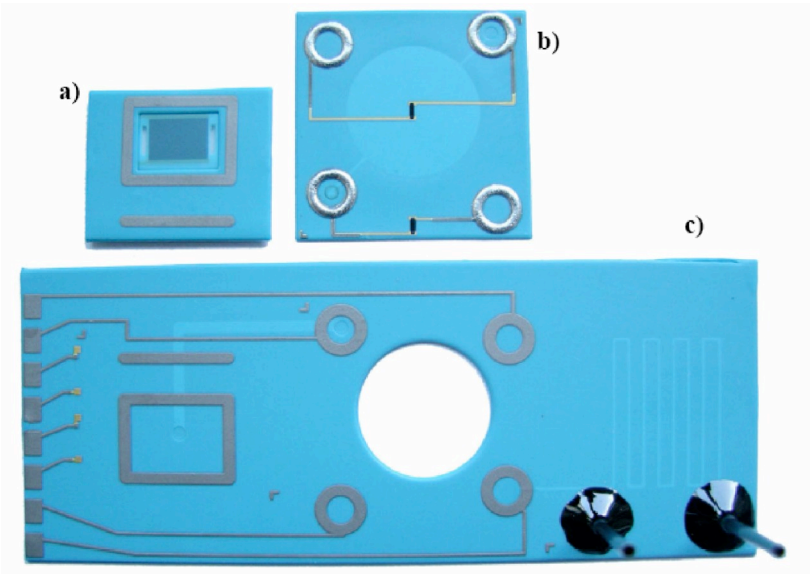

Figure 5.18. Components of the sensor: a) heater, b) pressure sensor, c) main block with integrated meander with inlet and outlet ports on the right hand side.

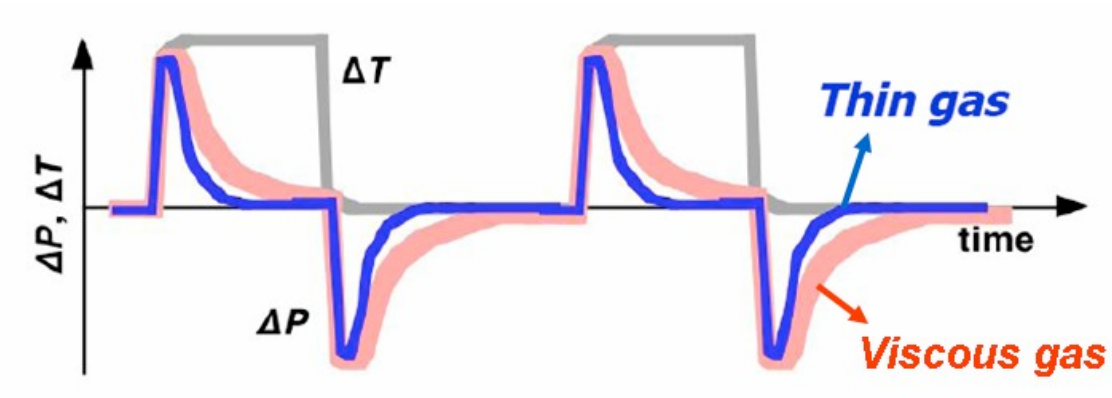

Figure 5.19. Relaxation behavior of a thick and thin gas in terms of temperature cycles.

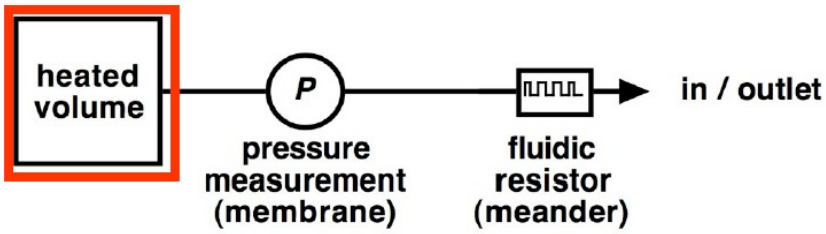

Figure 5.20. Principle of the viscosity sensor.

5.3.2 Force sensor

Force sensors, which can be fabricated using a broad range of technologies and materials, are extensively used in automotive and manufacturing industries, in household electronics, etc.

A typical thick-film force sensor, which is simple to fabricate and operative in a wide force range, is composed of two main parts: the beam, where the force is applied and the mechanical base (figure 5.21.). The beam is printed with thick-film piezoresistors, which convert mechanical strain (from force or pressure), into a change of resistance according to:

$$G_f = (\Delta R / R) / (\Delta l / l) = \text{Signal} / \delta \quad (3)$$

where G_f, R and l are the gauge factor, resistance and length, respectively. The numerator indicates the resistivity change (signal), whereas the denominator shows the strain (δ) upon applied force on the material.

From (3), it is clearly seen that improved signal can be achieved by increased strain. The key relations between the materials properties and the force sensor functions are given by:

$$E = \sigma / \delta \quad (4)$$

$$\sigma = (6FL) / bh^2 \quad \text{(nominal stress of a beam)} \quad (5)$$

where E, σ and F are Young's modulus, stress and force, respectively. The geometrical constraints are represented by L, b and h, which stand for the length, width and thickness of the beam (figure 5.21.). The previous relations can be further formulated both for LTCC and alumina (Al_2O_3) as:

$$\varepsilon_{LTCC} / \varepsilon_{Al2O3} = (b_{Al2O3} h^2_{Al2O3} E_{Al2O3}) / (b_{LTCC} h^2_{LTCC} E_{LTCC}) \quad (6)$$

which is obtained by assuming identical force applied on the beams with same length. It is important to note that strain and elastic constant are material characteristics and width and thickness can be defined by processability of the selected material.

Table 5.5. shows the comparison between the two materials in terms of the parameters shown in (6). Although the long-term design strains are similar [22], the LTCC, through its much lower modulus, availability of very thin sheets and possibility of 3D structuration, allows much higher sensitivity than alumina, making it especially suited to applications in the low force range.

3D structuration allows several improvements. First, using, at the point of measurement, a thick and narrow bottom layer and a thin and wide top layer (figure 5.22.) maximizes the degree of compressive strain at the bottom / measuring resistor (which determines the signal), compared to the tensile strain at the top side (which governs fracture). Therefore, the response is improved [12]. Additionally, restricting the narrowing of the bottom layer to the measurement zone increases the overall stiffness of the sensor (which is advantageous at low ranges), while allowing for better defined boundary conditions (less influence of parasitic stresses due to mounting on the base).

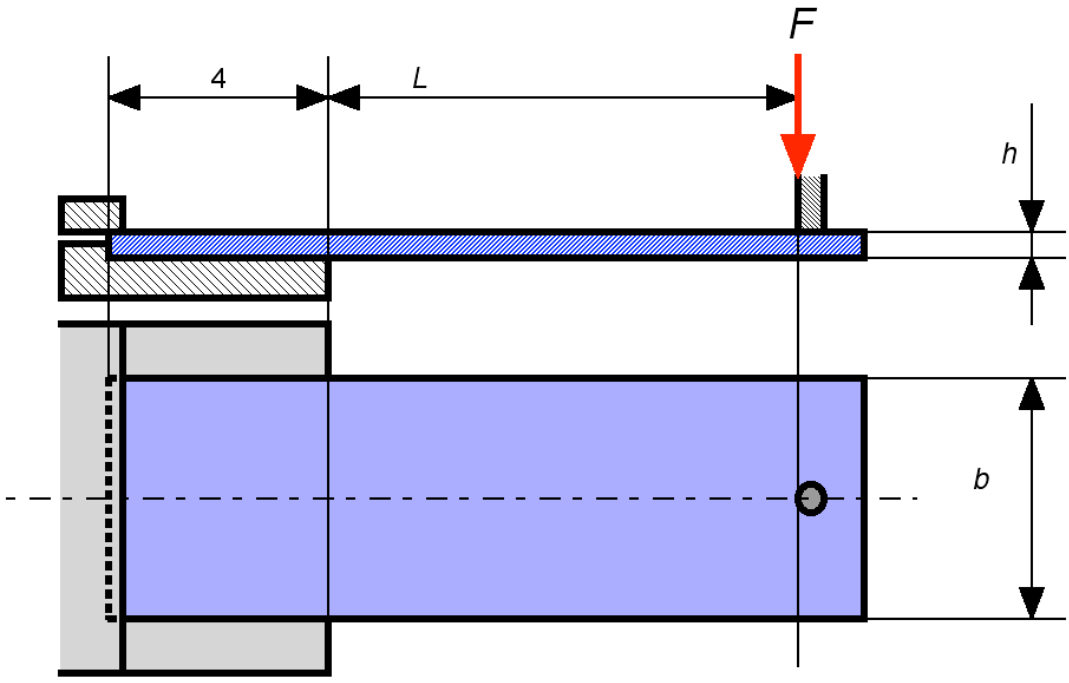

Figure 5.21. The beam from profile and top.

Table 5.5. LTCC versus alumina as the beam material

Properties	Du Pont LTCC 951 (fired)	Kyocera A-476 Al_2O_3 (96%)
Elastic modulus (GPa)	110 [23]	330 [25]
10-year design stress (MPa)	110 [22]	270 [22]
10-year design strain (ppm)	1000 [22]	800 [22]
Available thickness (mm)	0.04-0.21 [24]	0.25-1.00 [25]

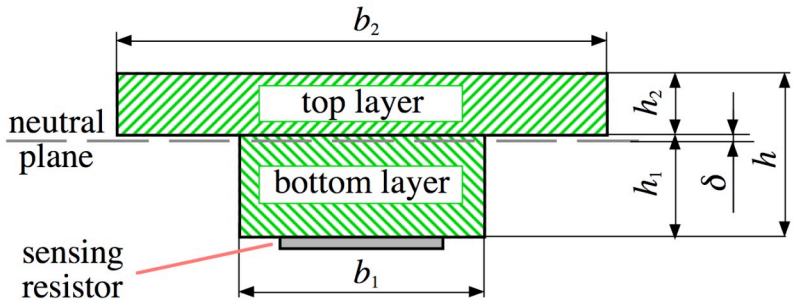

Figure 5.22. The cross section of the beam at the location of the measuring resistors. Width and thickness of the layers are shown as b and h, respectively and δ is the distance of the neutral plane to the planes' normal.

The beam of the millinewton force sensor can be analyzed in terms of its mechanical structure and functional elements. It consists of top and bottom LTCC layers – all from DuPont 951 series - (figure 5.23.), which are screen-printed, laminated under a uni-axial press that is heated to 70 °C (25 MPa) and co-fired at 875 °C, in air. The top layer, where the force is applied, is kept under tension, whereas the bottom layer is under compression. The compressive strain is maximized at specially designed neck regions in the bottom layer, which carry the measurement resistors (figure 5.24.). This layer also carries the other (inactive) half of the measurement bridge, which can therefore be deposited in a single screen printing step.

Terminations are selected from Au [26] and Ag/Pd (3/1) pastes (table 5.6.), the latter one being co-firable with LTCC [27]. To our experience, however, both conductors pose different problems. The organometallic Au paste, which has a very fine fired thickness, may become discontinuous as a buried layer due to islanding, and at the vias due to reactions with Ag-based materials [9]. The deformation due to the Ag/Pd paste, although very small with

thick LTCC structures, is far too high in the case of the thin LTCC beams that are the object of our study.

Therefore, a special paste is prepared by mixing another commercial paste (DuPont 9473 Ag/Pd) with 20 % by weight quartz (Sihelco, Sikron B 600), the details of which are previously explained. The shrinkage behavior of the modified paste (from here on) and its pure, commercial form is studied by dilatometer analysis, which is shown in figure 5.25. Moreover, comparison of warpage in co-fired LTCC samples using these pastes can be seen in figure 5.26. These results, which suggest warpage-free production of thinner LTCC sheets for beams, facilitated fabrication of sensors with increased performance.

The thick-film components used and their functions are shown in table 5.6. Common to all, solder contacts between the beam and the mechanical support and via filling are made using solderable Ag/Pd (Du Pont 6146). On the other hand, all of the three terminations, Au, Ag/Pd and modified paste, are used individually to evaluate their shrinkage compatibility with LTCC (visual observation). Overall, the modified Ag/Pd paste resulted in the minimum warpage after firing. Therefore, this material was selected for the beams used for electrical characterization.

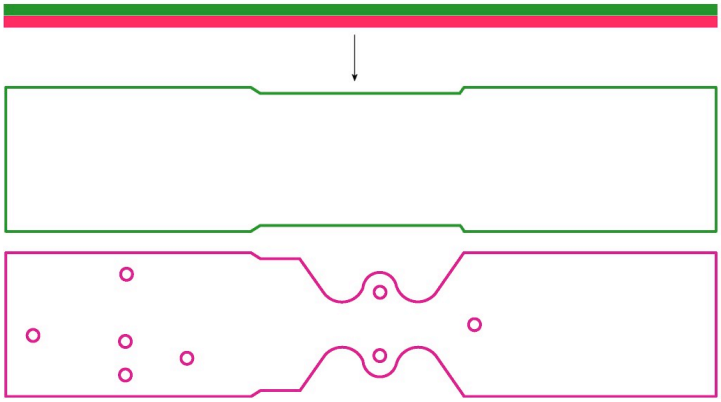

Figure 5.23. Individual layers of one single beam that is scored from a fired, 2X10 set of multiple beams. Unfired dimension is around of 18 mm x 4 mm.

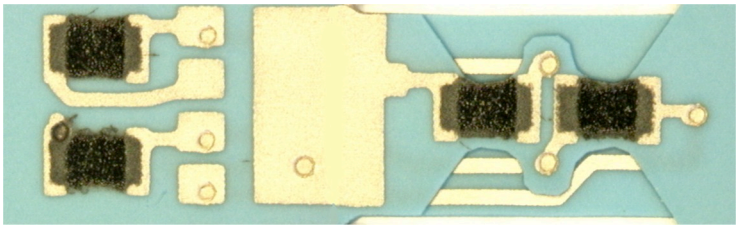

Figure 5.24. Part of the finished beam (~ 15 x 3 mm^2) with active (right) and passive piezoresistors and large rectangle area for soldering.

Table 5.6. Thick-film components used

Commercial name	Specification	Location in the sensor
ESL 8837	Organometallic Au [16]	Buried / in vias
Du Pont 6146	Co-firable, solderable Ag/Pd	Buried / on solder contact / in vias
(Du Pont 9473)	Modified (20 weight % SiO_2)	Buried / in vias
Du Pont 2041	Piezoresistor (RuO_2 + ruthenate) [19]	Sensing element

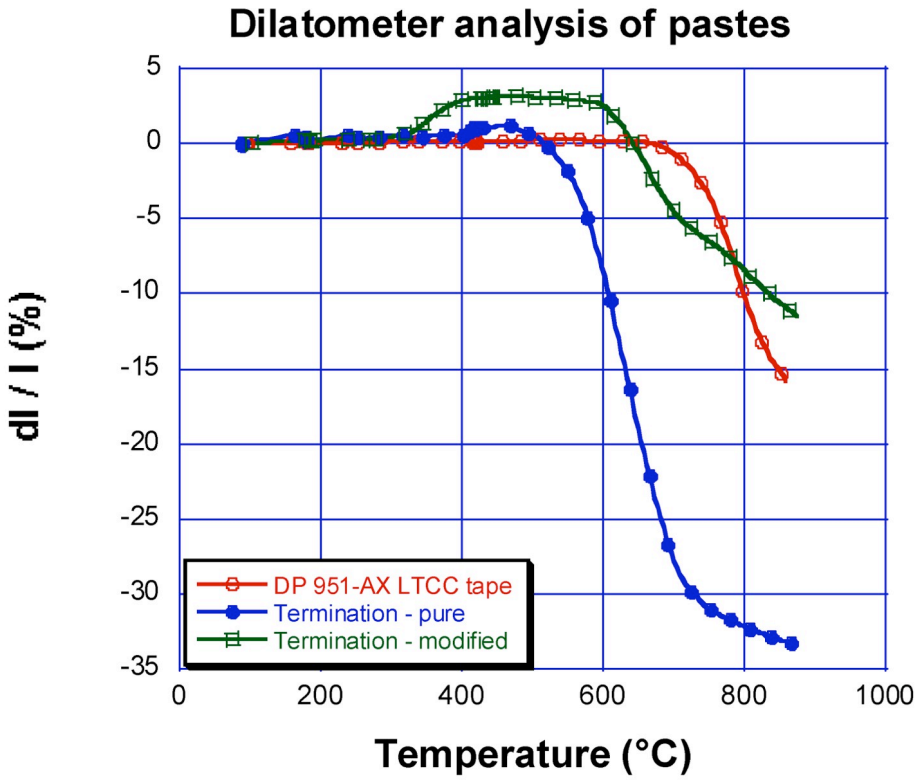

Figure 5.25. Dilatometer analysis showing the shrinkage delay of modified Ag-Pd paste by 140 °C and its reduced overall shrinkage (21 %).

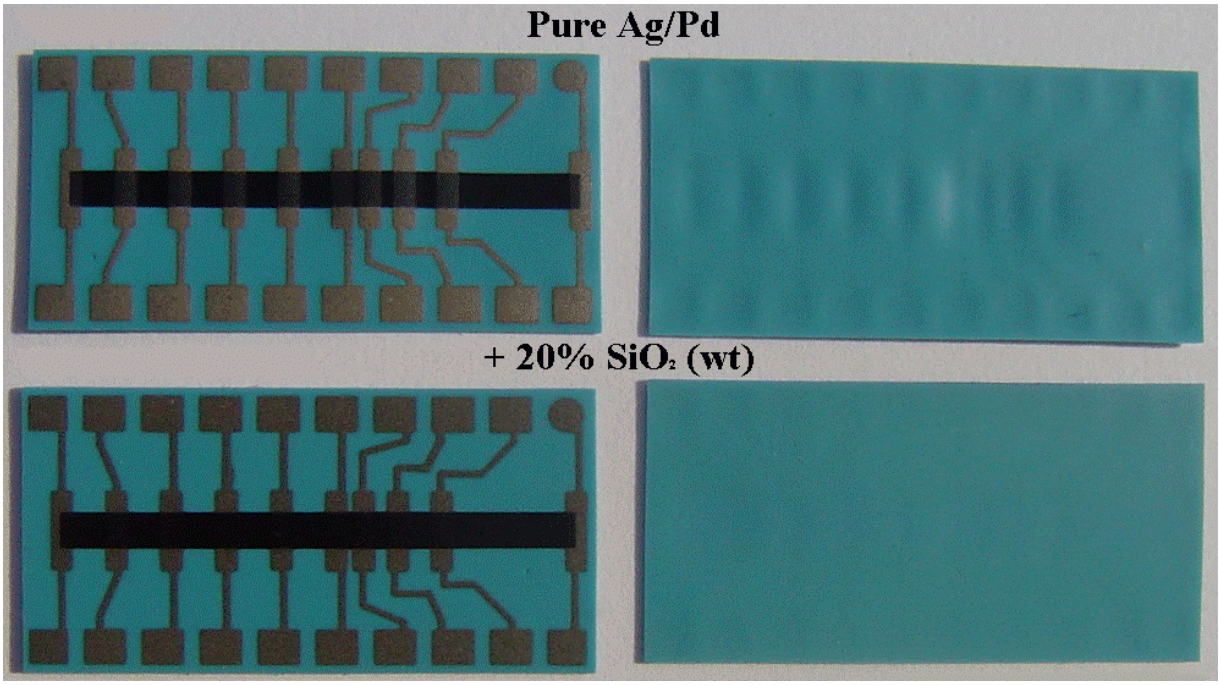

Figure 5.26. Comparison of test patterns co-fired with pure and modified Ag-Pd pastes. Latter shows reduced warpage on both faces of samples.

The fabricated beams were soldered on the mechanical support of the sensor and the force was applied by hanging weights on the beams. The output of the Wheatstone measurement bridge supplied with 5.00 V was used to characterize the response due to applied force. Used materials, beam layer configurations, fired thicknesses and the voltage changes recorded at 200 mN are listed in table 5.7. and the summary of the electrical characterization is shown in figure 5.27. Table 5.7. also gives approximate calculated responses (with G_F assumed to be 12 [28]).

As expected, thinner LTCC beams give a higher response than thicker ones. Also, the 116/254 configuration is more sensitive than the 254/116 one, according to the calculations. In spite of their half bridge design (only 2 active resistors), the LTCC beams are more sensitive than the reference alumina one (full bridge, 4 active resistors).

However, the sensitivity of the two thinnest beams are much lower than expected. This is ascribed to a strong stiffening effect brought about by warpage of the measurement cross section.

Table 5.7. Electrical characterization of the fabricated beams

Material	Configuration	Fired thickness (µm)	Delta Voltage at 200 mN (mV)	Approximately calculated response (mV)
Alumina*	Substrate	250	7.50	6.4
LTCC	254/116	290	12.00	14
LTCC	116/254	290	14.80	17
LTCC	116/116	180	15.35	39
LTCC	116/50	130	36.90	64

**Alumina: MillINewton force sensing cell (full bridge)*

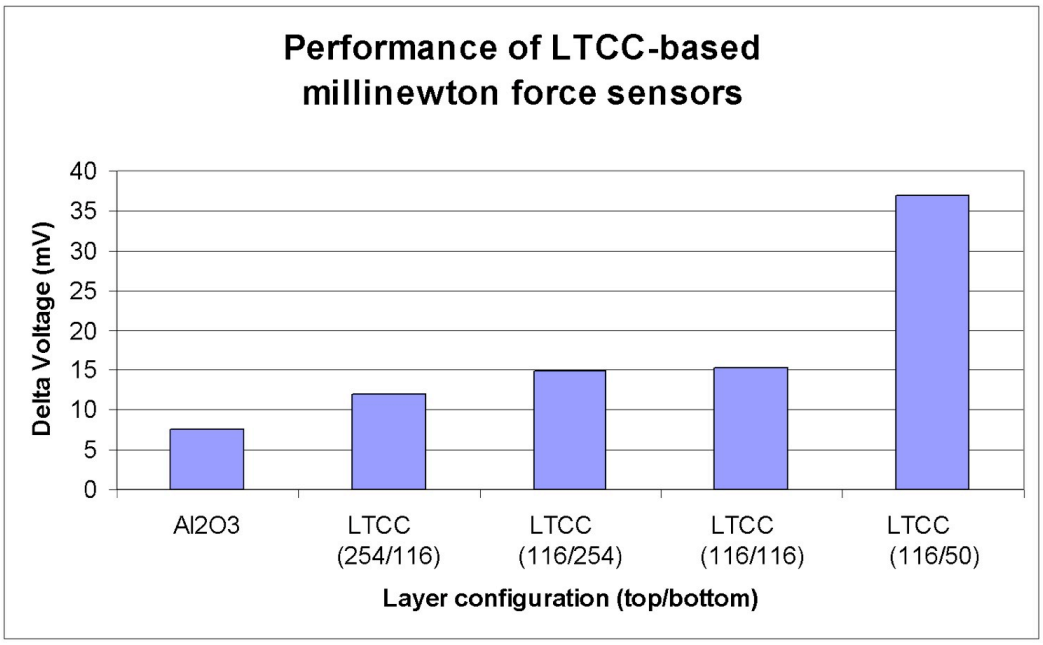

Figure 5.27. Signal change at 200 mN. Alumina used has a thickness of 250 µm.

As shown in detail, LTCC is a promising material to replace the traditional alumina for force and pressure sensing at low ranges. Its elastic modulus, available thickness and ease of processing allow fabrication of LTCC beams having sensitivities several times higher than that of alumina. However, progress is still needed in controlling warpage to fully utilize its potential.

5.3.3 Inclination sensor

LTCC has a very low thermal conductivity around 2-3 W/m/K (around one tenth of alumina), which, together with the availability of thin sheets and the ease of its structuration,

makes it an ideal substrate for “hot spot” applications: heat generated by the source is local due to limited heat dissipation.

The working principle of the sensor that is explained here is based on the heat loss on the PTC resistor (ESL 2612), which is screen-printed on the 100 µm-thick LTCC substrate (Heraeus CT 2000) (figure 5.28. a-b.). As it can be seen from the construction of the sensor (figure 5.28.), the heat loss on the resistor (hot spot) depends on the environment with which the resistor is in contact. Therefore, when there is no inclination, the bubble is directly over the resistor and so that the dissipated heat tends to remain in the resistor, increasing its temperature (figure 5.29.). In case of inclination, the heat over the resistor is dissipated more efficiently through the liquid, resulting in a lower resistor temperature at same power. The critical parameters for the sensor’s functioning can be listed as the thickness of the substrate, boiling temperature and surface tension of the liquid used and the operating parameters.

The performance of the sensor is shown in figure 5.30. The sensitivity can be increased further by thinner substrates, which minimizes the parasitic heat loss through the LTCC structure.

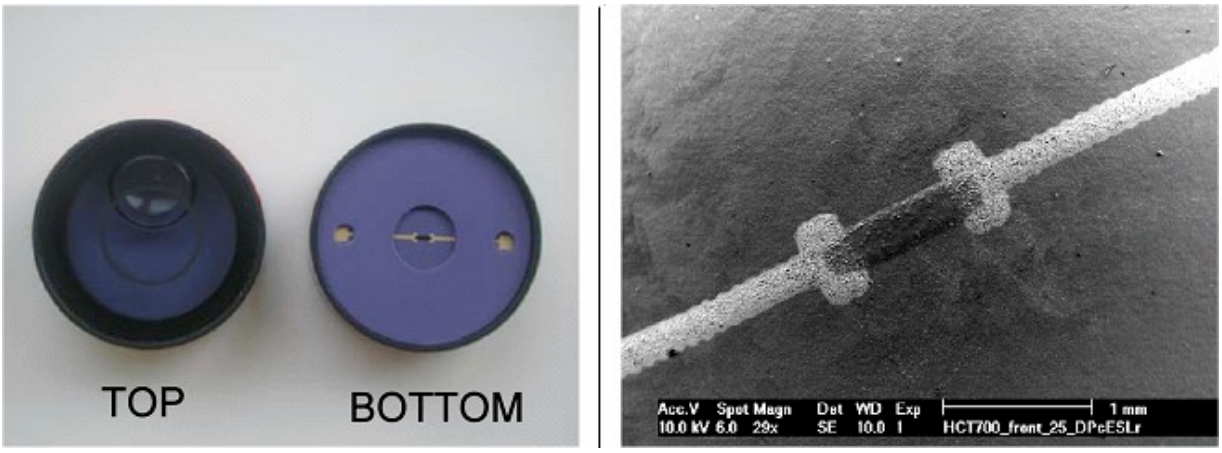

Figure 5.28. Top and bottom view of the inclination sensor (left) and the size of the hot-spot resistor on LTCC substrate imaged by SEM.

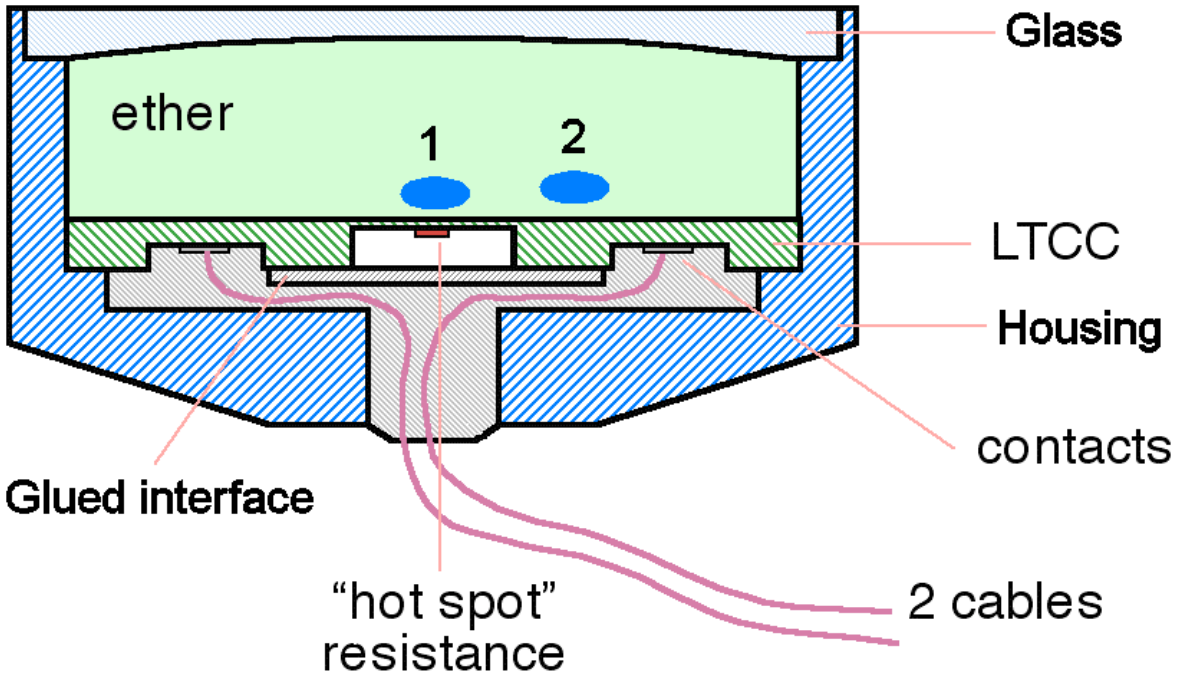

Figure 5.29. Sketch of the fabricated sensor: the bubble position in case of balance, α = 0 (position 1) and inclination, α ≠ 0 (position 2).

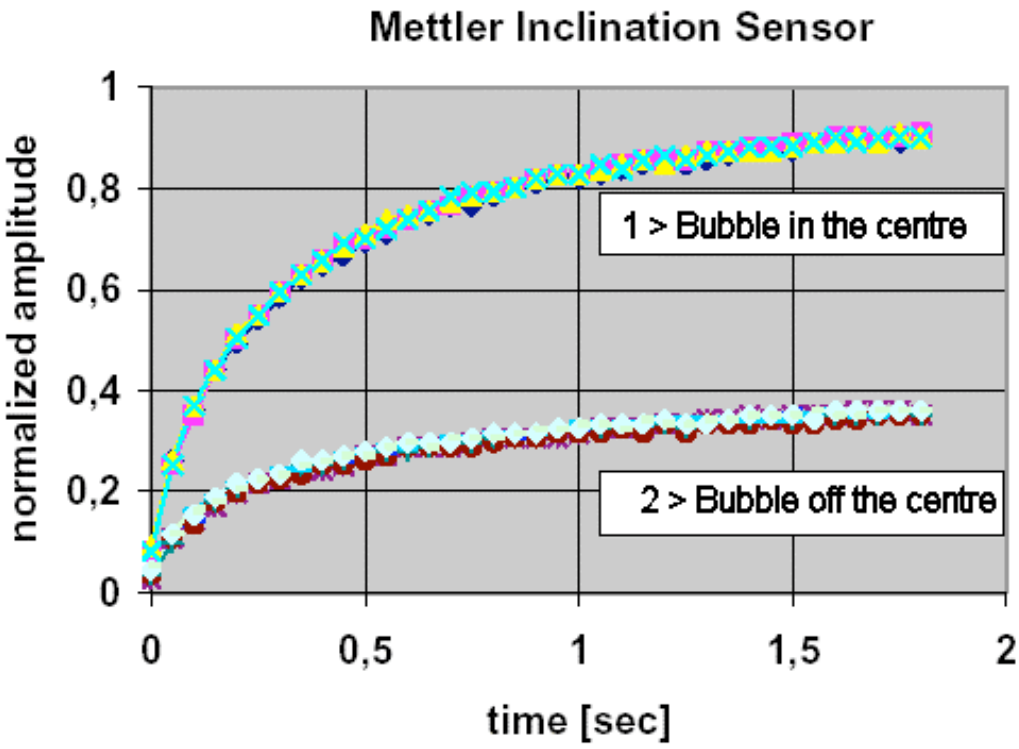

Figure 5.30. Performance of the sensor in balance (bubble in the centre) and tilted position.

Sensors and micro-fluidic structures for a broad range of applications are fabricated using LTCC technology. The performances shown are open to further improvement by reducing the materials incompatibility of co-fired materials such as differential shrinkage, chemical interaction, etc. Plasticity of tapes providing ease of fabrication of complex 3-D structures, integration of thick-film technology leading to high density packaging, hermeticity, thermal and chemical inertness of the fired tapes, etc. make the technology a reliable and efficient alternative to the widely-used alumina in certain critical applications.

References

1. “Thick-film Sensors”, Edited by M. Prudenziati, Elsevier, 1994, 59-71.

2. H. Birol, T. Maeder, I. Nadzeyka, M. Boers and P. Ryser, “Fabrication of a Millinewton Force Sensor Using Low Temperature Co-fired Ceramic (LTCC) Technology”, accepted for publication in Sens. Actuat. A: Physical, available online, 2006.

3. H. Birol, T. Maeder, C. Jacq, G. Corradini, M. Boers, S. Straessler and P. Ryser, “Structuration and Fabrication of Sensors Based on LTCC Technology”, Key Engineering Materials, High Performance Ceramics IV, 2006, 1849-1852.

4. H. Birol, T. Maeder, C. Jacq, S. Straessler and P. Ryser, "Fabrication of LTCC Micro-fluidic Devices Using Sacrificial Carbon Layers", Conference paper (IMAPS 2005, Baltimore) invited for publication in the International Journal of Applied Ceramic Technology, 2005, 2 [5], 364-373.

5. C.J. Ting, C.S. Hsi and H.Y. Lu, “Interactions between ruthenia-based resistors and corderite-glass substrates in low-temperature co-fired ceramics”, J. Amer. Ceram. Soc., 2000, 83 (12), 2945-2953.

6. P. Yang, M.A. Rodriguez, P. Kotula, B.K. Miera and D. Dimos, “Processing, microstructure and electric properties of buried resistors in low-temperature co-fired ceramics”, J. Appl. Phys., 2001, 89 (7), 4175-4182.

7. C.S. Hsi and M.W. Lee, “Properties of ruthenia-based resistors embedded in low-temperature co-firable ceramic substrates”, Jap. Journal Appl. Phys., 2002, 41 (8), 5323-5328.

8. H. Birol, T. Maeder, C. Jacq and P. Ryser,, "Effects of firing conditions on thick-film PTC thermistor characteristics in LTCC technology", Proceedings, IMAPS Conference on Ceramic Interconnect Technology, Denver, 2004, 106-109.

9. H. Birol, T. Maeder, C. Jacq and P. Ryser, “Investigation of Interactions Between Co-fired LTCC Components”, Journal of the European Ceramic Society, 2005, 25 [12], 2065-2069.

10. H. Birol, T. Maeder and P. Ryser, "Influence of Processing and Conduction Materials on Properties of Co-fired Resistors in LTCC Structures", Journal of the European Ceramics Society, 2006, 26 [10-11], 1937-1941.

11. K. Pitt, “Handbook of thick-film technology”, Electrochemical Publications, second edition, Bristol, 2005, Chapter 8, 181-209.

12. T. J. Garino, “The co-sintering of LTCC materials”, Ceramic Interconnect Technology Conference, 2003, 171-176.

13. G.Q. Lu, R.C. Sutterlin and T.K. Gupta, “Effect of mismatched sintering kinetics on camber in a low-temperature cofired ceramic package”, J. Amer. Ceram. Soc., 1993, 76 (8), pp.1907-1914.

14. http://www.netl.doe.gov/technologies/oil-gas/index.html

15. Press release euro gas Brussels 2004, 04M048 Natural Gas Consumption in Europe in 2003.

16. 2003 web site NaturalGas.org, Residential Uses.

17. 22nd World Gas Conference June 1—5, 2003 Tokyo, Japan, Working Committee 6, Utilization of Gases for Domestic, Commercial and Transportation Sectors, Study Group 6.1: Gas appliances for the 21st century Part 1 – Appliances.

18. Natural Gas Vehicle Technology Forum 2003, Natural Gas as a Transportation Fuel, http://www.ott.doe.gov/ngvtf.

19. K. Warwzinek and D. Trimis, “Development of a Wobbe number sensor for controlled combustion of gaseous fuels with varying quality”, Proceedings of the 6th International Conference on Technologies and Combustion for a Clean Environment (Clean Air VI), Porto, Portugal, July 2001.

20. K. Pickenäcker, D. Trimis and K. Warwzinek, “Excess air controlled operation of boilers and furnaces by means of Wobbe number measurement”, 5th European Conference on Industrial Furnaces and Boilers, Porto,11-14 April 2000.

21. T. Maeder, C. Jacq, I. Saglini, G. Corradini, S. Straessler, H. Birol, and P. Ryser, “LTCC thermal gas viscometer – heater module”, Proceedings of the 4th European Microelectronics and Packaging Symposium with Table-Top Exhibition, Terme Catez-Slovenia, May 22-24, 2006, 61-66.

22. H. Birol, M. Boers, T. Maeder, G. Corradini and P. Ryser, “Design and processing of low-range piezoresistive LTCC force sensors”, Proceedings of the XXIX International Conference of IMAPS Poland Chapter, Koszalin-Darlowko, 385-388, 2005.

23. M. Santo-Zarnik, D. Belavic, "Construction of a PZT actuator in an LTCC structure - a preliminary finite-element analysis", Proceedings, XXVIII International Conference of IMAPS Poland Chapter, 2004, 366-370.

24. http://www.dupont.com/mcm/gtapesys/part4.html

25. http://global.kyocera.com/prdct/fc/product/material/elec/

26. http://www.electroscience.com/pdf/8837.pdf

27. http://www2.dupont.com/MCM/en_US/PDF/datasheets/6146.pdf

28. C. Jacq, T. Maeder, S. Vionnet and P. Ryser, “Low-temperature thick-film dielectrics and resistors for metal substrates”, Journal of the European Ceramic Society, 2005, 25 [5], 2021-2024.

6 FUTURE PERSPECTIVES

6.1 Minerals based sacrificial layers

An alternative to the graphite-based sacrificial paste studied so far, which has a relatively narrow processing window and restricted range of applications for structuring LTCC, is minerals-based paste [1]. This technique suggests utilization of a sacrificial paste, which remains "permanent" during firing and is only later removed by chemical dissolution, thus providing an effective support throughout the firing. The paste is based on a mixture of B_2O_3 and alkaline earth oxides and screen-printed on an LTCC sheet that is laminated with additional LTCC layers. B_2O_3 forms a consolidated structure by melting at low temperatures (450 °C) and wetting alkaline earth oxide with high melting temperature (> 2000 °C), which can, after firing, be removed easily by acids. The basic characteristics that the pastes should possess can be summarized as: adequately formulated composition to allow easy etching, prevention of excessive reaction with the LTCC, and matching shrinkage behavior with LTCC.

Preparation of the paste

The selected materials for preparation of the “mineral” sacrificial layer are based on B_2O_3 (Sigma Aldrich H_3BO_3 with product number 339067) and CaO (Alfa Aesar $CaCO_3$ with product number 011403), where the former and the latter compounds are the fluxing agent and the alkaline earth mineral, respectively. Mass and enthalpy changes as a function of temperature are studied by TGA and SDTA (figure 6.1. a-b) and the decomposition reactions of the boric acid (H_3BO_3) and the carbonate can be written as:

$$2H_3BO_3 \rightarrow B_2O_3 + 3H_2O \text{ (at 300 °C)} \quad (1)$$

$$CaCO_3 \rightarrow CaO + CO_3 \text{ (at 600 °C)} \quad (2)$$

However, due to stoichiometry complications brought about by the carbonate decomposition in addition to visual observations, we decided to continue experiments with CaO (Alfa Aesar with product number 010923). The idea of using fluxing agent within an

alkaline earth mineral matrix, therefore, can be explained in light of these results: B_2O_3 (glass) decomposes around 160 °C (figure 6.1.b) and melts at 450 °C, which then wets and fills the porous CaO matrix that has a melting point of 2927 °C [2]. This leads to formation of a consolidated structure, which is not dense, thus etchable with the appropriate solvent.

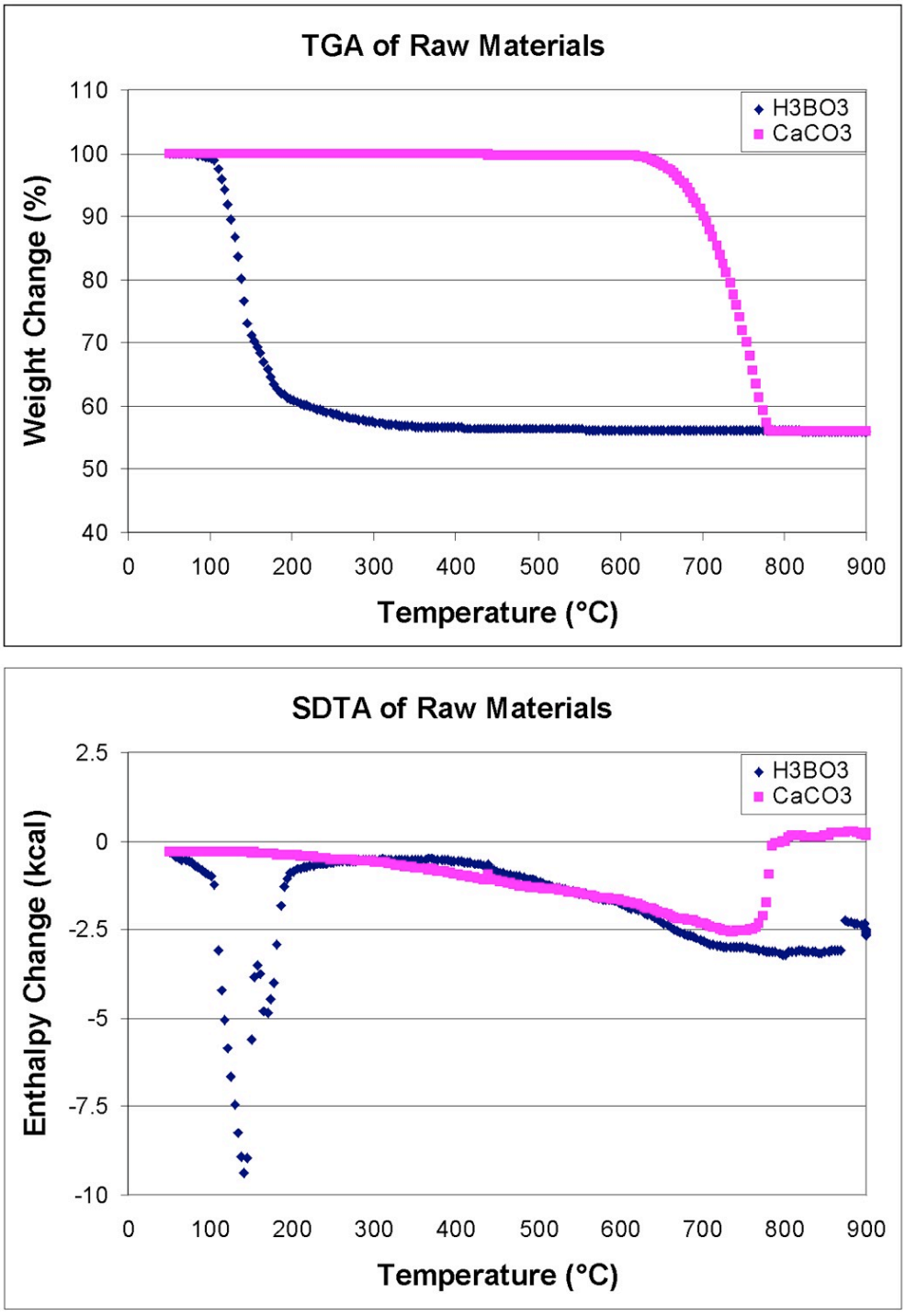

Figure 6.1. a) TGA (left), b) SDTA analysis (single differential thermal analysis obtained by superimposing DTA over TGA curve) of raw powders.

The starting powders are mixed at 10, 20, 30, 40, 60 and 80 molar percent of B_2O_3 according to the CaO-B_2O_3 phase diagram [2]. For efficient mixing and increased reactivity, powders are ball milled in isopropanol using zirconia media for 24 hours. The filtered and dried powders are finally crushed in agate mortar for finer size, prior to paste preparation. Humidity sensitivity and increased hardness of powders at higher B_2O_3 content are the primary observations concerning the state of powders.

Prior to paste preparation, the phases of the powders are investigated by X-ray diffraction (XRD). This is made on pellets, which are prepared by pressing the powders uni-axially. The pellets are then fired according to the identical profile for LTCC: 5 °C/min of heating rate with two dwell points at 440 (120 minutes) and 875 °C (25 minutes), respectively. Following firing, however, time-dependent disintegration is observed common to all pellets. This is ascribed to the hygroscopic nature of the B_2O_3. Therefore the XRD analysis is conducted on powders, which are obtained by crushing the disintegrated pellets.

The pastes are prepared by mixing the powders with the organic vehicle (table 1) at 42/58 solids to organics weight ratio. The mixed slurry is homogenized on a three roll mill and the prepared paste is transferred to the plastic crucibles for future use. Shrinkage compatibility with LTCC tapes is controlled by screen-printing pastes on blank, rectangular (30 x 5 mm^2) LTCC sheets (Du Pont 951-AX, 254 μm-thick), whereas their etchability using the appropriate solvent is controlled in membranes, where the paste is buried according to the layout shown in figure 6.2. Samples are fired according to the two-step profile, which is previously explained during pellet preparation.

Table 6.1. Materials used for the paste production

Product	Function	Supplier	Weight (%)
Ethyl cellulose	Binder	Aldrich, 43,383-7	50.5
Terpineol	Solvent	Fluka, 86480	2.3
Acetyl acetone	Dispersant	Sigma-Aldrich, P775-4	5.3
CBO* powder	Sacrificial		41.9

(*): CaO - B_2O_3 powder mixture

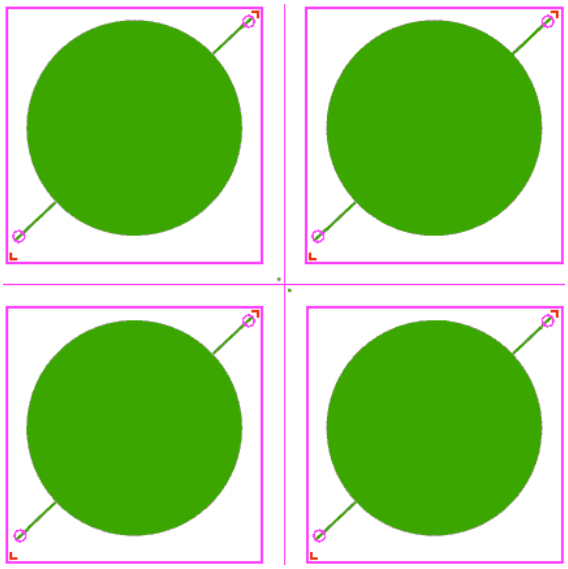

Figure 6.2. Layout for screen-printing permanent sacrificial pastes to check the etchability of the layer (circular area with 200 µm-wide inlet and outlet channels).

Results

XRD patterns of powders prepared at four different compositions (10-40 % B_2O_3) are shown in figure 6.3.a. Peak broadening is observed in powders with lower B_2O_3 concentration and peaks representing typical crystalline structure are observed in powder with the highest B_2O_3 concentration (40 %). The peaks in the latter case, however, belong to a phase with lower than nominal B_2O_3 composition: $3CaO.B_2O_3$ (JCPDS no: 48-1885 and shown in figure 6.3.b). This phase is one of the various intermediate compounds in the CaO-B_2O_3 system at approximately 25 % (molar) of B_2O_3. This is ascribed to the high volatility of B_2O_3 at elevated temperatures [3]. This estimation is also partially supported by the weight loss of the pellets, which exceeded in some cases the expected loss due to water vapor evolution. Unfortunately, these measurements were disturbed by water pickup after firing by the porous and hygroscopic samples, which did not allow us to calculate the B_2O_3 loss. Shrinkage of the samples is 7-8 % in thickness and diameter dimensions after firing and relatively independent of the B_2O_3 content.

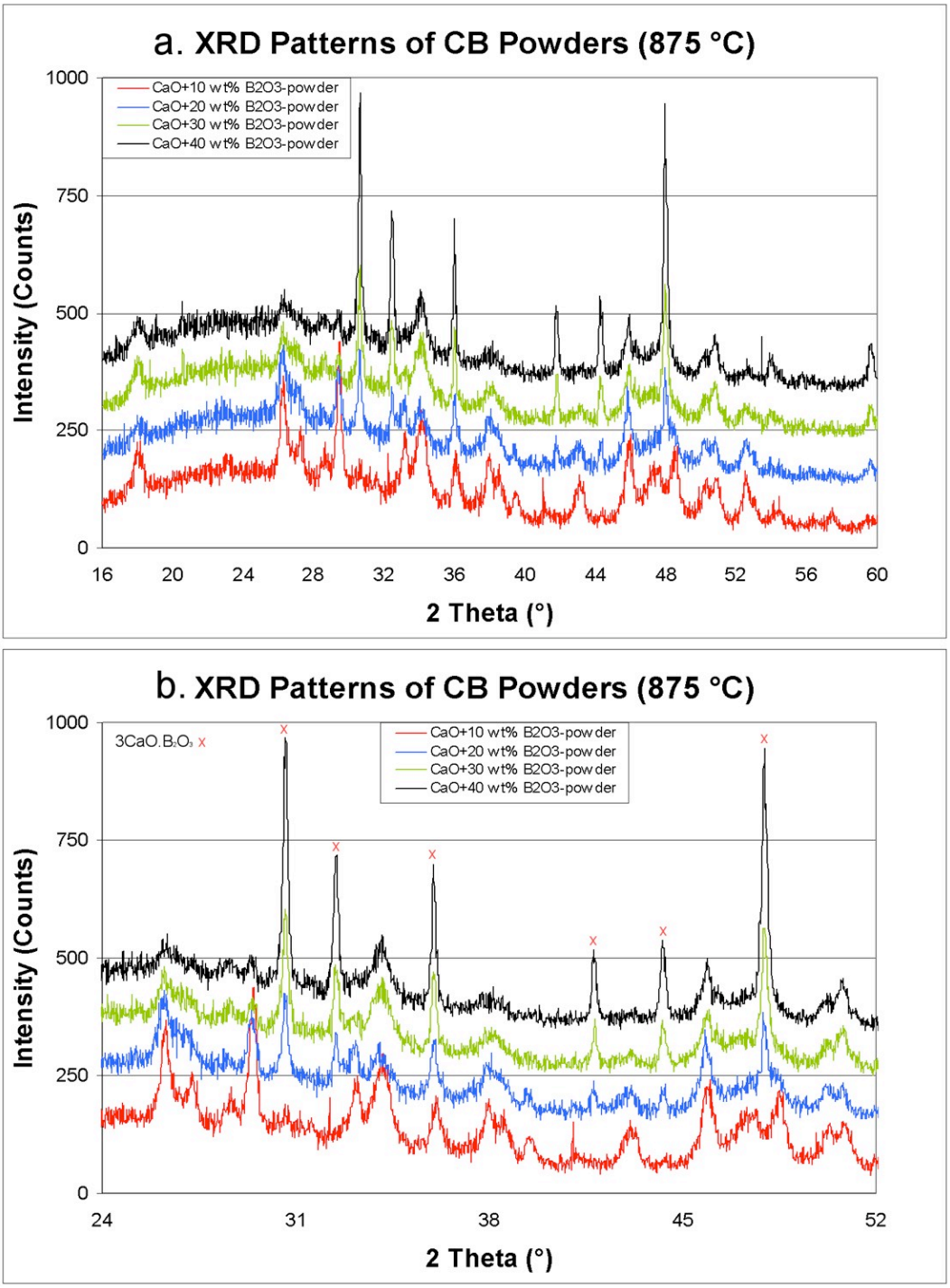

Figure 6.3. a) XRD analysis of powderized pellets for 4 compositions (patterns with lowest counts in both graphs representing the minimum B_2O_3 molar ratio (10 %), b) identification of primary phases (below).

The preliminary results show that shrinkage compatibility between the surface-printed paste and the LTCC tape must further be improved, although the obtained result is well comparable to most of the commercial thick-film products widely employed (figure 6.4.). The

buried paste within the membrane, on the other hand, is observed to exhibit larger deformation due to shrinkage incompatibility. However, it is found that the paste can be dissolved efficiently using hydrochloric acid (Fluka with product number 84419) in an ultrasonic bath. The overall etching period takes a maximum of 2 minutes and the results can be viewed in figures 6.5 and 6.6.

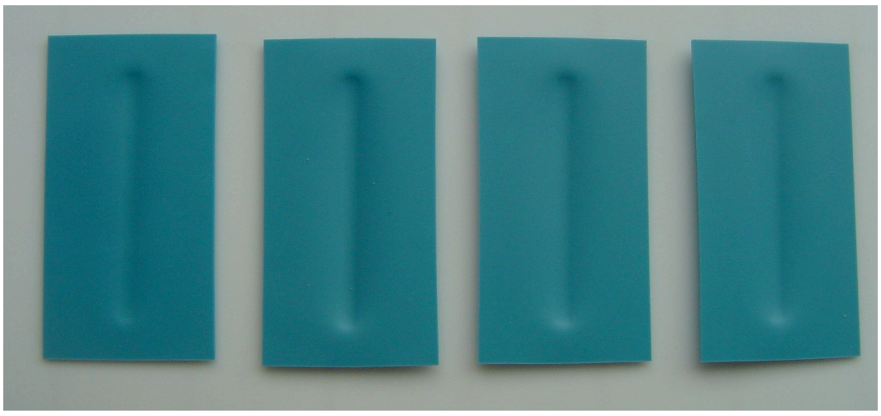

Figure 6.4. Back-sides of the printed LTCC sheets fired at 875 °C.

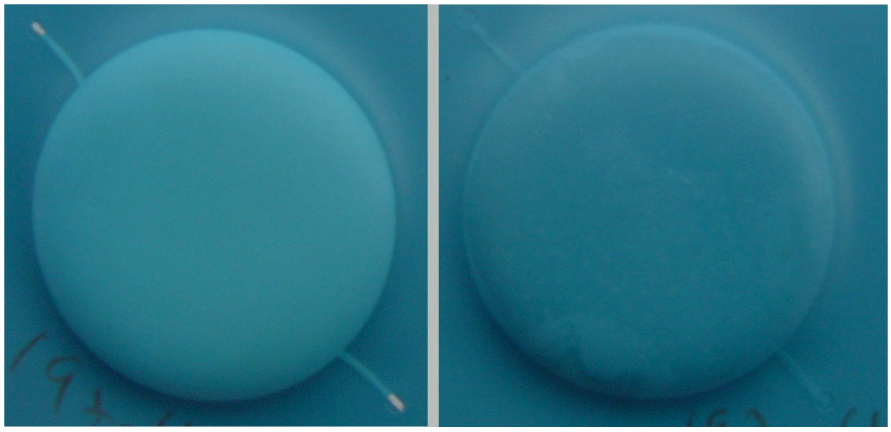

Figure 6.5. Membrane before (on the left) and after etching. The white sacrificial layer, which is clearly visible at the end of the channels, is removed following etching.

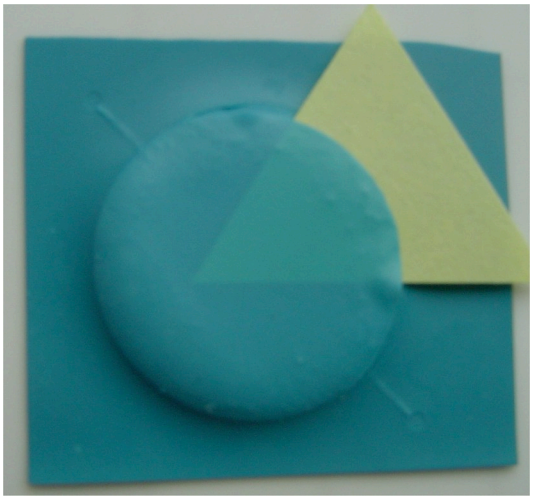

Figure 6.6. Spacing of a semi-open structure shown by a paper insert.

The spacing between the membrane and the base layer is controlled by cross-sectional analysis of the samples using SEM. Images demonstrate well-defined spacing as well as insufficient sacrificial layer removal at the edges of the membrane in figure 6.7. a and b, respectively. Therefore the removal of the etched paste, which is a common problem in such closed structures, requires special treatment for improved quality of the fabricated devices. It is observed that the spacing is constant over a wide range in longitudinal dimension.

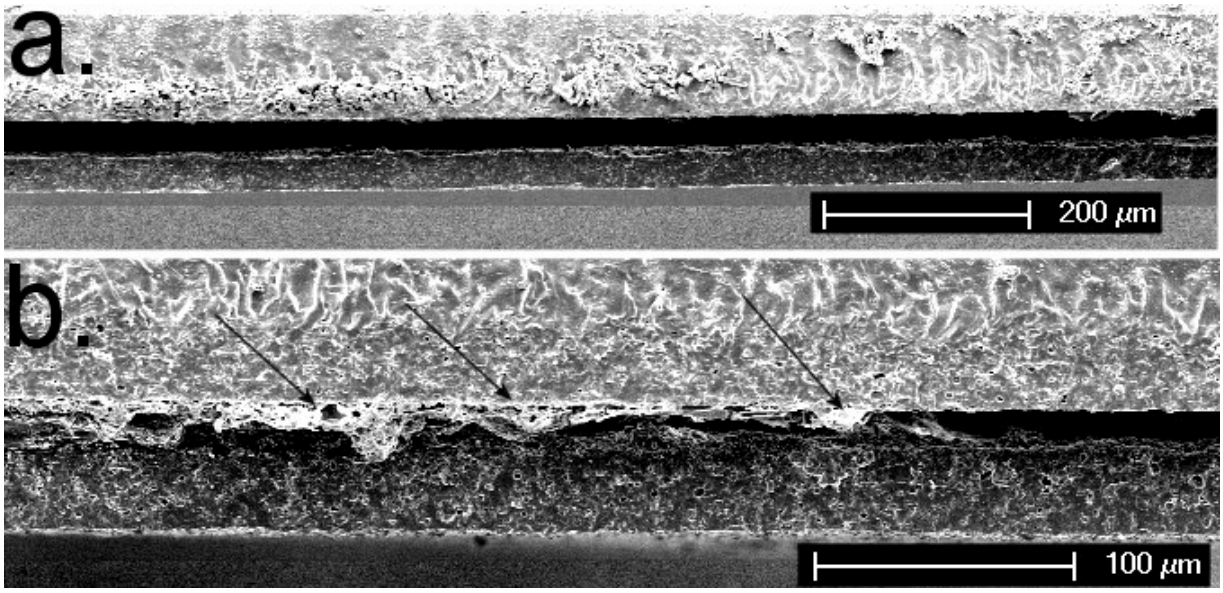

Figure 6.7. a) Well-defined spacing (above), b) insufficient etching at the edge of the membrane.

In spite of well defined spacing obtained in membranes in addition to ease of etchability, reducing the differential shrinkage between the paste and the LTCC tape remains

the major challenge for full-applicability of the proposed technique. On the other hand it is observed that the selected compositions, despite being over a wide compositional range, yield similar results and can be etched with great ease.

The remaining work, other than improving shrinkage compatibility, is foreseen to be on a detailed study of the compositional analysis of prepared pastes and the possible reaction of B_2O_3 with the LTCC sheets.

It is strongly thought that the proposed method can efficiently be used for fabrication of semi-open structures, which allows easy penetration of the etching liquid.

References

1. H. Birol, T. Maeder and P. Ryser, “Preparation and Application of Inorganic Materials-based Sacrificial Layers for Fabrication of LTCC Devices”, Proceedings of the 4th European Microelectronics and Packaging Symposium with Table-Top Exhibition, Terme Catez-Slovenia, May 22-24, 2006, 57-60.
2. H. Yu, Q. Chen and Z. Jin, “Thermodynamic assessment of the $CaO-B_2O_3$ system”, Calphad, 1999, Vol. 23, No. 1, 101-111.
3. EPRI/MRP Boric Acid Corrosion (BAC) Testing Program: Immersion Test Results, Electric Power Research Institute, 2005.

7 CONCLUSIONS

The potential of graphite-based sacrificial pastes for structuring LTCC devices was investigated in consecutive steps as listed in the following:

- paste preparation, characterization and selection,
- qualitative determination of LTCC permeability elimination temperature,
- kinetics competition between paste oxidation and LTCC open porosity elimination,
- determination of model device and critical design parameters related to LTCC processing,
- device fabrication and characterization

Pastes were prepared using design of experiments, where the amounts (in weight %) of graphite powder, binder and solvent were selected as the independent factors of the experiments. The powder was mixed with the organic vehicle and homogenized on a three roll mill and the prepared pastes were characterized in terms of their oxidation kinetics, rheology and stability. The solvent content, as expected, was observed to have a strong influence on paste viscosity, although the apparent viscosity at similar solvent ratios was found to have stronger influence. Among all, pastes those exhibiting minimum viscosities such as P4 and P7 showed extreme sedimentation, which is ascribed to precipitation of graphite particles in the solvent-excess environment. These pastes (also P1, P8) could not be screen-printed either, immediately after thorough mixing.

According to the experimental conditions selected, 35% by weight of graphite was found to be the upper limit for the powder content. The best compatibility with screen-printing (rheology) and resistance to sedimentation (stability) were achieved in P2, P3 and P5. In light of these results, P2 was selected as the paste for the forthcoming experiments, having an apparent viscosity of 442 Pa.s at 100 Pa and exhibiting sufficient stability.

LTCC green tapes, as well as pastes, were also studied in terms of different heating rates. Two major issues at this point were of utmost interest for the proposed technique to function: determination of full oxidation temperature of pastes and open-porosity elimination temperature of LTCC at different heating rates, the latter being determined by a leakage

detection system specially manufactured for this study based on pressure sensor. It was seen that the paste oxidation (P2), which occurs at 800 °C and at a heating rate of 2 °C/min, is shifted to higher temperatures at higher rates (i.e. 900 °C at 8 °C/min) as expected, whilst the shift in LTCC open pore elimination temperature was confined to a much narrower window: a change of heating rate from 2 to 8 °C/min resulted in a temperature shift from 765 °C to 775 °C for 254 μm-thick LTCC and from 785 to 795 °C for 50 μm-thick LTCC.

These values, which were measured solely for the paste and LTCC substrates, were re-evaluated under real-time conditions after the model device was selected. A membrane geometry was selected as the model device comprising inlet and outlet channels. In this case, the effects of kinetic competition between paste oxidation and LTCC open pore elimination on fabricated structures was studied as a function of heating rate, thickness of the deposited carbon paste and width of the inlet/outlet channels. It was observed that fast heating rates resulted in swelling of the membranes, which was due to LTCC open porosity elimination occurring at temperatures much lower than full paste oxidation. This resulted in incompletely oxidized paste being entrapped within the cavity and exerting pressure on the LTCC membrane. Changing the channel width, on the other hand, was observed to control the degree of swelling independently of other parameters by affecting the ease of oxidation of graphite and degassing of oxidized gases.

The major effect, however, was observed in case of the paste amount deposited, which was determined by the screen. Thicker paste deposition (using 165/80 type screens) was seen to reduce swelling from by an order of magnitude and yield reproducible results.

The membranes, which were fabricated in terms of the selected experimental conditions, were finally characterized as a function of their displacement as a function of pressure. It was observed and confirmed by quantified results that swelling had a strong and direct influence on the membrane displacement: swollen membranes such as those fabricated at 2.50 °C/min heating rate with low paste depositing screens and narrower channels resulted in hysteresis, whereas relatively flat ones were free of hysteresis. Swollen membranes can be used for bistable devices such as relays, pressure switches, et., whereas flat ones are useful for low-range pressure sensors.

Although the characteristics of the fabricated membranes were studied as a function of paste ingredients and LTCC properties under various processing conditions simultaneously, it is important to note the following points:

1. The sacrificial layer removal, which is based on oxidation of the graphite-based paste, is a far more complex process than described briefly in here. The exact mechanism is yet an open issue to the corresponding communities such as electrochemistry, metallurgy, etc. It is believed that the gap, which remains to explain the exact nature of graphite oxidation and its influence on membranes, will be closed by new studies and findings in the domain.

2. The open porosity elimination temperature, which is measured for the DuPont 951 LTCC series in this study, is a characteristic feature of the selected LTCC: the overall data, therefore, should be modified in case of a different LTCC system. In this case the densification mechanism and ranges of the new system should be determined and adopted (if possible) to the sacrificial layer features.

A selection of other devices those fabricated for sensor applications were also presented, with an insight to their fabrication and characterization. It has been demonstrated that the differential shrinkage between LTCC tape and the commercial thick-film conductor can be reduced significantly by addition of SiO_2 powder into the latter, which reduced deformation and thus allowed utilization of thinner LTCC sheets for the beam of the force sensor, enhancing improved device performance. Additionally an alternative approach to temporary –sacrificial layer removed during firing as in case of graphite-based sacrificial paste- sacrificial paste was introduced which is based on minerals and removed after firing. Although they could be removed efficiently using acid, their shrinkage compatibility to LTCC remains to be a major optimization issue.

List of Figures

Chapter 1.

Chapter 2.

Chapter 3.

Chapter 4.

Chapter 5.

Figure 5.23. Individual layers of one single beam that is scored from a fired, 2X10 set of multiple beams. Unfired dimension is around of 18 mm x 4 mm.

Figure 5.24. Part of the finished beam (~ 15 x 3 mm^2) with active (right) and passive piezoresistors and large rectangle area for soldering.

Figure 5.25. Dilatometer analysis showing the shrinkage delay of modified Ag-Pd paste by 140 °C and its reduced overall shrinkage (21 %).

Figure 5.26. Comparison of test patterns co-fired with pure and modified Ag-Pd pastes. Latter shows reduced warpage on both faces of samples.

Figure 5.27. Signal change at 200 mN. Alumina used has a thickness of 250 μm.

Figure 5.28. Top and bottom view of the inclination sensor (left) and the size of the hot-spot resistor on LTCC substrate imaged by SEM.

Figure 5.29. Sketch of the fabricated sensor: the bubble position in case of balance, $\alpha = 0$ (position 1) and inclination, $\alpha \neq 0$ (position 2).

Figure 5.30. Performance of the sensor in balance (bubble in the centre) and tilted position.

Chapter 6.

Figure 6.1. a) TGA (left), b) SDTA analysis (single differential thermal analysis obtained by superimposing DTA over TGA curve) of raw powders.

Figure 6.2. Layout for screen-printing permanent sacrificial pastes to check the etchability of the layer (circular area with 200 μm-wide inlet and outlet channels).

Figure 6.3. a) XRD analysis of powderized pellets for 4 compositions (patterns with lowest counts in both graphs representing the minimum B_2O_3 molar ratio (10 %), b) identification of primary phases (below).

Figure 6.4. Back-sides of the printed LTCC sheets fired at 875 °C.

Figure 6.5. Membrane before (on the left) and after etching. The white sacrificial layer, which is clearly visible at the end of the channels, is removed following etching.

Figure 6.6. Spacing of a semi-open structure shown by a paper insert.

Figure 6.7. a) Well-defined spacing (above), b) insufficient etching at the edge of the membrane.

List of Tables

Table of Abbreviations

LTCC: low temperature co-fired ceramic

IC: integrated circuit

MCM: multi chip module

PCB: printed circuit board

MLC: multilayer ceramic

MCIC: multi-chip integrated circuits

HTCC: high-temperature co-fired ceramic

Q: quality factor

T_f: temperature coefficient of resonant frequency

RF: radio frequency

SMD: surface mount(able) device

TCE: thermal coefficient of expansion

LPS: liquid phase sintering

NLPS: non-reactive liquid phase sintering

TFR: thick-film resistor

TCR: temperature coefficient of resistance

R_{sq}: sheet resistance

SD: standard deviation

PTC: positive temperature coefficient

NTC: negative temperature coefficient

PLAS: Pressureless assisted sintering

TOS: Tape on substrate

PAS: Pressure assisted sintering

υ: media speed

ε: dielectric constant

f_o: frequency

Δf: band-width

c: speed of light

TGA: thermo gravimetric analysis

BSE: back scattered electron

SEM: scanning electron microscopy

EDXS: electron dispersive X-ray analysis

MEMS: micro electro-mechanical systems

W_o: Wobbe number

XRD: X-ray diffraction

G_f: gauge factor

R: resistance

E: elastic modulus

σ: stress

δ: strain

F: force

SDTA: single differential thermal analysis

DTA differential thermal analysis

Acknowledgements

I would like to thank to these wonderful people for their generous support in making this work come through: my thesis director, Prof. Peter Ryser, who gave me this great opportunity to get into the exciting world of LTCC and microelectronics packaging, in a wonderful lab ambience that is situated at a perfect balance between basic and applied research. I appreciate your passion to share your thoughts spontaneously and your true support that arrives right on time, when necessary. I wish to thank to my thesis supervisor, Dr. Thomas Maeder, who is an amazing source of knowledge and intelligence and yet so will-full to offer and share every bit of it until the very end. Thank you for your support and your generosity for sharing all these nice things you have, both as a scientist and a human being.

I would like to thank to each and all of my colleagues at LPM, particularly to Ms. Caroline Jacq, Ms. Karine Genoud, Mr. Giancarlo Corradini, Mr. Matthias Garcin, Mr. Igor Saglini, Mr. Timothée Haller, Mr. Boris the Moll Brothers, Mr. Fabien Bourgeois. I would like to acknowledge: Dr. Sigfrid Strässler for sharing his infinite knowledge and ideas that is blended with passion for striving the unique and with such modesty, the CIME crew - Prof. Dr. Philippe Buffat, Mr. Brian Senior, Ms. Danièle Laub, Ms. Fabienne Bobbard, Mr. Guido Milanesi and Mr. Marco Cantoni-, for their availability and generous support, Ms. Evelyn Hollenstein and Dr. Philip Nissing for their whenever-necessary-help in various measurements, Mr. Marc Boers and Mr. Ingo Nadzeyka for doing such wonderful semester projects, Mr. Georges Brélaz for his endless commitment to make things work with great professionalism. I do not bother myself writing their names one by one but send big hugs to all ST*Rs dispersed all around the world.

I truly appreciate the precious efforts of my primary school teachers Sayın Mehmet Küçükekşi and Sayın Seval Kahraman and my dear Professor from METUniversity, Sayın Macit Özenbaş. I also would like to acknowledge my best friends with whom I have had the best moments over long years: Cemil, Seltaç, Zındık, Özbalta, Arbaş, Canguz, Bobo, Özcan, Hamde, Götan (Cem Kofoğlu, Serkan Şahinöz, Mustafa Pektaş, Alper Özçelik, Arda Çetin, Cem Selçuk, Ozan Bilge, Özgür Özzeybek, Hande Uçartürk, Gökhan Uysal).

I would like to thank to the members of my thesis committee for improving the quality of my thesis by sharing their technical and personal excellence; Prof. Gary L. Messing for coming a long way to here, Dr. Andrzej Dziedzic for showing a true interest and Prof. Paul Muralt for his presence.

I also wish to acknowledge Sayin Dr. Kahraman Tunaboylu and his dear family, who have warmly and strongly embraced me in the hardest times: you are the real “Kahraman” (= hero) of this work and I will always remember your care and indescribable humanity with utmost appreciation.

I would like to give my THANKS to my parents Sevgili Arıgül ve Coşkun Birol, who has sacrificed nothing from my education and has always been with me, providing their endless warmth and support: “Sizleri çok seviyorum. Sonsuz sevginiz ve emeğiniz, eşsiz insanlığınız, sınırsızca tattırdığınız ve bir ömre sığamayacak kadar çok ve içten güzellikler için çok şanslı ve minnettarım; sağolun, varolun”.

My utmost appreciations go also for my Dayıcığım , Yengeciğim, Tubişim ve Minik gurk-ufak tavuğum (Çok değerli Metin, Bedriye, Tûba ve Burak Şenocak) for their true and pure belief in me and for their strong support since my childhood: “Çocukluğumdan beri verdiğiniz gerçek sevgi, mutluluk ve sınırsız destekle bana herzaman hem ana-baba, hem kardeş oldunuz. Sizleri çok seviyor ve bir kez daha en içten sevgi, saygı ve teşekkürlerimi iletiyorum”.

I also would like to thank my “mae e pai” querida Marlo Pedra e querido Sergio Abilio Jorge in Brazil, for their infinite wisdom and positivism that has reached undisturbed over a long way: “Eu amo vocês e obrigado pela coisa mais bonita que vocês botaram na minha vida”.

Finally my most special thanks and appreciation would go for my “life time love” and *farol*, Alline, who is my magic window opening to the sunny side of life, even during the heaviest showers. Your endless support, commitment, joy and humor are everywhere in my life; I love you so and I am grateful for your existence.

Publications

Reviewed Journal Papers

1. H. Birol, T. Maeder, C. Jacq and P. Ryser, “Investigation of Interactions Between Co-fired LTCC Components”, Journal of the European Ceramic Society, 25 [12], 2065-2069, 2005.

2. H. Birol, D. Damjanovic and N. Setter, “Preparation and Characterization of $KNbO_3$ Ceramics”, Journal of the American Ceramics Society, 88 [7], 1754-1759, 2005.

3. H. Birol, D. Damjanovic and N. Setter, “Preparation and Characterization of $(K_{0.5}, Na_{0.5})NbO_3$”, Journal of the European Ceramics Society, 26 [6], 861-866, 2006.

4. H. Birol, T. Maeder, C. Jacq, S. Straessler and P. Ryser, "Fabrication of LTCC Micro-fluidic Devices Using Sacrificial Carbon Layers", International Journal of Applied Ceramic Technology, 2 [5], 364-373, 2005.

5. H. Birol, T. Maeder and P. Ryser, "Influence of Processing and Conduction Materials on Properties of Co-fired Resistors in LTCC Structures", Journal of the European Ceramics Society, 26 [10-11], 1937-1941, 2006.

6. H. Birol, T. Maeder and P. Ryser, "Processing of Graphite-Based Sacrificial Layer for Microfabrication of Low Temperature Co-fired Ceramics (LTCC)", Sensors and Actuators A: Physical, 130-131, 560-567, 2006.

7. H. Birol, T. Maeder and P. Ryser, “Modification of Thick-film Conductors Used in IP Technology for Reduction of Warpage during Co-firing of LTCC Modules”, Key Engineering Materials, High Performance Ceramics IV, 746-749, 2006.

8. H. Birol, T. Maeder, C. Jacq, G. Corradini, M. Boers, S. Straessler and P. Ryser, “Structuration and Fabrication of Sensors Based on LTCC Technology”, Key Engineering Materials, High Performance Ceramics IV, 1849-1852, 2006.

9. H. Birol, T. Maeder, Ingo Nadzeyka, Marc Boers and P. Ryser, “Fabrication of a Millinewton Force Sensor Using Low Temperature Co-fired Ceramic (LTCC) Technology”, accepted for publication in Sensors and Actuators A: Physical, available online, 2006.

10. H. Birol, T. Maeder and P. Ryser, “Application of Graphite-based Sacrificial Layers for Fabrication of LTCC (Low Temperature Co-fired Ceramic) Membranes and Micro-channels”, Journal of Micromechanics and Microengineering, 17, 50-60, 2007.

Reviewed Conference Papers

11. H. Birol, T. Maeder, M. Boers, C. Jacq, G. Corradini and P. Ryser, “Millinewton Force Sensor Based on Low Temperature Co-fired Ceramic (LTCC) Technology”, Proceedings of the Conference on Ph.D. Research in Micro-electronics and Electronics (PRIME), Lausanne, 2, 343-346, 2005.

12. H. Birol, T. Maeder and P. Ryser, “Low Temperature Co-fired Ceramic (LTCC) Technology: General Processing Aspects and Fabrication of 3-D Structures for Micro-fluidic Devices”, Proceedings of the 4th International Conference on Science, Technology and Applications of Sintering, Grenoble-France, 216-219, August 2005.

Proceedings

13. T. Maeder, C. Jacq, H. Birol and P. Ryser, "High-strength ceramic substrates for thick film sensor applications", Proceedings, IMAPS Friedrichshafen-Germany, 133-137, 2003.

14. T. Maeder, C. Jacq, H. Birol and P. Ryser, "Integrated Microfluidic Devices Based on Low-Temperature Co-Fired Ceramic (LTCC) Technology", Proceedings, 4th Korea-Switzerland Joint Symposium, Materials and MEMS for Life Science Applications, Les Diablerets-Switzerland, 2004.
15. H. Birol, T. Maeder, C. Jacq and P. Ryser, "Effects of firing conditions on thick-film PTC thermistor characteristics in LTCC technology", Proceedings, IMAPS Conference on Ceramic Interconnect Technology, Denver-USA, 106-109, 2004.

16. H. Birol, T. Maeder, C. Jacq and P. Ryser, "3-D structuration of LTCC for Sensor Micro-fluidic Applications", Proceedings, European Microelectronics and Packaging Symposium, Prague-Czech Republic, 366-371, 2004.

17. T. Maeder, C. Jacq, H. Birol and P. Ryser, "Strength of ceramic substrates for piezoresistive thick-film sensor applications", Proceedings, European Microelectronics and Packaging Symposium, Prague-Czech Republic, 272-276, 2004.

18. H. Birol, T. Maeder, C. Jacq, G. Corradini, R. Passerini, Y. Fournier, S. Straessler and P. Ryser, "Fabrication of LTCC Micro-fluidic Devices Using Sacrificial Carbon Layers", Proceedings of the 1st CICMT Conference on Ceramic Interconnect Technology, Baltimore-USA, 59-66, April 2005.

19. H. Birol, T. Maeder and P. Ryser, "Materials Compatibility Issues in LTCC Technology and Their Effects on Structural and Electrical Properties", Proceedings of the 1st CICMT Conference on Ceramic Interconnect Technology, Baltimore-USA, 300-309, April 2005.

20. H. Birol, T. Maeder, C. Jacq, G. Corradini, Y. Fournier, I. Saglini, S. Straessler and P. Ryser, "Structuration of Micro-fluidic Devices Based on Low Temperature Co-fired

Ceramic (LTCC) Technology", Proceedings of the 15th European Microelectronics and Packaging Conference and Exhibition, Brugge-Belgium, 243-247, 2005.

21. C. Jacq, T. Maeder, S. Menot-Vionnet, H. Birol, I. Saglini and P. Ryser, “Integrated thick-film hybrid microelectronics applied on different material substrates”, Proceedings of the 15th European Microelectronics and Packaging Conference and Exhibition, Brugge-Belgium, 319-324, 2005.

22. H. Birol, M. Boers, T. Maeder, G. Corradini and P. Ryser, “Design and processing of low-range piezoresistive LTCC force sensors”, Proceedings of the XXIX International Conference of IMAPS Poland Chapter, Koszalin-Darlowko, 385-388, 2005.

23. H. Birol, T. Maeder, M. Boers, C. Jacq, G. Corradini, and P. Ryser, “Fabrication and Characterization of LTCC-based Millinewton Force Sensor: Influence of Design and Materials Compatibility on Device Performance”, Munich-Germany, October 2005.

24. S. Straessler, P. Ryser, H. Birol, S. Kuenzi, A. Barraud and J. Hilbert, “Few is more”, IIS/EPFL/KIMM Symposium on Nano/Micro Science and Technology: Seiken Symposium No 41, Neuchatel-Switzerland, October 17-19, 2005.

25. H. Birol, T. Maeder and P. Ryser, “Preparation and Application of Inorganic Materials-based Sacrificial Layers for Fabrication of LTCC Devices”, Proceedings of the 4th European Microelectronics and Packaging Symposium with Table-Top Exhibition, Terme Catez-Slovenia, 57-60, May 22-24, 2006.

26. T. Maeder, Caroline Jacq, Igor Saglini, Giancarlo Corradini, Sigfrid Straessler, H. Birol, and P. Ryser, “LTCC thermal gas viscometer – heater module”, Proceedings of the 4th European Microelectronics and Packaging Symposium with Table-Top Exhibition, Terme Catez-Slovenia, 61-66, May 22-24, 2006.

Curriculum Vitae

Name and family name: Hansu Birol

Date and place of birth: July 4, 1976, Karacabey / Bursa

Nationality: Turkish

Civil status: Married to Mrs. Alline Pedra Jorge-Birol

EDUCATION

2002-2006

Ph.D. in Micro-engineering

Swiss Federal Institute of Technology, Lausanne (EPFL), Switzerland

1999-2001

M.Sc. in Sensor Systems Technology

Karlsruhe University of Applied Sciences, Karlsruhe, Germany

1994-1999

B.Sc. in Metallurgical and Materials Engineering

Middle East Technical University, Ankara, Turkey

PROFESSIONAL EXPERIENCE

Research assistant

December 2002 – September 2006

Swiss Federal Institute of Technology, Lausanne (EPFL)

Micro-engineering Department (SMT)

Laboratory for Production of Micro-technology (LPM)

LANGUAGE SKILLS

Turkish: mother tongue

English, German, French, Italian, Portuguese: advanced level